Evolution of Metabolism in Pseudomonas aeruginosa During Adaptation to the Cystic Fibrosis Airways

Pedersen, Bjarke Haldrup

Publication date:
2023

Document Version
Publisher's PDF, also known as Version of record

Infection Microbiology Group
Novo Nordisk Foundation Center for Biosustainability

Evolution of Metabolism in *Pseudomonas aeruginosa* During Adaptation to the Cystic Fibrosis Airways

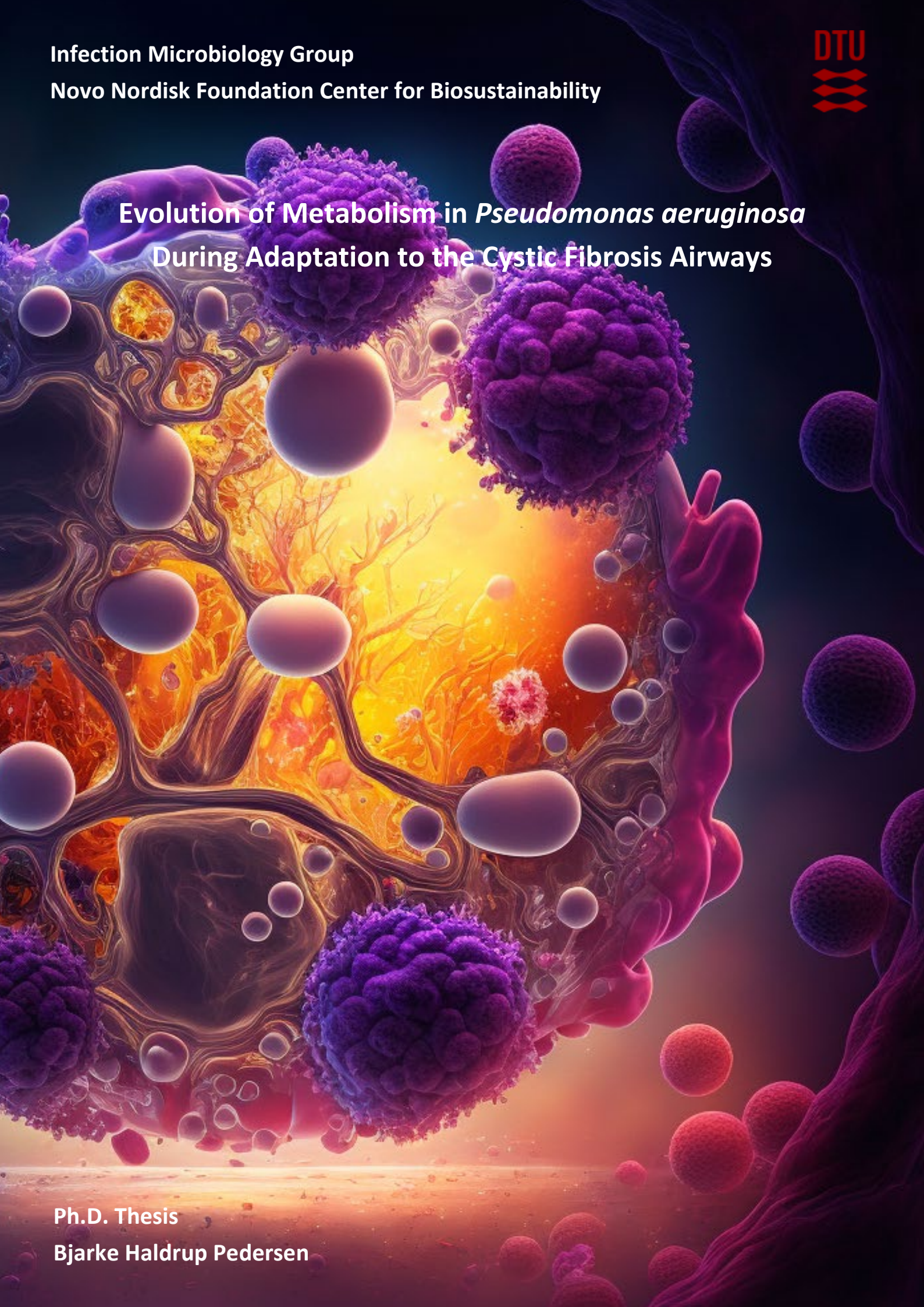

Ph.D. Thesis
Bjarke Haldrup Pedersen

Evolution of Metabolism in *Pseudomonas aeruginosa* During Adaptation to the Cystic Fibrosis Airways

Ph.D. Thesis

Bjarke Haldrup Pedersen

Infection Microbiology Group

Novo Nordisk Foundation Center for Biosustainability

Technical University of Denmark

Cover Art by author, using MidJourney with prompt: "*Beautiful world of enzymes carrying out metabolism inside bacterial cell, cover art, 8K, scientific, purple theme*".

"The gods did not reveal, from the beginning,
All things to us; but in the course of time,
Through seeking we may learn, and know things better…
This, as we well may conjecture, resembles the truth.
But as for certain truth, no man has known it,
Nor will he know it; neither of the gods,
Nor yet of all the things of which I speak.
And even if by chance he were to utter
The perfect truth, he would himself not know it;
For all is but a woven web of guesses."

- Xenophanes. Translation by Karl Popper, "The World of Parmenides."

"So we seek explanations that remain robust when we test them against those flickers and shadows, and against each other, and against criteria of logic and reasonableness and everything else we can think of. And when we can change them no more, we have understood some objective truth. And, as if that were not enough, what we understand we then control. It is like magic, only real."

- David Deutsch, "The Beginning of Infinity: Explanations That Transform the World."

Preface

This thesis is submitted as a partial fulfilment of the requirements to obtain the Ph.D. degree at the Technical University of Denmark (DTU). The work presented was carried out in the Infection Microbiology Group, led by Søren Molin and Helle Krogh Johansen, at the Novo Nordisk Foundation Center for Biosustainability and under the supervision of Ruggero La Rosa and Pablo Ivan Nikel. The work was performed from November 2019 to 2022 and the thesis was submitted at the end of January 2023. This Ph.D. was co-financed by the Novo Nordisk Foundation Center for Biosustainability and the Cystic Fibrosis Trust.

Bjarke Haldrup Pedersen

Kgs. Lyngby

January 2023

Acknowledgements

This Ph.D. project has been an incredible experience full of both amazing opportunities as well as many difficult challenges and could not have been done without the support of the many extraordinary people that I was lucky enough to be surrounded by during my studies.

First of all, I want to thank my co-supervisor Ruggero La Rosa both for his mentorship and collaboration in absolutely everything during these last three years, from when I first arrived at the group until the conclusion of my Ph.D. project. I also want to thank my supervisor Pablo Ivan Nikel and my group leaders Søren Molin and Helle Krogh Johansen for their valuable feedback and support in the conception of this project and for giving me this opportunity and the many that followed.

Thank you to all the wonderful people in the CfB Infection Microbiology Group for their company and comradery throughout the years and especially to all of the researchers at CfB that I had the chance to directly learn from, including Jennifer Bartell, Lise Goltermann, Ifigeneia Kyrkou, Filipa Simões, Ivan Pogrebnyakov, Antonella Colque, Akbar Espaillat, Daniel Volke and Nicolás Gurdo, as well as Head of Analytics Tune Wulff and Laboratory Technicians Lizzie Eriksen and Lars Boje Petersen.

I also want to thank Martin Welch for graciously welcoming me into his group at the University of Cambridge, Department of Biochemistry during my external stay. Thank you to Meng Wang, Stephen Trigg and everybody else in the Welch Group for their help and advice in getting me acquainted with the new lab. Importantly, I want to give a special thank you to all of the amazing people I met at Coronation Street that made my stay there an amazing and unforgettable experience.

I want to thank the Cystic Fibrosis Trust and the Novo Nordisk Foundation for funding this project and the European Molecular Biology Organization (EMBO) for the Scientific Exchange Grant to support my external stay at the University of Cambridge.

Finally, I want to thank my friends and family for their constant support during both the most exciting and the most difficult times of this journey.

Popular Science Summary

Since the beginning of the antibiotics revolution almost 100 years ago, the ability to control bacterial infections has transformed society in numerous ways, from the treatment of what used to be deadly diseases to how we produce food and do biological research. However, with the widespread use of antibiotics, the evolution of antibiotic *resistance* in bacteria is inevitable and the sparsity of novel antibiotic development in recent years means we now face a crisis of a globalised society reliant on antibiotics that every year becomes less effective at preventing the spread of infectious disease in humans, plants and animals. One of the areas where this is already a major health issue is in patients with Cystic Fibrosis, which is a heritable disease that makes the person highly vulnerable to chronic airway infections from pathogens with high degrees of antibiotic resistance – most notoriously the pathogen *Pseudomonas aeruginosa*. In the current project, I study the evolution of *P. aeruginosa* during its adaptation towards chronic airway infection in patients with Cystic Fibrosis. Specifically, I study the changes in metabolism, which is the term used for all of the processes related to the production and use of energy in the cell.

In a collaboration between DTU and Rigshospitalet, the Molin/Johansen group has established a collection of more than 500 clinical isolates of *P. aeruginosa*, sampled from patients with Cystic Fibrosis over the course of their infection. By selecting 8 pairs of early- and late-stage isolates from highly adapted infection scenarios and comparing changes in how nutrients are taken up and processed, as well as which proteins are being expressed at relatively high or low levels, I was able to identify several changes in bacterial metabolism and general physiology that appear characteristic of adaptation to the patient environment. One apparent adaptation of particular interest was the dysfunction of the enzyme “pyruvate dehydrogenase”, which plays a key role in determining how much of the cells energy is derived from its most central and energy-efficient metabolic pathway, known as the Krebs Cycle.

When inserting clinically evolved mutations of the genes encoding this enzyme into a laboratory strain of *P. aeruginosa*, it leads to many of the same changes in metabolism and general physiology seen in highly adapted clinical isolates. Furthermore, when tested in a stem cell-derived model system for airway infections, these mutant strains showed similar changes in pathology as those commonly seen for adapted isolates, most notably a reduced

immune response. In the thesis, I propose a mechanism by which this dysregulation directly affects the pathology of the bacteria, by increasing secretion of certain toxins and reducing e.g. growth and movement of cells to help avoid the immune system. By showing that metabolic adaptations directly regulate pathology and infection-specific mechanisms, this work provides evidence for the idea that metabolism is an important target for the development of next generation therapeutics and diagnostics, aimed toward chronic infections. Additionally, it suggests the key metabolic regulator pyruvate dehydrogenase as a specific example of such a target.

Abstract (English)

Pseudomonas aeruginosa is a highly versatile pathogen with several mechanisms both for immune escape and antibiotic resistance, making it one of the most critical pathogens to develop new treatments against to mitigate the antibiotic crisis. Because of its metabolic versatility, *P. aeruginosa* is able to undergo rapid adaptation and specialization toward a diverse range of environmental niches. This is evident in the case of patients with the heritable disease Cystic Fibrosis, where mutations in the Cystic Fibrosis Transmembrane Conductance Regulator dysregulates epithelial fluid transport. This leads to abnormal accumulation of dehydrated mucus in the lungs, which provides a nutrient-rich environment for infecting microbes. By adjusting its metabolism and physiology to the solutions available for the various niches that exist in the CF airways, *P. aeruginosa* is able to achieve persistent infections, which cause chronic lung inflammation that can last for more than 30 years and is the predominant cause of morbidity and mortality.

This study focuses on the evolution of *P. aeruginosa* metabolism during adaptation to the CF airways to identify key aspects of the strategies by which it achieves chronicity, and by extension how within-patient evolution of bacteria more generally leads to persistent infections, in order to identify potential targets for the development of novel therapeutic and diagnostic measures.

The first chapter gives a general introduction to the clinical relevance and molecular biology of *P. aeruginosa* CF airway infections and elaborates on the specific aims and design of the project. The second chapter describes a study in which we develop a high-throughput method for dynamic exo-metabolomic analysis in order to screen large collections of clinical isolates for metabolic changes. The study demonstrates how dilution-resolved sampling from several time-shifted growth curves accurately captures the metabolic dynamics of traditional low-throughput methods. The third chapter describes another study, where we select 8 pairs of clinical strains from different infection scenarios of *P. aeruginosa* in patients with Cystic Fibrosis based on reduction in growth rates as proxy for metabolic rewiring and apply the method described in Chapter 2 to identify commonalities in adapted metabotypes. Doing so, we identify clinical mutations in the *aceEF* genes encoding the key metabolic regulator pyruvate dehydrogenase as central to the adapted metabotypes and insert these mutations into the clean genetic background of PAO1. We combine this with proteomic analysis of both

clinical and genetically recombinant strains and demonstrate that these mutations in PAO1 leads to a partial recapitulation of the persistent phenotype. We then verify the pathoadaptive nature of these mutations by testing the mutant strains in an air-liquid-interface airway infection model system where they show reduced virulence and immunogenicity reminiscent of persistent infections. The fourth chapter gives a discussion of specific topics, where the obtained results may have interesting implications and finally, the fifth chapter gives a summary of the key findings and conclusions of the project and suggests some important directions for future research.

Altogether, this work provides evidence that evolution of metabolism is not simply a biproduct, necessary for accommodating the persistent phenotypes, but directly promotes the establishment of persistent infections without relying on traditional antibiotic resistance mechanisms. Furthermore, it suggests that dysregulation of pyruvate dehydrogenase and the consequent change in the flux of pyruvate is a common strategy by *P. aeruginosa* to achieve chronicity in CF airway infections.

Resume (Dansk)

Pseudomonas aeruginosa er et særligt fleksibel patogen med adskillige mekanismer for både undvigelse af immunsystemet og antibiotika resistens, hvilket gør det til en af de vigtigste bakterier at udvikle nye behandlinger imod for at forebygge antibiotikakrisen. På grund af ets metaboliske fleksibilitet, *P. aeruginosa* er i stand til at undergå hurtig tilpasning og specialisering imod en bred række miljøer. Det er tydeligt i tilfældet af patienter med den arvelige sygdom Cystisk Fibrose, hvor mutationer i proteinet "Cystic Fibrosis Transmembrane Conductance Regulator" dysregulerer væsketransport i epitellaget. Dette leder til anormal ophobning af dehydreret slim i lungerne, hvilket fungerer som et næringsrigt miljø for inficerende mikrober. Ved at justere dets metabolisme og fysiologi til de løsninger der er tilgængelige i diverse nicher der eksisterer i CF-luftvejene, *P. aeruginosa* er i stand til at opnå vedvarende infektioner der forårsager kronisk lungeinflammation, som kan vare i mere end 30 år og er den ledende årsag til morbiditet og dødelighed.

Dette studie fokuserer på evolution af *P. aeruginosa* metabolisme under tilpasning til CF-luftvejene for at identificere nøgleaspekter af de strategier det benytter for at opnå kronicitet og derved hvordan patient-specifik evolution mere generelt leder til vedvarende infektion med henblik på at identificere potentielle sårbarheder for udviklingen af nye behandlinger og diagnosticeringsmetoder.

Det første kapitel giver en generel introduktion til den kliniske relevans og molekylærbiologi af *P. aeruginosa* CF luftvejsinfektioner og uddyber om de specifikke mål og design af projektet. Det andet kapitel beskriver et studie hvor vi udvikler en "high-throughput" metode for dynamisk exo-metabolomisk analyse med henblik på at screene store samlinger af kliniske isolater for metaboliske ændringer. Studiet demonstrerer hvordan fortyndings-baseret sampling fra adskillige tidsforskudte vækstkurver korrekt fanger de metaboliske dynamikker fra traditionelle " low-throughput" metoder. Det tredje kapitel beskriver et andet studie, hvor vi udvælger 8 par af kliniske isolater fra forskellige infektionsscenarier af *P. aeruginosa* i patienter med Cystisk Fibrose, baseret på deres reduktion i vækstrate som proxy for metaboliske ændringer og anvender metoden beskrevet i Kapitel 2 til at identificere fællestræk i tilpassede metabotyper. Ved at gøre dette identificerer vi kliniske mutationer i *aceEF* generne, der koder for den vigtige metaboliske regulator "pyruvate dehydrogenase", som centrale for de tilpassede metabotyper og indsætter disse mutationer i den rene

genetiske baggrund af PAO1. Vi kombinerer dette med proteomisk analyse af både kliniske og genetisk rekombinerede stammer og demonstrerer at disse mutationer i PAO1 leder til en delvis rekapitulering af fænotypen for vedvarende infektioner. Derefter verificerer vi den patoadaptive karakter af disse mutationer ved at teste de genetisk rekombinerede stammer i en luft-væske-interface luftvejsinfektionsmodel, hvor de udviser reduceret virulens og immungenkendelse der minder om vedvarende infektioner. Det fjerde kapitel giver en diskussion af specifikke emner, hvor projektets resultater kan have interessante implikationer og til slut giver det femte kapitel en opsummering af de vigtigste resultater og konklusioner fra projektet og foreslår vigtige retninger for fremtidig forskning.

Tilsammen udgør arbejdet evidens for, at evolution af metabolisme ikke blot er et biprodukt, nødvendigt for at akkommodere fænotypen af vedvarende infektioner, men at det direkte fremmer etableringen af vedvarende infektioner uden at være afhængig af traditionelle mekanismer for antibiotikaresistens. Derudover så indikerer det at dysregulering af "pyruvate dehydrogenase" og de konsekvente ændringer i flux af pyruvat er en ofte anvendt strategi af *P. aeruginosa* for at opnå kronicitet i CF luftvejsinfektioner.

Table of contents

Chapter 1: Introduction

1.1 The antimicrobial resistance crisis

The development of antimicrobial resistance (AMR) is specifically pointed to as one of the main challenges to address in the UN 2015-2030 sustainable development goals, with regards to health and well-being [1]. In the widely cited *Review on Antimicrobial Resistance (2016)* commissioned by the UK government, it is projected that if the AMR crisis continues its current trajectory, absent novel solutions, by 2050 it will lead to an additional 10 million deaths annually and a cumulative loss of 100 trillion USD [2]. It is important to note that this review has been strongly criticized by academic researchers for lacking reliable and comprehensive data leading to inappropriate extrapolations of e.g. resistant proportion of incidence rates and from bloodstream infection data to other infection types, as well as potential bias in the methods for attributing mortality to resistance – all pointing in the direction of overestimating the burden of resistance [3]. In their critique, de Kraker et al., (2016) acknowledges that AMR presents a serious public health burden requiring urgent action as it is likely to increase over time but warns against forecasting decades into the future based on assumptions with no underlying empirical data to support them.

More recently, a comprehensive empirical study of the global burden of antibacterial resistance was published, looking specifically at actual deaths associated with or attributable to antibacterial resistance in 2019 [4]. This found that AMR is one of the leading causes of death globally, especially severe in resource-poor areas, such as sub-Saharan Africa. In 2019, an estimated 4.95 million deaths were associated with AMR, with 1.27 million of those deaths being directly attributable to AMR [4]. Using these results would make AMR the 12th leading GBD Level 3 cause of death globally, if based on directly attributable deaths, and the 3rd leading if based on AMR associated deaths [5].

More than half of the worlds small and medium-sized enterprises focused on development of novel antibacterial drugs are located in the United States [6] and in 2019, the number of antibacterial investigational new drug applications (INDs) in active development in the US had declined to an 11-year low, while the number of new antibacterial INDs initiated had reached the lowest in three decades [7]. Furthermore, the current global clinical pipeline is dominated by derivatives of already established classes with the same mode of action, which is likely to

lead to issues of cross-resistance for multidrug resistant gram-negative pathogens, such as *P. aeruginosa* [8]. Of the 76 drugs in the current pipeline, 54 % are targeted at these most critical pathogens and only 5 % were based on new modes of action, while only one of the 12 new antibacterial drugs approved in the last 5 years was not a derivative of a previously approved class – stressing the urgent need for basic research and high-risk R&D into new antibiotics with novel modes of action [9].

According to a 2017 World Bank Report and the Center for Global Development, this is due to a number of market failures with respect to development of novel antibiotics [5,10]. In the World Bank Report, Jonas et al., (2017) predict that by 2050, AMR will lead to a decrease in annual GDP between 1.1 % - 3.8 %, which would be more severe than the 2008 global financial crisis, but for a longer time and disproportionally impacting low-income countries [10]. One example of an attempt to circumvent these market failures is the US PASTEUR Act, a commitment to subscription-based purchasing of novel antimicrobials, which the US Center for Global Development estimates, when limiting the analysis to only antibacterials, to have a national return on investment (ROI) of 6:1 over 10 years and 28:1 over 30 years, while the global ROI is estimated to be 27:1 over 10 years and 125:1 over 30 years [5], with similar estimates for such a programme in the EU, UK, Canada and Japan [11–14]. In their report, they describe the problem as follows:

> "*There are three main pathways of impact. First, common infections will become less easily treated, causing more people to fall ill and die. Second, first-line antimicrobials are generally well-tolerated and easily administered; current second-and third-line antibiotics often come with more serious side-effects, and require intravenous administration or hospitalization. Finally, and perhaps most frightening, is the "nightmare scenario" in which modern medicine collapses because surgeries, chemotherapy, and other common interventions are no longer viable due to infection risk*"
>
> - Towse and Bonnifield, (2022)

It is also worth noting that according to the US Center for Disease Control, the Covid-19 pandemic has further exasperated the situation by overwhelming the health sector and negatively impacting prevention, control and tracking practices for resistant infections, as well as leading to misdiagnosis and prescription of antibiotics to patients with Covid-19. This

has led to increased case-rates for many types of resistant infections, including a 32 % increase in hospital-onset multi-drug resistant (MDR) *P. aeruginosa* infections from 2019-2020 [15].

1.2 Clinical relevance of *P. aeruginosa* airway infections of patients with Cystic Fibrosis

In my project, I focus on the specific pathogen *P. aeruginosa*, which is one of the six most impactful pathogens identified in Murray et al., (2022). *P. aeruginosa* has also been listed by the WHO as one of three pathogens of critical priority for development of new antibiotics [16] and is one of the six so-called "ESKAPE" pathogens which, in addition to being responsible for the vast majority of nosocomial infections, represent the most important paradigms of pathogenesis, transmission and resistance that we must learn to control, in order to deal with virtually any pathogen that might take their place [17].

Specifically, this project relates to *P. aeruginosa* airway infections in patients with Cystic Fibrosis (CF), where it represents the leading cause of morbidity and mortality [18]. CF is a heritable disease caused by a mutation in the Cystic Fibrosis Transmembrane Conductance Regulator (CFTR) protein, which affects the activity of chloride ion-transport channels in the airway epithelia. Dysregulation of this gene affects the osmolarity of the mucus, which is a part of our innate immune system, leading to dehydration and preventing its normal clearance by cilial cell beating. This in turn leads to abnormal accumulation of dehydrated mucus in the airways, which provides a nutrient-rich environment for infecting microbes, making the patients highly vulnerable to airway infections (La Rosa et al., 2019).

The study by Murray et al., (2022) found that lower respiratory infections were the most impactful type of infection, making up more than 30 % of the deaths associated with AMR globally [4]. It also found *Pseudomonas aeruginosa* to be one of the six leading pathogens for death associated with AMR, which together are responsible for more than 70 % of the 1.27 million deaths directly attributable to AMR, and of the 4.95 million deaths associated with AMR [4], as seen on Figure 1.

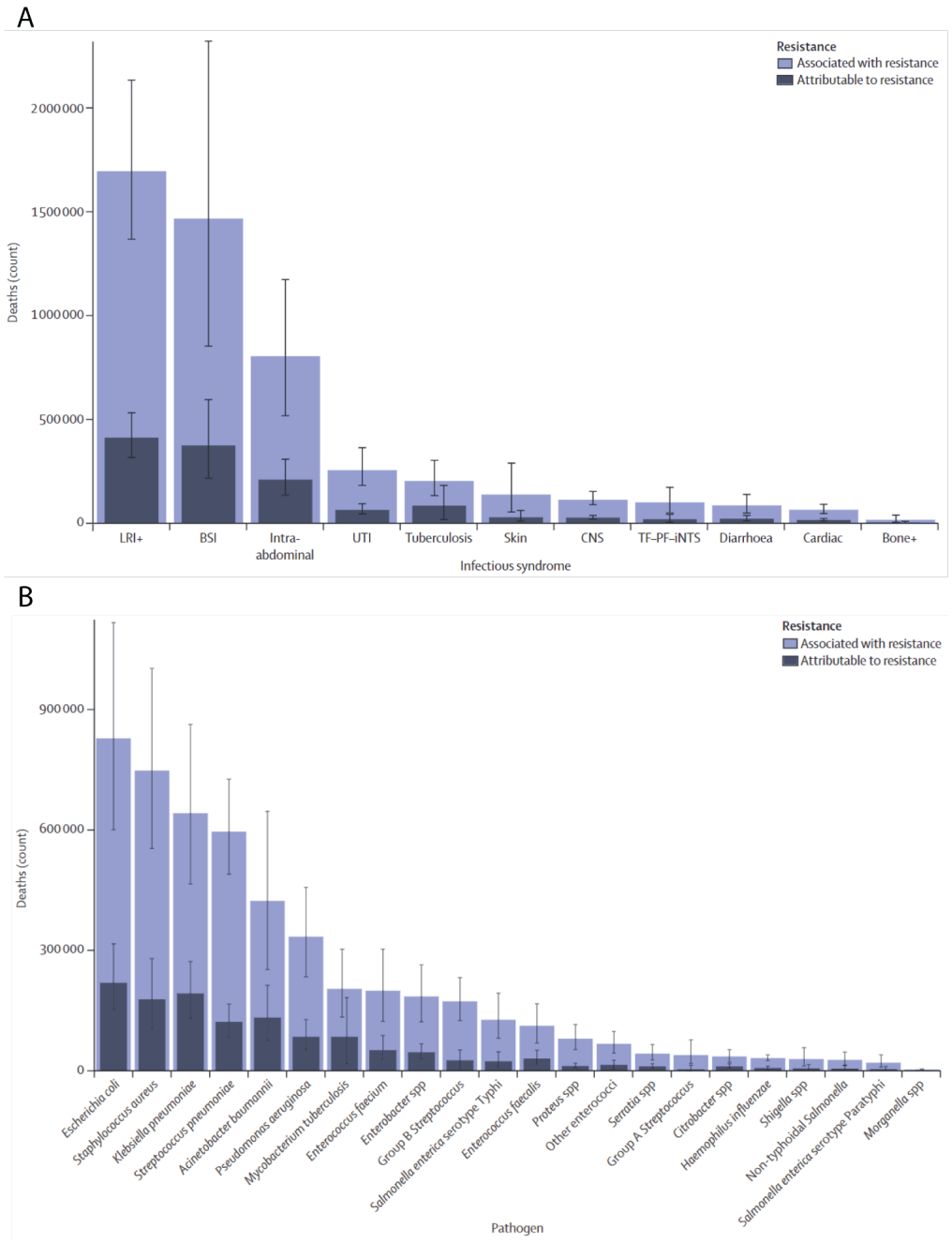

Figure 1: Figures 3 and 4 from Murray et al., (2022) showing the death counts of different types of (A) infections and (B) pathogens.

Thus, in addition to being an important health challenge in its own right, *P. aeruginosa* infections of the CF airways represents a model system that reveals insight applicable to both one of the most critical pathogens, as well as the specific environment of the lower airways, which is the most impactful type of infection of the modern world.

Staphylococcus aureus is the organism causing most respiratory infections for CF patients earlier in life and was the primary cause of death before modern intensive antibiotic

treatments were introduced. However, the success of anti-staphylococcal therapies revealed *P. aeruginosa* to be an important pathogen in the context of CF [20]. Today, *P. aeruginosa* is associated with more severe outcomes, i.e. more pulmonary exacerbations and higher CRP levels than *S. aureus* [21]. Moreover, once the patient has been exposed to *P. aeruginosa*, it tends to outcompete and replace *S. aureus* and all other microbes present in the airways, leading to reduced microbial diversity. For patients >34 years old, 60 % of airway infection cases involve *P. aeruginosa* and almost 40 % show *only P. aeruginosa* [22], as can be seen on Figure 2.

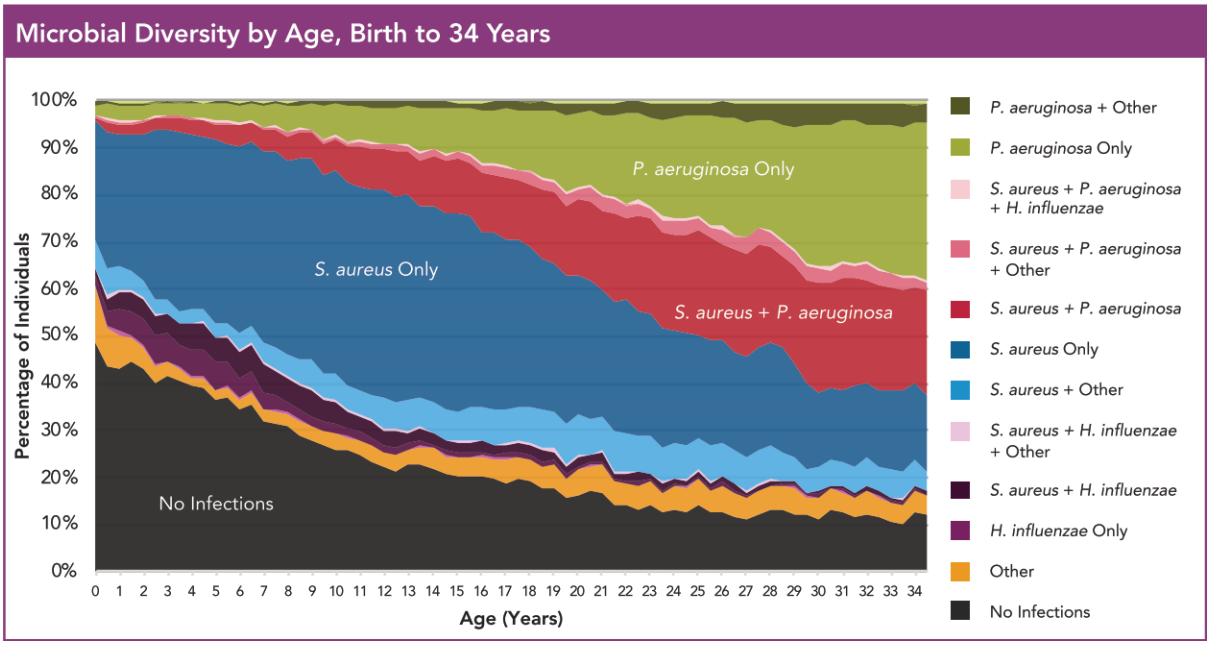

Figure 2: Figure from the Cystic Fibrosis Foundation 2018 Patient Registry Annual Data Report (Cystic Fibrosis Foundation, 2018) showing the change in microbial diversity in CF patients by age.

This eventual take-over of *P. aeruginosa* is in large part due to its highly flexible metabolic repertoire, which allows rapid adaptation and specialization toward the various niches available in the CF airways [19]. The colonization by *P. aeruginosa* induces the host immune system, as seen on Figure 3 from the rapid build-up of *P. aeruginosa* specific antibodies. This immune response is maintained constantly in the case of chronic infections, leading to chronic lung inflammation that causes tissue damage and impairs normal lung function. Eventually this results in respiratory failure, which is the reason for 95% of deaths in patients with CF [20,23].

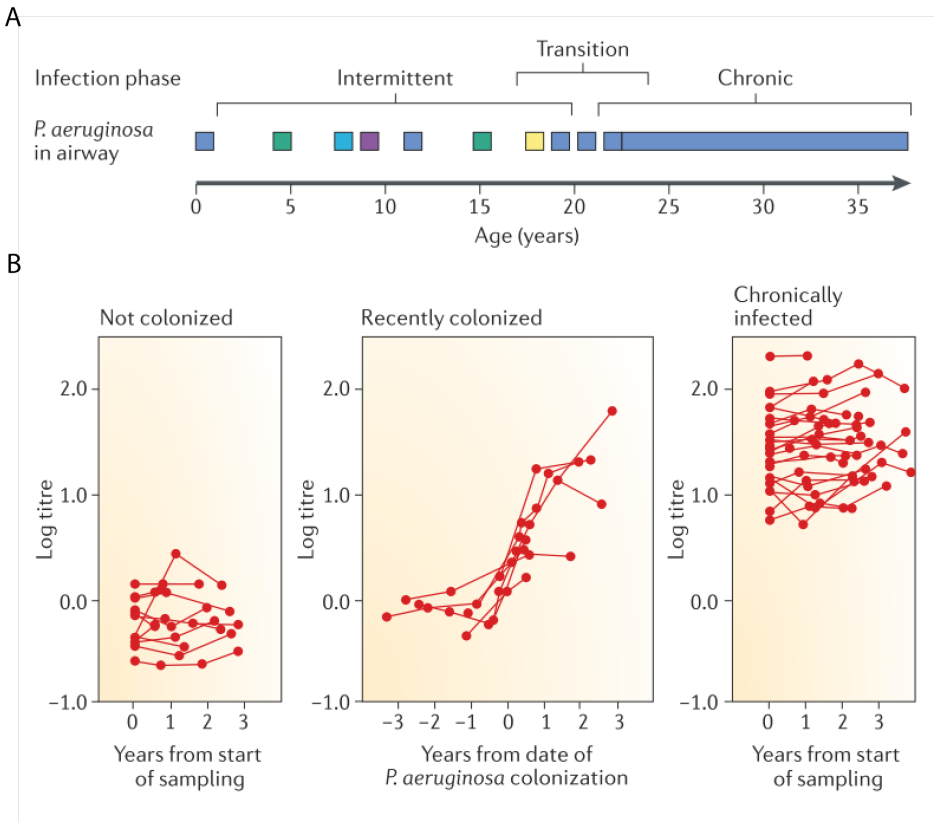

Figure 3: From Figure 2 of Folkesson et al., (2012) showing (A) schematic of typical progression of CF patients with P. aeruginosa airway infections and (B) the effect this has on the log titre of P. aeruginosa specific antibodies.

These infections require severe and continuous antibiotic treatments, which help maintain lung function and has extended media life-span of patients to almost 50 years [24]. However, these treatments also have many severe adverse effects and eventually the persistent infection develops resistance. Indeed, chronic *P. aeruginosa* infections often exhibit resistance toward all clinically relevant antibiotic classes [23].

A more recent strategy that has seen substantial success are CFTR modulator treatments that focus on directly targeting the defective CFTR protein, either by improving its gating function ("potentiators"), helping to stabilize 3D conformation ("correctors") or increase CFTR protein production ("amplifiers") depending on the type of mutation in the patient [25–31]. In addition to improving overall lung function, body mass index and sputum production [32], some studies also show a reduced prevalence of *P. aeruginosa* airway infections [33] although the remaining 7-15 % yearly incidence rates still remain concerning and require further development of antimicrobial therapies especially targeted toward chronic phenotypes that may work synergistically with CFTR modulator treatment to improve long-term outcomes [34].

One area that has been historically understudied but is becoming increasingly relevant is the role of metabolism in antibiotic resistance [35–42]. This also represents a novel area of targets for the development new antimicrobial treatments [6,9]. Given that metabolism is known to function radically different in chronic infections [19,43] it may be possible to target metabolism of persistent phenotypes specifically, which could help to reduce adverse effects, as well as the selective pressure for development of resistance.

1.3 *Pseudomonas aeruginosa*

1.3.1 Metabolically versatile pathogen

Pseudomonas aeruginosa is a Gram-negative bacterium ubiquitous in soil and water environments but primarily associated with habitats affected by human activity [44]. It is an opportunistic pathogen capable of infecting both plants [45] and animals [46,47], as well as humans. Besides the CF airways, *P. aeruginosa* can also cause infections in people with other pulmonary obstructions [48], bladder catheters or intubations [49], burn wounds, diabetic foot ulcers and even in healthy subjects with no particular vulnerabilities [50,51].

It is known to be highly ecologically versatile and resilient to changes in the environment, owing to its very large genome (5.5-7 Mb) that rivals even the size of simple eukaryotes [52]. This large genome encodes many different regulators and transporters, as well as a diverse set of virulence factors and catabolic functions that provide it with responses to the wide array of challenges it may face in different environments [51]. Its core genome consists of 665 genes encoding essential functions [53], which is similar to the number of genes thought to be essential in CF airway environment [54]. The remaining 99% of its pan-genome [53] is more flexible, leaving room for substantial genomic diversity within the species [55]. *P. aeruginosa* has generally been separated into three phylogenetic groups represented by the common strains PAO1, PA7 and PA14 respectively [56], although recent studies suggest there may be two other phylogenetically independent groups [53]. Most strains belong either to the PAO1 or PA14 group, with PAO1 being used as the reference strain to clinical isolates in this study.

Because *P. aeruginosa* is often found in environments where nutrient availability is limited, it has evolved a broad metabolic network capable of adapting it catabolic and anabolic pathways to the nutritionally and chemically diverse niches of both water, plants and animals

and allowing it to utilize a variety of both complex and recalcitrant carbon sources for growth and biosynthesis of specialized secondary metabolites [57–59]. For example, the coupling of glycolysis with both the Entner–Doudoroff and Pentose Phosphate Pathways (EDP/PPP) supports high levels of reducing equivalents through hexose sugar assimilation [60,61] as well as the biosynthesis of alginate required for the mucoid phenotype often employed in infection scenarios [62]. Organic and amino acids are assimilated and funnelled through the tricarboxylic acid (TCA) cycle, which provides the building blocks necessary to maintain relatively high growth rates [63–65].

The TCA cycle also supports aerobic respiration, which is the most efficient pathway for energy production but also leads to the accumulation of Reactive Oxygen Species (ROS) that cause oxidative stress. This is likely to be exasperated by the host immune response during infection and so it may be adaptive to mitigate oxidative stress by reducing TCA activity e.g. by decoupling glycolysis from the TCA cycle and/or redirecting flux through the glyoxylate shunt [37,40,66]. One potential mechanism for this, which will be studied in detail in this thesis is the dysregulation of the pyruvate dehydrogenase (PDH) complex, which connects glycolysis to the TCA cycle through the conversion of pyruvate (the end product of glycolysis) to acetyl-CoA, which enters the TCA cycle. Mutations in the *aceEF* genes encoding the PDH-E1 and E2 subunits respectively both appear to be selected for during adaptation to the CF airways [18] and both genes show reduced expression in the transcriptional programme of *P. aeruginosa* when grown in CF sputum of chronically infected patients compared with the same strains grown under laboratory conditions, suggesting reduced activity *in vivo* [67]. The fact that the *aceA* gene, which encodes the enzyme isocitrate lyase responsible for redirecting flux through the glyoxylate shunt, also shows increased expression under the same conditions suggest a synergistic effect where glucose metabolism and the TCA cycle are decoupled, with the TCA cycle working through the glyoxylate shunt, most likely supported by the assimilation of amino acids. Under most conditions, such an adaptation would need to have substantial benefits to off-set the fitness cost of the loss in capacity for energy production through aerobic respiration.

P. aeruginosa is a facultative anaerobic meaning it can survive and grow both in the presence and absence of oxygen. This does not function as an either-or response dictated e.g. by a discrete regulon for low oxygen conditions but rather *P. aeruginosa* can modulate its

transcriptome to balance anaerobic and micro-aerophilic respiration in response to different oxygen conditions as seen for example in the case of adaptation CF airways where oxygen availability is often limited [67,68]. Even in the absence of oxygen, it is able to use nitrogen and potentially larger molecules such as thiosulfate to replace oxygen as electron acceptors for respiration [69]. Indeed several operons related to denitrification (nir, nar, nos and nap) as well as one thought to encode thiosulfate reductase are all activated in the lung microenvironment, along with high oxygen affinity terminal oxidases that are able to make use of oxygen even at very low concentrations [67]. Additionally, *P. aeruginosa* can make use of both pyruvate and arginine for fermentation to produce energy and support long-term survival without growth under anaerobic conditions when both oxygen and nitrogen are depleted [70–72].

The CF airways generally provide an abundance of nutrients compared with most other environments but has limited availability of important cofactors such as iron and zinc due to the host activity restricting access to these in an attempt to inhibit bacterial growth. *P. aeruginosa* however has several strategies for adapting to this restriction, including the expression of iron- and zinc-independent variants of metabolic enzymes and stress regulators that typically rely on these as cofactors, as well as the production of a wide array of metal scavenging systems including the siderophores pyoverdine and pyochelin and molecules for zinc-sequestration and transport [67,73,74].

1.3.2 Virulence factors

In addition to the metal-scavenging molecules, *P. aeruginosa* produces many other types of virulence factors including phenazines that function as electron acceptors to maintain redox balance and protect against oxidative stress [75]. It also produces five different secretion systems for delivering effector proteins into the extracellular space as well as directly injecting them into both the host and competing microbes as seen on Figure 4 [76].

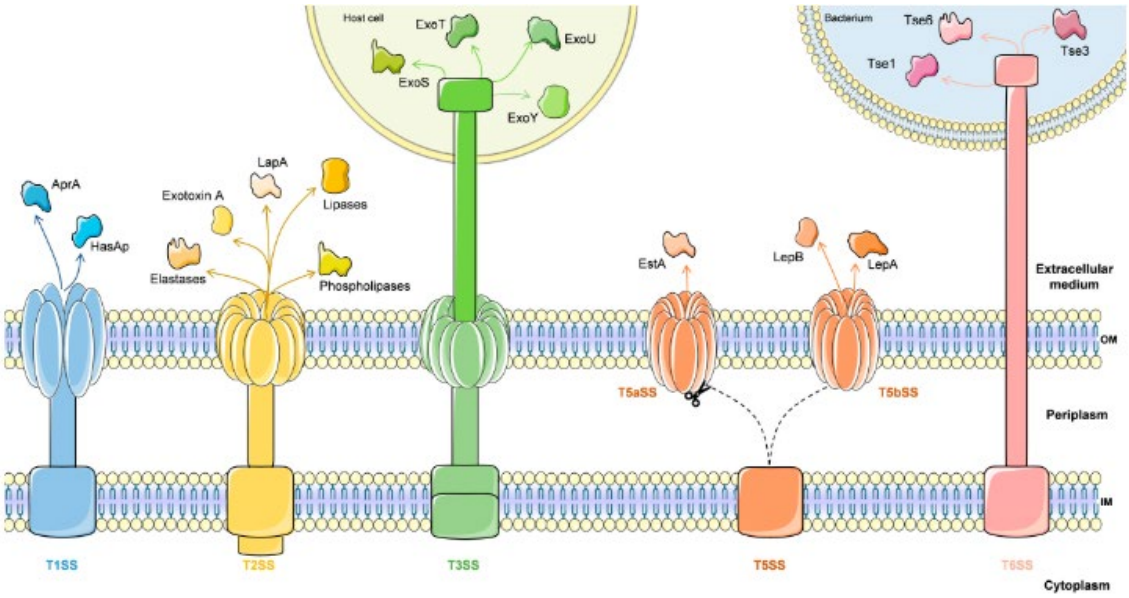

Figure 4: Figure 2 from de Sousa et al., (2021) showing the five different secretion systems encoded by P. aeruginosa.

The type I secretion system (T1SS) is a simple system consisting of an outer membrane protein, an inner membrane ATP-binding cassette (ABC) transporter providing the necessary energy for transport and an adaptor protein connecting the two in the periplasm [77]. This can produce e.g. the HasAp protein, which is important for early infections because it can bind to heme, allowing it to steal iron from the host haemoglobin [77,78]. The T1SS can also secrete the virulence factors AprX [79] and the alkaline protease AprA [77,80].

The type II secretion system (T2SS) transports large multimeric proteins that were folded in the periplasm through the outer membrane into the extracellular environment [81,82]. This includes at least 14 different proteins with different effects such as elastases (LasB, LasA), phospholipases and lipases (PlcN, PlcH, LipA and LipC) and exotoxin A (ToxA) through the Xcp system, as well as the alkaline phosphatase LapA through the Hxc system under phosphate-limiting conditions [83]. Exotoxin A leads to the death of host cells through ADP-ribosylation of the host cell elongation factor-2, which inhibits protein synthesis [84]. Elastases cleaves the main component of lung connective tissue elastin, thus degrading it [85] while phospholipases and lipases degrade surfactants, also in the pulmonary system, and interfere with normal immune function [86,87].

The type III secretion system (T3SS) is a needle-like complex that can directly inject effectors such as the cytotoxic proteins ExoS, ExoT, ExoU and ExoY into the host cells [88]. ExoS and ExoT disrupt the host cells' signalling pathways through ADP-ribosylation of Ras [89–91], while ExoY

disrupts the actin in their cytoskeleton by increasing intracellular cAMP levels and ExoU causes tissue destruction through its activity as a lipase [92]. The T3SS is also known to be related to the assembly of flagellar and is subject to highly complex regulation by at least 36 genes in 5 different operons [93]. It can be induced by several different signals including contact with host cells [94,95], Calcium limitation [93], cAMP levels [96] and spermidine [97].

The type V secretion system (T5SS) is a simple system composed of autotransporters and two-partner secretion systems [93] that transport proteins to the outward-facing side of the outer membrane where they remain unless released into the extracellular space by proteolytic cleavage [98]. This includes EstA which is important for rhamnolipid production and affects motility and biofilm formation [99,100] and CdrA which also promotes biofilm formation, as well as LepA/LepB that secrete proteases that interfere with the host immune response [101,102].

The type VI secretion system (T6SS), like the T3SS, is another needle-like complex that directly injects effectors into the target cells [103]. It is a widespread strategy in gram-negative bacteria used for killing competing microbes but is employed slightly differently in *P. aeruginosa* following the game-theoretical tit-for-tat strategy [104]. The T6SS is used by *P. aeruginosa* to inject both host cells and competing bacteria with effectors, such as the Tse1-6 proteins. While Tse1/3 hydrolyse peptidoglycan in periplasm of competing bacteria and Tse4-6 function directly as antibacterials, Tse2 works to arrest growth of both prokaryotes and eukaryotes [76,105,106]. There are three different loci encoding T6SS components referred to as H1-, H2- and H3-T6SS, all controlled by the global regulator RsmA [103]. H1-T6SS encodes the phage-like needle structure responsible for projection of payloads onto bacterial surfaces [106,107] while H2-T6SS has been implicated in the internalization of *P. aeruginosa* in epithelial cells to evade the immune system and H3-T6SS is associated with pathogenesis [108]. Both H2- and H3-T6SS are also regulated by the quorum sensing regulator PqsR [103,109].

1.3.3 Quorum sensing and biofilm formation

There are three Quorum Sensing (QS) systems in *P. aeruginosa* responsible for regulating bacterial communication and responding to the presence and density of other cells [110] by producing small signalling molecules called autoinducers that coordinate the activity of several functions including virulence factors, adhesion, motility and formation of biofilm

[111,112]. These three systems are the Las-, Rhl-, and *Pseudomonas* Quinolone System (PQS) [113,114], which act in a highly coordinated way where the Las system induces both the rhl system and PQS, while the PQS induces the rhl system and the rhl system in turn inhibits PQS [115]. Rhl is mainly responsible for inducing the expression of proteases, elastases, rhamnolipids, pyocyanin and HCN [116]. PQS also regulates the biosynthesis of pyocyanin and rhamnolipids [109] and has been associated both with iron acquisition, cytotoxicity, biogenesis of outer-membrane vesicles, reduced metabolic activity to mitigate oxidative stress and immune modulation [117,118].

All three QS systems are also involved in the formation of biofilms, which are structured communities of cells embedded in a matrix composed of e.g. polysaccharides and extracellular DNA [119,120]. LasR regulates biofilm formation through the Psl system which in turn increases cell surface adhesion and synthesis of galactose/mannose-rich polysaccharides [121–124], whereas RhlI regulates the Pel system, which relies on glucose-rich polysaccharides instead [125,126]. Both are related to the initial stages of biofilm formation [120]. Biofilm formation is also regulated by the two-component regulatory systems (GacS/GacA) and the nucleotide c-di-GMP, which coordinates a switch between and motility and polysaccharide biosynthesis [109,127–129].

Figure 5 shows the five stages of biofilm formation [130], the first being flagellar-mediated reversible surface-attachment by planktonic cells followed by a second stage characterized by the influx of motile cells to the location of the attachment which maintain Type IV pili mediated twitching motility to form microcolonies and upregulate expression of the *algC*, *algD*, and *algU* genes to promote the biosynthesis of alginate for the extracellular matrix. The third stage is defined by proliferation and loss of motility while the fourth stage is defined by the transition from a monolayer of cells into a three-dimensional structure. Finally, the fifth stage is the dispersion of new planktonic cells from the biofilm which can generate new biofilms [120,131].

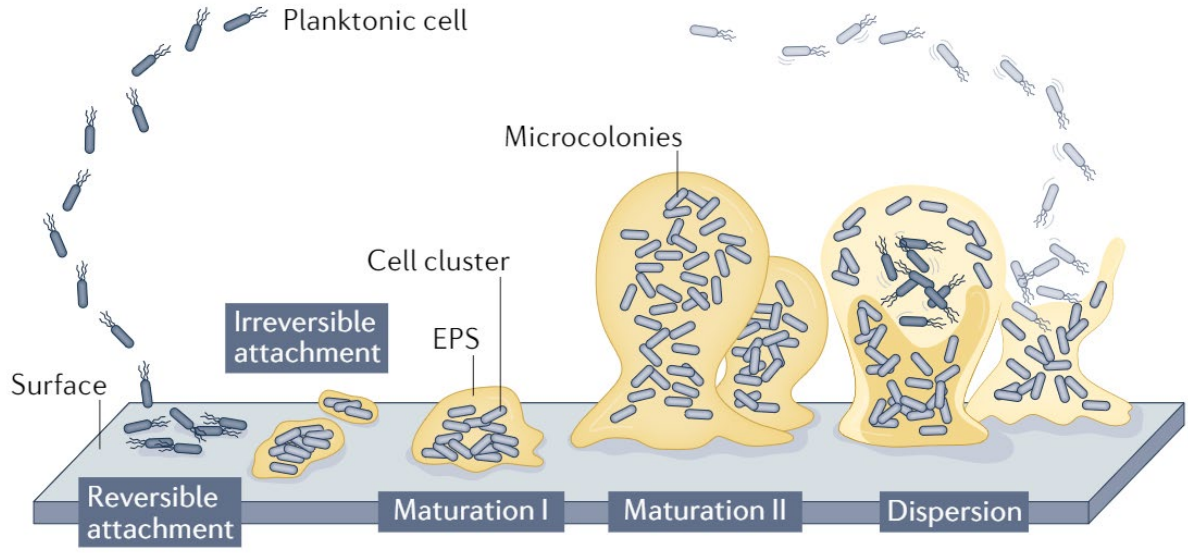

Figure 5: Figure 1 from Saur et al., (2022) showing the five stages of biofilm formation.

Because of the architecture of biofilms, they typically exist under oxygen-limiting conditions with increasingly low oxygen-availability at the deeper levels [132,133]. Indeed, low oxygen availability seem to promote more robust biofilms for *P. aeruginosa* [134], which also means the oxygen-limited environment of the CF airways is highly suitable for biofilm formation [135]. The same architecture also restricts access of antibiotics to lower levels of the biofilm and contributes to the increased tolerance observed for biofilms against surfactants, antibiotics and phagocytosis [136–138].

In addition to biofilm formation, alginate production is also linked to the development of mucoidity, which protects *P. aeruginosa* from physical stress [139] and inflammation [140–143]. Alginate production often appears to be upregulated in chronic *P. aeruginosa* CF airway infections [144] and is associated with worse outcomes for patients [145]. This phenotype is most commonly derived from mutations in MucA which inhibits expression of the *algD* operon required for alginate biosynthesis by sequestering the σ-factor σ22 [146–152]. This same σ22 is also involved in the regulation of many genes related to virulence, motility and general stress response [145,153–155] suggesting mucoidity is coordinated with many other functions important for infection.

1.3.4 Adaptation of P. aeruginosa to the CF airways

Despite the overall abundance in nutrients, the CF airways still present many complex challenges to the colonizing *P. aeruginosa* including oxidative stress from reactive nitrogen and oxygen species (RNS and ROS) released by the immune system to kill infecting bacteria [156,157], limited access to e.g. oxygen, zinc and iron and high concentrations of antibiotics from modern intensive treatment regimens [67,73,74]. *P. aeruginosa* responds by undergoing substantial metabolic rewiring to support a new balance between growth and more specialized functions such as the production of virulence factors for metal scavenging, exopolysaccharides for biofilm formation and surface modifications of both lipid composition and loss of O-antigen to help evade the immune system [67,158–161]. It also has several strategies for mitigating the oxidative stress caused by the immune response, including the expression of enzymes that are either ROS-insensitive variants, RNS/ROS-scavenging or help repair other oxidized proteins or maintain redox balance [67,73,74]. This, combined with its intrinsic antibiotic tolerance allows small subpopulations to persist despite the hostile conditions and eventually, through continuous selective pressure, transition to a chronic phenotype that is highly specialized to the CF airways [69]. Figure 6 shows how *P. aeruginosa* adapts during transition to chronic infections.

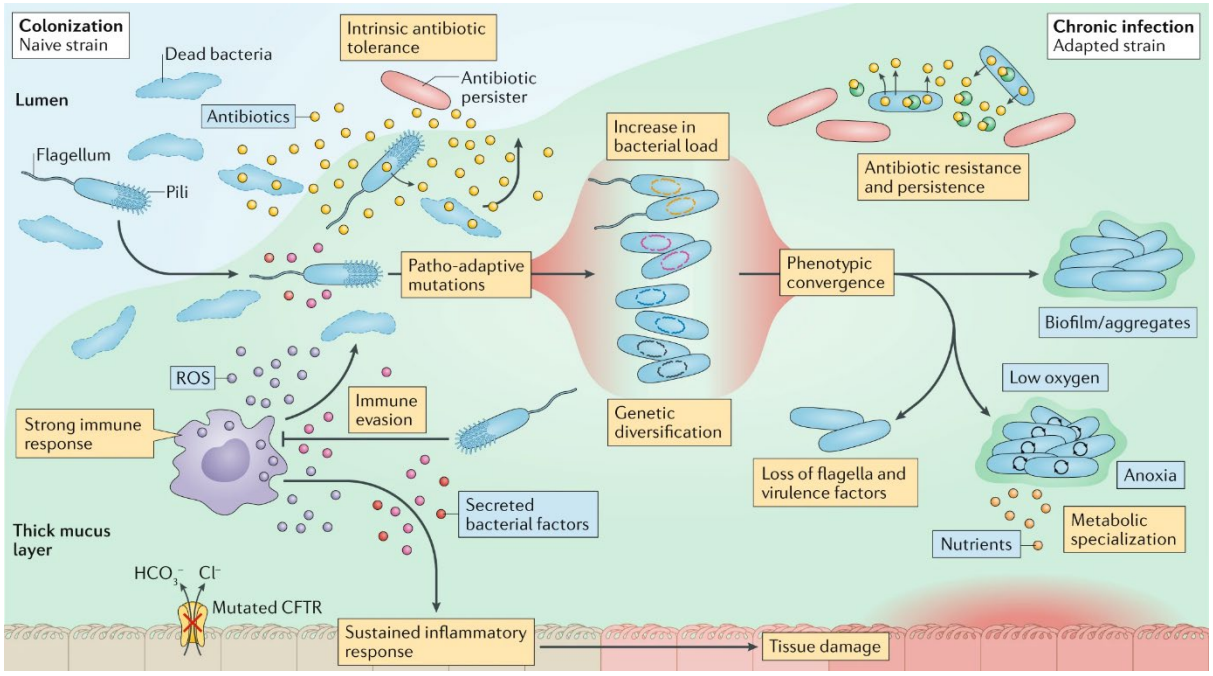

Figure 6: Figure 1 from Rossi et al., (2020) showing the convergent evolution of persistent phenotypes in P. aeruginosa CF airway infections.

Genomic analysis of large longitudinal collections of clinical isolates from different CF clinics have found frequent mutations in specific genes associated with metabolism (*aceE*, *aceF*) biofilm formation (*mucA*, *algU*, *morA*), antibiotic resistance (*mexZ*, *nfxB*, *mexR*, *gyrA*, *gyrB*, *mpl*), loss of virulence factors (*ykoM*, *mpl*), quorum sensing (*lasR*) and other regulatory systems (*rpoN*, *nfxB*, *mexR*, *gacA*, *gacS*) [18,162,163]. However, in general, chronic infections are characterized by substantial genetic diversity and unique evolutionary trajectories in different patient lineages leading to a highly conserved set of phenotypic traits such as reduced growth rate, increased biofilm formation, protease secretion, reduced motility and loss of certain quorum sensing and virulence functions through convergent evolution [18,23,162–165]. These studies also reveal that phenotypic changes occur rapidly in the first 2-3 years of infection in a manner dependent on genotypic changes but after that, further accumulation of mutations have little effect on the overall phenotype [164,165]. Surprisingly, the development of antibiotic resistance is typically not among these initial phenotypic changes. Rather it can take decades before the strains acquire mechanisms that confer full antibiotic resistance. This remains a puzzle but some explanations that have been offered are centred around the intrinsic antibiotic tolerance that may be conferred either by the biofilm lifestyle or by slow stationary growth mediated by reduced metabolism [23].

1.4 Project design

1.4.1 Strain collection at Rigshospitalet

To address this challenge of chronic *P. aeruginosa* CF airway infections, the Copenhagen CF Centre has established a strain collection of more than 500 longitudinally sampled clinical *P. aeruginosa* isolates across more than 34 different patients, which has been studied by the Molin/Johansen group to map out the evolution of *P. aeruginosa* in CF airway infections through Whole-Genome Sequencing, as well as transcriptomic, metabolomic and phenotypic analysis [18,43,67,164]. Figure 7 shows the collection from a 2015 study where 474 clinical strains were Whole-Genome sequenced.

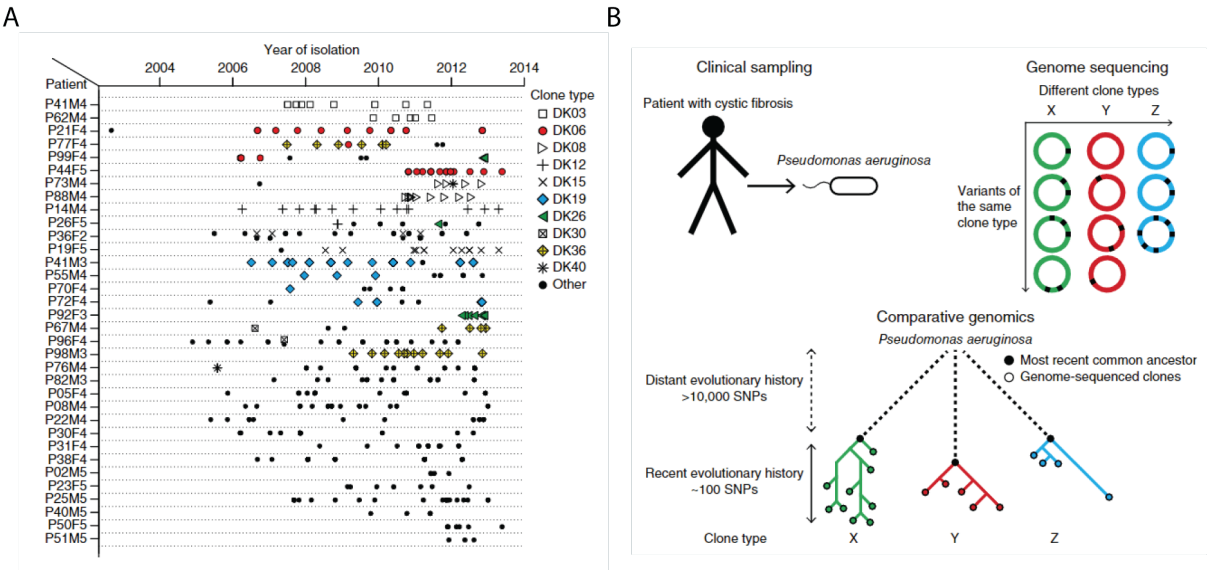

Figure 7: Figures 1-2 of Marvig et al., (2015a) showing (A) the collection of isolates, as of 2015, with icons indicating Clone Type of individual isolates separated by year of isolation on x-axis and patient on y-axis, as well as (B) schematic of the procedure of sampling, then carrying out Whole Genome Sequencing followed by comparative genomics to track evolutionary history of the clinical strains.

Initially, the aim was to find genetic markers that could predict the potential for establishment of chronic infections in the clinic. In many ways, we are now understanding the role of specific mutations in different evolutionary trajectories leading to chronic infections. However, the multitude of different mutational profiles that can support similar persistent phenotypes makes it unlikely that chronic infections can be inferred from specific mutations alone. Rather, diagnostics based on such markers will require additional types of phenotypic markers that generalize to different evolutionary trajectories.

1.4.2 Objectives of PhD project

In this project, I investigated the metabolic changes that underlie the transition to persistent phenotypes. First, I selected out the most relevant clinical isolates based on reduction in growth rate from early to late clinical isolates of different infection lineages as proxy for metabolic adaptation to the CF airways to screen them for convergent changes in nutrient utilization using dynamic exometabolomics. I also investigated if frequently occurring clinical mutations in the *aceE* and *aceF* genes, encoding the key metabolic regulator pyruvate dehydrogenase, promote persistent phenotypes by testing the extent to which the persistent phenotype was recapitulated when these mutations were inserted into the clean genetic background of PAO1.

Overall, the aims of this project were:

- First, to develop a high-throughput method for dynamic exo-metabolomic analysis of large numbers of strains, which was required to be able to screen our collection in sufficient detail for convergent changes in metabolic profiles.
- Second, to apply this method to the selected clinical strains to find links between adapted metabotypes and infection-related functions.
- Third, to determine the specific effects of the metabolic adaptation of pyruvate dehydrogenase dysregulation and its role in transition to a persistent phenotype.

Chapter 2: High-throughput dynamic exo-metabolomics

2.1 Metabolomics as tool for studying metabolism

Metabolomics is the direct study of the many metabolites produced and consumed by the organism as part of its metabolic activity. Broadly, this can be divided into endo-metabolomics, which is the study of the metabolites inside the organism, and exo-metabolomics, which focuses on the effect of metabolism on metabolites outside the organism. Exo-metabolomics is done by analysing changes in extracellular metabolite concentrations of a defined growth medium caused by the specific assimilation and secretion of metabolites during cell growth [166].

While endo-metabolomics generally provides a more direct description of the physiological state of the cell when sampled, there are several advantages to exo-metabolomics that are the reason it was used in this study. First, endo-metabolomics requires careful quenching of the sample to freeze metabolic activity at exactly the right time to get snapshots of the cell-state that are comparable between samples. Second, the destructive nature of the sampling means that time-resolved data quickly becomes unfeasible to collect when scaling up the experiment. The comparable simpleness of exo-metabolomic sampling and the fact that multiple time-resolved samples can be collected from the same culture makes it an effective tool for large-scale applications, such as broad screening of metabolism for many strains. Additionally, endo-metabolomics is generally focused on the effect of the environment on the physiology of the organism, but information about the effect of the organism on the environment is highly relevant to the biological context of an infection, where you have a complex environment with competing microbes and antagonistic immune cells.

2.2 Widespread applications of exo-metabolomics

The method has widespread applications and has been used for basic research in the metabolism of bacterial species such as *Escherichia coli, Corynebacterium glutamicum, Bacillus licheniformis* and *Saccharomyces cerevisiae* [167], as well as strain classification [168–170]. It has been used as biosensor e.g. for contamination in micro-algal fermentation [171] and toxins in wastewater [172], as a bioremediation tool for the decontamination of polluted soils [173] and for monitoring flavor-impacting bioprocesses in wine fermentation. [174,175]. Exo-metabolomics

has also been used to study the metabolism of key organisms of interest in the design of cell factories for sustainable bioproduction, e.g. through metabolic pathway discovery in *Aspergillus nidulans* [176] and interrogation of the role of carbon catabolite repression in *Pseudomonas putida* [177,178]. It has also been suggested as a promising approach for identifying quorum sensing molecules in pathogens that can be targeted by drugs in a way that prevents biofilm formation without threatening survival, thus allowing for the development of resistance-resistant antibiotics [179].

2.3 Need for high-throughput method for dynamic exo-metabolomic sampling

Characterizing bacterial metabolic profiles has so far largely been limited to low-throughput methods, making in-depth analysis of large collections of strains across several conditions challenging. To solve this issue, we applied a serial-dilution method similar to those described in previous papers [180,181] studying growth and biofilm formation and investigated whether this method might be suitable for dynamic exo-metabolomic studies as well. For this method to be a reliable tool, it is important to establish whether or not metabolism is conserved among cells of one biological replicate growing in the different wells of a dilution-row during cultivation, such that the metabolomes of dilution-resolved samples at different growth states correspond to the metabolomes of one culture at all of those growth states.

For this reason, the method was benchmarked against a conventional low-throughput time-resolved cultivation approach using laboratory strains of *P. aeruginosa* in Synthetic Cystic Fibrosis Medium (SCFM) – a rich media mimicking the CF airway environment and *Pseudomonas putida* in minimal media similar to that used for this organism in industrial bioproduction. This was done by comparing biological parameters such as metabolic profiles, rate of assimilation and, in the case of *P. aeruginosa* in SCFM, assimilation hierarchy. Both microtiter- and deep well plates were tested to optimize the method with respect to oxygen conditions, culture volumes and dilution factor.

The study reveals an overlap between the bacterial metabolic profiles and assimilation hierarchy, irrespective of the cultivation strategy, suggesting high robustness and flexibility of the high-throughput dilution-resolved method. Deep-well plates provided the best cultivation setup yielding consistent and comparable metabolic profiles across conditions and strains.

Altogether, the results illustrate the usefulness of this technological advance for high-throughput analyses of bacterial metabolism for both biotechnological applications and automation purposes. The following section encloses the paper published on this work in *Microbial Biotechnology*, (2021).

Following the validation of the method, we applied it to all clinical isolates selected for study in the current project for a total of 272 samples analysed, which will be discussed further in Chapter 3.

2.4 "High-throughput dilution-based growth method enables time-resolved exo-metabolomics of *Pseudomonas putida* and *Pseudomonas aeruginosa*", Microbial Biotechnology (2021)

microbial biotechnology

Open Access

High-throughput dilution-based growth method enables time-resolved exo-metabolomics of *Pseudomonas putida* and *Pseudomonas aeruginosa*

Bjarke H. Pedersen,[1] Nicolás Gurdo,[1] Helle Krogh Johansen,[1,2,3] Søren Molin,[1] Pablo I. Nikel[1] and Ruggero La Rosa[1]

[1]*The Novo Nordisk Foundation Center for Biosustainability, Technical University of Denmark, Kgs. Lyngby, 2800, Denmark.*

[2]*Department of Clinical Microbiology, 9301, Rigshospitalet, Copenhagen, 2100, Denmark.*

[3]*Department of Clinical Medicine, Faculty of Health and Medical Sciences, University of Copenhagen, Copenhagen, 2200, Denmark.*

Summary

Understanding metabolism is fundamental to access and harness bacterial physiology. In most bacteria, nutrient utilization is hierarchically optimized according to their energetic potential and their availability in the environment to maximise growth rates. Low-throughput methods have been largely used to characterize bacterial metabolic profiles. However, in-depth analysis of large collections of strains across several conditions is challenging since high-throughput approaches are still limited – especially for non-traditional hosts. Here, we developed a high-throughput dilution-resolved cultivation method for metabolic footprinting of *Pseudomonas putida* and *Pseudomonas aeruginosa*. This method was benchmarked against a conventional low-throughput time-resolved cultivation approach using either a synthetic culture medium (where a single carbon source is present) for *P. putida* or a complex nutrient mixture for *P. aeruginosa*. Dynamic metabolic footprinting, either by sugar quantification or by targeted exo-metabolomic analyses, revealed overlaps between the bacterial metabolic profiles irrespective of the cultivation strategy, suggesting a certain level of robustness and flexibility of the high-throughput dilution-resolved method. Cultivation of *P. putida* in microtiter plates imposed a metabolic constraint, dependent on oxygen availability, which altered the pattern of secreted metabolites at the level of sugar oxidation. Deep-well plates, however, constituted an optimal cultivation set-up yielding consistent and comparable metabolic profiles across conditions and strains. Altogether, the results illustrate the usefulness of this technological advance for high-throughput analyses of bacterial metabolism for both biotechnological applications and automation purposes.

Received 10 May, 2021; revised 5 July, 2021; accepted 18 July, 2021.
For correspondence. E-mail rugros@biosustain.dtu.dk; Tel: (+45) 9351 1647.
Microbial Biotechnology (2021) **0**(0), 1–13
doi:10.1111/1751-7915.13905

Introduction

Bacterial metabolism comprises sets of biochemical reactions that are tightly regulated spatio-temporally. This complex network of reactions interacts dynamically with the external environment. Thus, changes in the surrounding conditions (e.g. nutrient availability) are propagated to the intracellular metabolites' fluxes to optimize cellular physiology (Chubukov *et al.*, 2014). Microbial growth is, indeed, influenced by the availability of the nutritional resources, which is often a matrix of several different components (Sezonov *et al.*, 2007; Molina *et al.*, 2019b).

Due to the tight relationship between exo- and endo-metabolism, variations in exo-metabolites provide important information on the intracellular metabolic status of the cell (Mapelli *et al.*, 2008). Metabolic footprinting analysis allows quantification of metabolite depletion and/or synthesis as function of the cellular growth, which can be further used as constraints for genome-scale metabolic models for the computation of intracellular metabolite distribution and fluxes (Mapelli *et al.*, 2008; O'Brien *et al.*, 2015). For this reason, exo-metabolomic analyses have been extensively used for a variety of both biotechnological applications and for basic research, such as the functional characterization of uncharacterized genes, selection of evolved strains, identification of relevant bacterial mutants, and description of metabolic pathways in several bacterial species (Kaderbhai *et al.*, 2003; Howell *et al.*, 2006; Henriques *et al.*, 2007; Paczia *et al.*, 2012; Deutschbauer *et al.*, 2014).

In Pseudomonads, metabolic footprinting has been primarily used to characterize regulatory processes such

as Carbon Catabolite Repression (CCR), proteome composition changes as function of cellular growth, and to identify links between metabolism and infection (Behrends *et al*., 2009, 2013; La Rosa *et al*., 2016, 2018; Yung *et al*., 2019; Arce-Rodríguez *et al*., 2021; McGill *et al*., 2021). Pseudomonads constitute a large group of bacterial species of high interest, both from biotechnological and clinical points of view (Weimer *et al*., 2020; Rossi *et al*., 2021). *Pseudomonas putida* is a valuable chassis organism due to its broad metabolic capability, high tolerance to harsh conditions (oxidative stress and toxic compounds), fast growth in multiple laboratory conditions, and for the availability of a vast spectrum of genetic tools to manipulate its genome (Nikel *et al*., 2014). *P. aeruginosa* is a ubiquitous human opportunistic pathogen present in different natural environments, and associated with pulmonary infections in cystic fibrosis (CF) patients, burn wounds, urinary tract infections and hospital-acquired infections (Crone *et al*., 2020). In both *P. putida* and *P. aeruginosa*, the utilization of essential metabolites in simple or complex mixtures is a dynamic process orchestrated by several regulators (Behrends *et al*., 2013; Nikel *et al*., 2014, 2015; La Rosa *et al*., 2016, 2019; Molina *et al*., 2019a, 2019b; Dolan *et al*., 2020). Glucose assimilation occurs through oxidization in the periplasm, first to gluconate (GA) and then to 2-ketogluconate (2-KGA), which are subsequently phosphorylated to glucose-6-phosphate (G6P), 6-phosphogluconate (6PG) or 2-keto-6-phosphogluconate (2KG) to enter the cytoplasm (del Castillo *et al*., 2007; Nikel *et al*., 2015, 2021). In rich complex media, the CCR complex Crc/Hfq represses the assimilation of less preferred carbon sources, such as glucose or branched-chain amino acids, favouring the assimilation of other more energetically preferred nutrients, such as glutamine, asparagine, aspartate, alanine and glutamate (Rojo, 2010; La Rosa *et al*., 2016).

Conventionally, to study exo-metabolite dynamics, cell cultures are established in Erlenmeyer flasks and supernatant samples are continuously collected from the same culture. This classical approach is called the 'time-resolved' method (Fig. 1). Importantly, the higher the number of data points to collect, the higher the volume of cell culture needed. This reduces the effect of sampling on the physiology of the cell as a consequence of the shift in the culture volume/conditions over time (Behrends *et al*., 2014). Although the conventional time-resolved method provides detailed analyses of metabolite uptake/secretion profiles, it is clearly a low-throughput method when many samples are needed, and many strains are analysed. High-throughput methodologies such as 'dilution-resolved' synchronized cell culture can, theoretically, be applied to multiple conditions and several strains on 96-well plates, substantially increasing the throughput (Govantes, 2018). This method, first described by van Ditmarsch and colleagues (van Ditmarsch and Xavier, 2011; López-Sánchez *et al*., 2013), takes advantage of the relationship between the lag phase of growth and the cell density, and offers a great potential for many biotechnological applications. In practice, serial dilutions of bacterial cell cultures are established to generate shifts in the growth curves reflecting the differences in the initial biomass concentration. After incubation, all samples are simultaneously harvested, and each end-point sample from the different dilutions is synchronized to reconstruct the time-dependent trajectory of a conventional time-resolved growth curve (Fig. 1). A detailed description of the method and a detailed protocol are available in REF (Govantes, 2018). However, even though this method appears to be very promising, only a limited number of examples are available in literature (van Ditmarsch and Xavier, 2011; López-Sánchez *et al*., 2013, 2016; Jiménez-Fernández *et al*., 2015, 2016; Govantes, 2018). Whether the dilution-resolved method for high-throughput applications secures flexibility in terms of cultivation set-ups which entails reconstruction of the time-dependent trajectory of a conventional time-resolved growth curve, and whether it is sufficiently robust in relation to the degree of physiological and metabolic agreement of cell cultures cultivated in separate wells with increasing dilutions, is still under-described. Moreover, it is also not clear whether reliable quantification of assimilation and secretion profiles of compounds from simple and complex mixtures of carbon sources can be made. Establishing the dilution-resolved method as gold standard platform for high-throughput metabolomic analyses would, therefore, be a step forward in connection with both biotechnological applications and automation purposes.

Here, we applied both time-resolved and dilution-resolved methods for metabolic footprinting analyses of the model species *P. putida* KT2440 and *P. aeruginosa* PAO1. Since most biotechnological applications rely on inexpensive and simple carbon sources, we analysed *P. putida* KT2440 when growing in the presence of glucose as an archetypal sugar substrate. In contrast, *P. aeruginosa* PAO1 was analysed when growing in the defined rich Synthetic Cystic Fibrosis Medium (SCFM) that reproduces the CF lung milieu, thereby, representing the nutrient composition relevant for an infection. Comparative analyses demonstrated that the dilution-resolved method produces metabolic footprinting data from both simple and complex media, similar to those produced by the conventional time-resolved method. Moreover, this approach provides flexibility as it can fulfil diverse experimental needs by merely changing the cultivation set-up, therefore, supporting its use for high-throughput

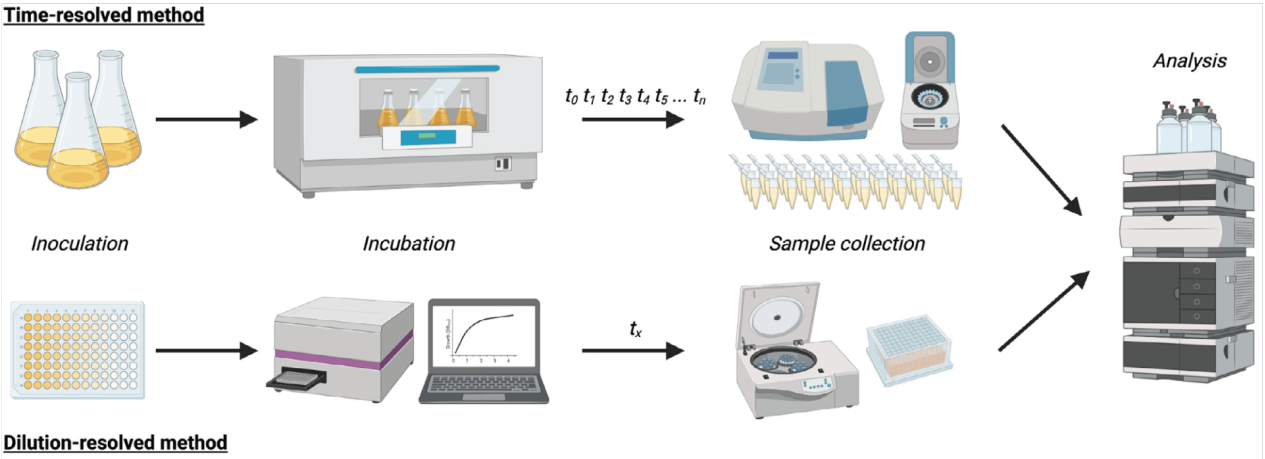

Fig. 1. Schematic representation of the time-resolved and dilution-resolved workflow for exo-metabolomic analyses. For the time-resolved method, bacteria are cultivated in Erlenmeyer flasks and incubated in a flask shaker incubator. Samples are collected over time (t_1 t_2 t_3 t_4 t_5 ... t_n) for OD measurement to follow bacterial growth and supernatants are collected by centrifugation. For the dilution-resolved method, bacteria are inoculated in 96-well plates in serial dilutions and incubated in a microtiter plate reader to follow the growth in real time. At the time of sampling (t_x), all supernatant samples are harvested simultaneously by centrifugation.

screening of large collections of strains and/or growth conditions.

Results and discussion

Sampling by time-resolved and dilution-resolved methods provide comparable sample distributions

Dilution-resolved growth curves in 96-well deep-well plates and microtiter plates were compared with conventional time-resolved growth curves from continuous sampling over time from Erlenmeyer flasks to compare the distribution of the collected samples. *P. putida* KT2440 was cultivated in de Bont minimal medium (Hartmans *et al.*, 1989) with glucose as sole carbon source and *P. aeruginosa* PAO1 in the defined rich SCFM medium containing amino acids, glucose and lactate as carbon and nitrogen sources (Palmer *et al.*, 2007). *P. putida* was cultivated in Erlenmeyer flasks, 96-well deep-well and microtiter plates, while *P. aeruginosa* was only cultivated in Erlenmeyer flasks and 96-well deep-well plates. Many clinical isolates of *P. aeruginosa* create free-floating bacterial aggregates in microtiter plates which interfere with the optical density (OD) acquisition and, therefore, producing unreliable measurements. Moreover, while production strains are routinely screened in microtiter plates, few large-scale screenings have been performed with clinical isolates in microtiter plates (Wewetzer *et al.*, 2015; Kragh *et al.*, 2018; Bartell *et al.*, 2019). For these reasons, we excluded microtiter plates for *P. aeruginosa* analyses and focussed only on deep-well plates and flasks. Dilution-resolved plates were prepared by serial dilutions of overnight cultures of *P. putida* in fresh de Bont minimal medium and of *P. aeruginosa* in fresh SCFM. To adequately cover the growth phases of interest, the dilution factor, the number of dilutions, the inoculum density and the incubation time must be chosen appropriately. The dilution factor, together with the number of dilutions, controls the growth time-shift between the cultures, while the incubation time, together with the inoculum density, controls the range of ODs at which the cultures are sampled. Changing either the dilution factor or the inoculum density makes it possible to carry out the cultivations by the incubation time which best suits the specific needs. To describe two very different approaches and assess the adaptability of the method, we selected a low inoculum density and a long incubation time for *P. putida* and a high inoculum density and a short incubation time for *P. aeruginosa*. It should be noted that while quantification of sugars by HPLC is inexpensive and widely accessible, amino acid quantification is still more costly and requires an *ad hoc* set-up due to the complexity of the amino acid chemistry. For this reason, for *P. putida* we prioritized a high resolution of the growth curve, whereas for *P. aeruginosa*, we reduced the number of dilutions to a minimum, which could provide full coverage of the growth curve.

For *P. putida*, a low inoculum density with OD_{600} values (OD at 600 nm) between 5.0×10^{-2} and 9.5×10^{-8} and an array of 20 serial dilutions was used (Fig. 2A). For *P. aeruginosa*, a high inoculum density with OD_{600} between 2.0×10^{-1} and 3.9×10^{-4} and an array of 8 serial dilutions was used (Fig. 2B). A dilution factor of 1:2 was applied for both strains (see Experimental Procedures for a full description of the method). To produce time-shifted cultures mirroring 12 and 9.5 h of bacterial growth in conventional Erlenmeyer flasks, an

incubation time of 22 h for *P. putida* and 5.5–6.5 h for *P. aeruginosa* was required (Fig. 2). Independently of the specific set-up and strain, the distribution of the OD values of the samples collected using the dilution-resolved method showed coverage of ODs similar to the conventional time-resolved growth curves (*Z*-score range = 0.08–0.23) (Fig. 2).

These results suggest that the samples collected using the high-throughput dilution-resolved method can capture the same growth states as in the time-resolved method. Moreover, they confirm the relationship between lag phase and cell density at any given time for the strains and laboratory conditions used in this study, indicating robustness and simultaneous flexibility of the dilution-resolved method in the presented experimental set-up and with the specific analysed strains. Importantly, the relationships between inoculum density, dilution factor and incubation time should be specifically explored for each combination of media condition, numbers of samples required, and specific bacterial strains in order to identify the optimum conditions.

The dilution-resolved method captures the different phases of initial glucose processing in P. putida

For applications of the dilution-resolved method, it is important that the relationship between the metabolomes of the different cultures growing in different wells, progressively diluted, is analogous to the relationship between the metabolomes of a single culture sampled continuously over time. The metabolite concentration in supernatant samples from both time-resolved and dilution-resolved methods should, therefore, change similarly maintaining a linear relationship between the samples. To test this possibility, supernatant samples collected from *P. putida* cultures, established using the dilution-resolved method, were analysed by HPLC to quantify glucose metabolism intermediates, and compared to samples collected using the time-resolved methods (Fig. 2A). Regardless of the method used and the cultivation set-up (flask, deep-well or microtiter plates), the relationship between the samples, that is the relationship between the metabolites abundance and the OD, was maintained, making it possible to determine profiles of assimilation and secretion for glucose, GA and 2-KGA (Fig. 3A and Table S1). In all cases, glucose was assimilated during the entire cultivation while GA and 2-KGA were initially secreted and catabolized by the cells at later stages during late exponential and stationary phase. Interestingly, the cultivation set-up imposed a specific metabolic constraint, resulting in slightly different assimilation and secretion profiles. While the maximal concentration of GA was comparable between the cultivation setups (~3.2 mM), the growth phase at which it was secreted varied between flask and deep-well plate (exponential phase) and microtiter plate (stationary phase) (Fig. 3A). 2-KGA was detected only in flask cultures and deep-well plates, although secretion occurred

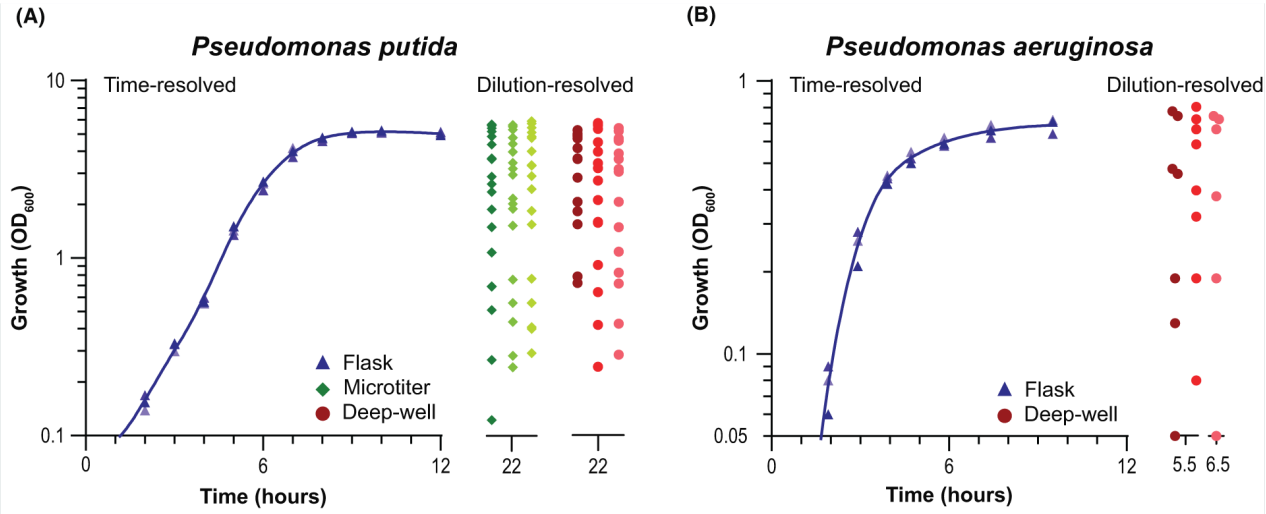

Fig. 2. Time-resolved and dilution-resolved growth curves of *Pseudomonas putida* and *Pseudomonas aeruginosa*.
A. Growth curve and distribution of samples of *P. putida* cultivated in de Bont minimal medium in the presence of glucose in Erlenmeyer flasks (blue symbols and lines), deep-well plates (red symbols) and microtiter plates (green symbols).
B. Growth curve and distribution of samples *P. aeruginosa* cultivated in SCFM in Erlenmeyer flasks (blue symbols and lines) and deep-well (red symbols) plates. Each symbol represents a sample collected during the growth using the time-resolved method (blue symbols) or at incubation time using the dilution-resolved method (red and green symbols). Shades of colour represent three independent biological replicates. For comparison, the distribution of the samples collected using the dilution-resolved method is shown at the side of each graph. Time-resolved growth curves were inferred by fitting a spline/LOWESS curve to the OD_{600} (OD at 600 nm) and time data.

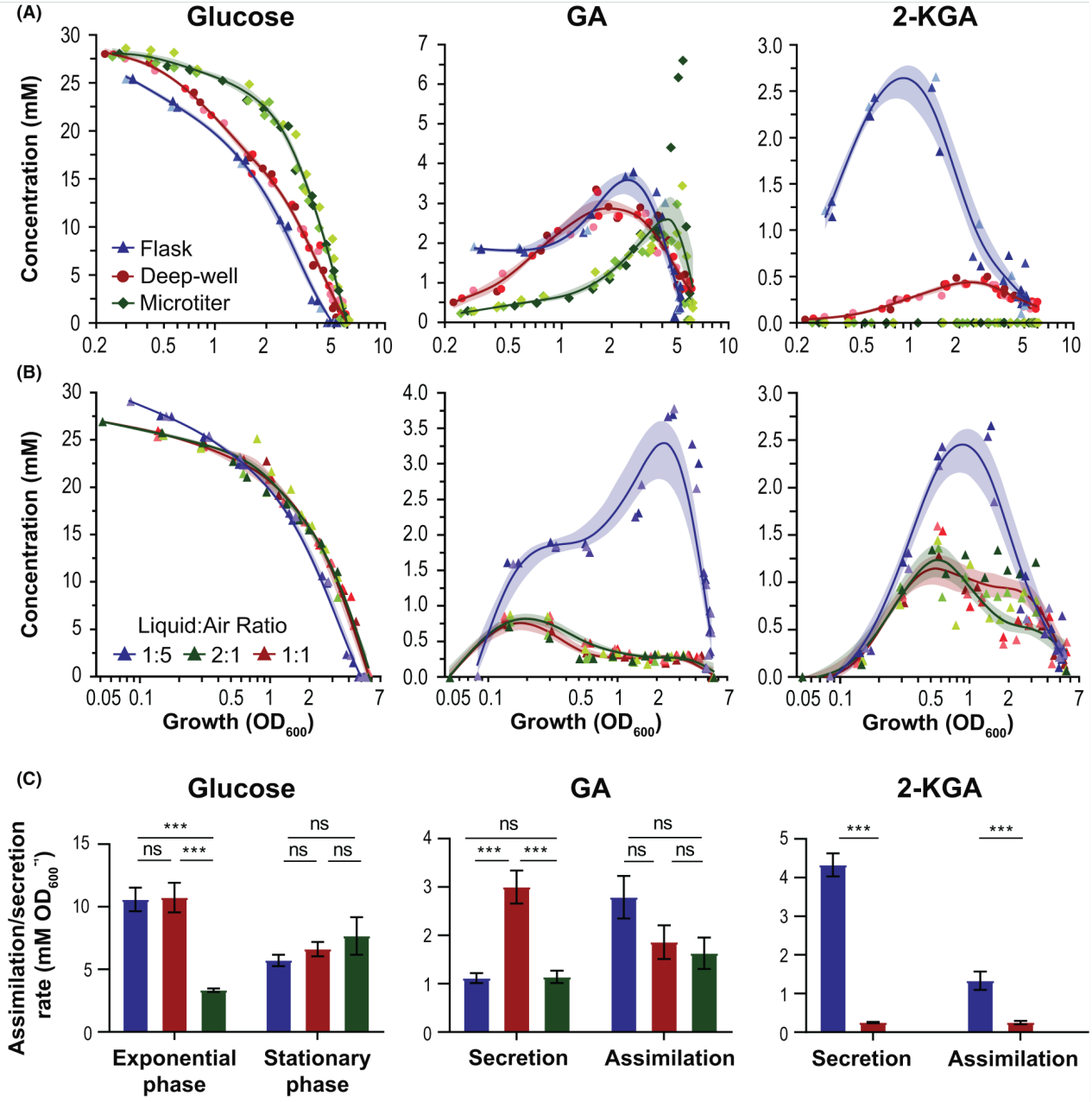

Fig. 3. Dynamics of sugar uptake and its conversion into oxidized products in *P. putida*.
A. The concentration of glucose, gluconate (GA) and 2-ketogluconate (2-KGA) in Erlenmeyer flasks (blue symbols and lines), deep-well plates (red symbols and lines) and microtiter plates (green symbols and lines) is shown relative to the OD_{600} (OD at 600 nm) at which supernatant samples were collected. The time-resolved method was used for cultivation of *P. putida* in Erlenmeyer flasks while the dilution-resolved method for deep-well and microtiter plates in de Bont minimal medium in the presence of 27.7 mM of glucose as sole carbon source. Shades of colour represent three independent biological replicates while shaded areas indicate the 95% confidence intervals of the curves (cubic spline fitting).
B. Concentration of glucose, gluconate and 2-ketogluconate in Erlenmeyer flasks in de Bont minimal medium in the presence of 27.7 mM of glucose as sole carbon source at ratios of culture media to air volume of 1:5 (blue symbols and lines), 1:1 (red symbols and lines) and 2:1 (green symbols and lines) relative to the OD at which supernatant samples were collected. Shades of colour represent three independent biological replicates while shaded areas indicate the 95% confidence intervals of the curves (cubic spline fitting).
C. Maximal assimilation and secretion rate for glucose, gluconate and 2-ketogluconate in Erlenmeyer flasks (blue bars), deep-well plates (red bars) and microtiter plates (green bars). Parameters were calculated by linear regression from the six samples that produced the highest rate. For glucose, assimilation rate was calculated during both exponential and stationary phase. The error bar indicates the SEM (Standard Error of the Mean). Differences between rates were evaluated by Unpaired Welch *t*-test with significance indicated as 'ns' where $P > 0.05$, and '***' where $P < 0.001$.

at later time points and at lower concentration (fivefold reduction; Fig. 3A). No 2-KGA was identified in microtiter plate cultures. We hypothesize that limited oxygen availability in multi-well plates, mostly due to the different ratios between medium and air volume (1:5 for flasks, 1:1 for deep-well plates, and 2:1 for microtiter plates) and the different oxygen-transfer rate (OTR) between setups, led to reduced 2-KGA formation (Duetz and Witholt, 2004; Wewetzer *et al*., 2015). Oxygen is an important factor for glucose assimilation, and if limited may cause rearrangement of the metabolite fluxes within the glucose catabolic pathway (Davis *et al*., 2015). To substantiate this hypothesis, we quantified the glucose, GA and 2-KGA assimilation and secretion profiles in flasks using a ratio of medium versus air of 1:1 and 2:1 and compared it with the 1:5 set-up (Fig. 3B). Glucose assimilation pattern overlapped between conditions, while GA showed a threefold reduction relative to the 1:5 set-up and it was secreted only during early exponential phase in both 1:1 and 2:1 flasks (Fig. 3B). Moreover, while in microtiter plates no 2-KGA was identified, in the corresponding 2:1 flask set-up, 2-KGA was still secreted albeit at lower concentration (twofold reduction) (Fig. 3B). This indicates that in our experimental set-up, oxygen availability is still higher in flasks relative to deep wells and microtiter plates due to the different OTR which ultimately depends on the shape and size of the vessel, on the orbital diameter and on the rate of shaking (Duetz and Witholt, 2004; Wewetzer *et al*., 2015).

Maximal rates of glucose consumption and secretion of GA and 2-KGA, computed at the six OD points that produced the highest rates, deviated between the methods as a consequence of the different cultivation setups (Fig. 3C and Table S1). While the specific glucose consumption rate was similar in flasks and deep-well plates, it was threefold lower in microtiter plates during exponential phase (Unpaired Welch *t*-test) (Fig. 3C). For GA, there was no significant difference between the assimilation rates using the different methods, but its secretion rate was 2.7-fold higher in deep-well plates (Unpaired Welch *t*-test) (Fig. 3C). For 2-KGA, both assimilation and secretion rates differed significantly between the methods (Unpaired Welch *t*-test) as also shown by the secretion plot (Fig. 3A).

Regardless of the underlying regulatory mechanism, it is worth noting that the cultivation set-up should be taken into account while planning high-throughput experiments using the dilution-resolved method. Indeed, OTR should be specifically analysed to match the desired oxygen availability for the specific cultivation (Duetz, 2007). Parameters such as cultivation volume, shape of the vessel, orbital diameter and rate of orbital shaking can be specifically selected to perfectly match the desired final cultivation set-up. Nonetheless, these results confirm the reliability of the method for analyses of targeted metabolites assimilated or secreted during bacterial cultivations in the presence of a single carbon source.

P. aeruginosa's *complex metabolic behaviour in SCFM is maintained irrespective of the cultivation method*

To further test whether the dilution-resolved method can be applied to assess complex metabolic patterns from a rich defined complex medium such as SCFM, the supernatant samples collected from *P. aeruginosa* cultivations using both the dilution-resolved and time-resolved methods (Fig. 2B), were analysed by targeted exometabolomics and compared with respect to changes in metabolite composition over time and dilution.

Performing a Principal Component Analysis (PCA), which explains 89% of the variance on PC1, shows how the exo-metabolomes overlap between the two sampling methods and follow the same trajectory as a function of growth and metabolite assimilation (Fig. 4A). Similarly, a hierarchical clustering analysis (HCA) of the variance of each specific metabolite, summarizing the reduction in concentration across all samples of a given experiment, shows a mixed clustering of the experiments regardless of the sampling method (Fig. 4B). Compounds such as aspartic acid, glutamic acid, proline, alanine, arginine and serine show the highest variance being assimilated during the early stages of growth. The remaining compounds, in contrast, show low variance since they were not assimilated in the analysed growth window (Fig. 4B and Fig. S1). It should be pointed out that for *P. aeruginosa*, samples were collected mainly during exponential and early stationary growth phase to maximize the resolution of the most preferred carbon sources. Therefore, to cover the assimilation profiles of the remaining compounds, a higher number of dilutions or a higher dilution factor should be selected. Similar to what was shown for *P. putida*, assimilation curves overlapped using the two methods, both for the fully (aspartic acid), partially (proline) and not (tyrosine) assimilated compounds without showing significant differences based on the cultivation method (Fig. 4C, Fig. S1 and Table S1).

To further investigate whether the hierarchy and rates of assimilation were similar between methods, we fitted mechanistic growth models and linear regression models to the data of the seven metabolites, which were either completely or partially assimilated during the exponential growth phase (Fig. 4D and E and Table S1). The mechanistic growth model allows quantifying important parameters such as the metabolite half-life (OD_{50} value), which represents the OD at which 50% of a compound has been assimilated. When metabolites are ordered by their OD_{50} value, the hierarchy of assimilation can be defined

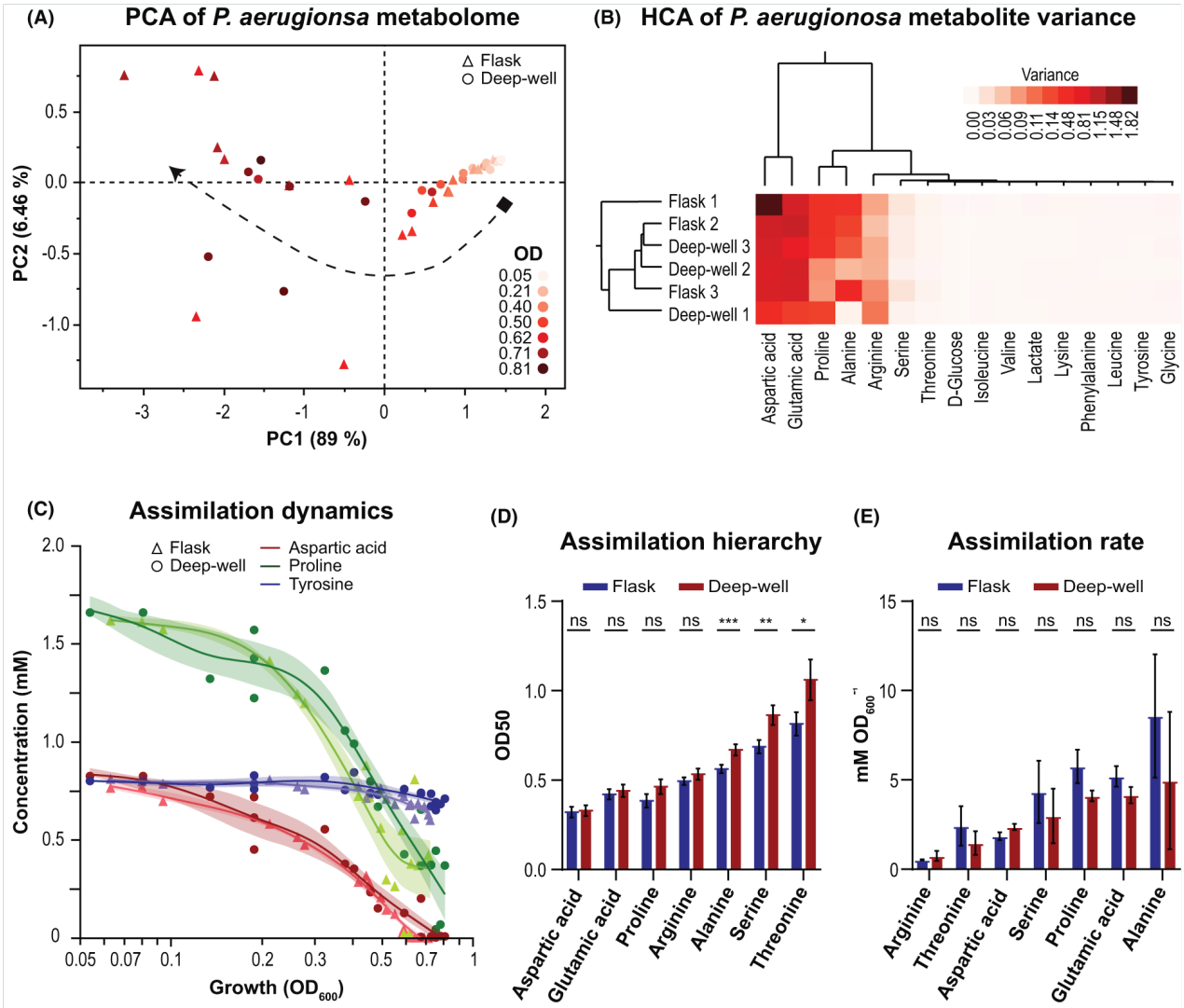

Fig. 4. Metabolism dynamics of *Pseudomonas aeruginosa* cultivated in SCFM rich medium.
A. Principal Component Analysis (PCA) of the exo-metabolomes of *P. aeruginosa* collected using the time-resolved (triangles) and dilution-resolved methods (circles). Dots represent the metabolome of each supernatant sample at a given OD. The OD is represented by a colour gradient and the black dashed arrow indicates the trajectory of the metabolome during growth.
B. Two-way hierarchical cluster analysis (HCA) of the quantified metabolites grouped by cultivation methods and metabolite dynamics. The heat map shows the variance of the concentration of each compound which is a proxy of the shift in metabolite concentration within the samples of a specific method. Compounds with higher variance are assimilated earlier than those with lower variance. Compounds not assimilated show null variance.
C. Assimilation of aspartate (red lines and symbols), proline (green lines and symbols) and tyrosine (blue lines and symbols) during cultivation using either the time-resolved (triangles) or the dilution-resolved (circles) method in Erlenmeyer flasks and deep-well plates respectively. The plot shows examples of metabolites completely assimilated (aspartate), partially assimilated (proline) and not assimilated (tyrosine) by *P. aeruginosa* when growing in SCFM respectively. Shaded areas indicate the 95% confidence intervals of the curves (cubic spline fitting).
D and E. Assimilation parameters of the compound uptaken during exponential growth. The maximal assimilation rate was calculated by fitting a linear regression model to the five data points which showed the highest reduction in concentration. The hierarchy of assimilation was defined by ordering the assimilated metabolites by their half-life (OD_{50}), which represents the OD at which the concentration of each compound halved. The OD_{50} were calculated by fitting a mechanistic growth model to the metabolite's concentration relative to the OD. The error bar indicates the SEM (Standard Error of the Mean). Differences between rates were evaluated by Unpaired Welch *t*-test with significance indicated as 'ns' where $P > 0.05$, '*' where $P < 0.05$, '**' where $P < 0.01$ and '***' where $P < 0.001$.

based on the cellular metabolic preference (Behrends *et al.*, 2014). When comparing the OD_{50} values between methods, no statistical differences (Unpaired Welch *t*-test) were shown for the four most preferred carbon sources. Although the latter three showed some small differences between methods, the hierarchy is clearly preserved, supporting the constancy of the hierarchy of assimilation in SCFM (Fig. 4D and Table S1). Similarly, the assimilation

rates were comparable between methods confirming the reliability of the dilution-resolved method for the characterization of complex metabolic behaviours (Fig. 4E and Table S1). Interestingly, even using only the data of two biological replicates, the hierarchy and the rates of assimilation were comparable, irrespective of the method, confirming the robustness and the potential of the dilution-resolved method (Fig. S2 and Table S1).

Opposite to what was shown for *P. putida*, no considerable difference in assimilation profiles was observed when using the two cultivation methods (flask versus deep-well). The OD_{50} assimilation hierarchy of PAO1 has been previously described in LB medium (La Rosa *et al*., 2018). Arginine was not identified in that study, but the order of assimilation for the remaining six preferred metabolites is identical between studies, indicating a common metabolic preference of *P. aeruginosa* PAO1, independent of the growth medium.

Altogether, these results show that metabolism is conserved in individual wells in the high-throughput dilution-resolved method, reflecting changes in the metabolome composition during growth, as accurately as in the time-resolved method. Moreover, it suggests that complex patterns of metabolic behaviour are maintained independent of the cultivation set-up and/or sampling method.

Discussion

Metabolic characterization of bacterial strains is usually carried out in a low-throughput manner, which is time and resource consuming. Only a limited number of high-throughput methods are available (Zampieri *et al*., 2017), mostly devoted to strain characterization towards biotechnological applications. Here, we have shown that a dilution-resolved method for dynamic sugars quantification and targeted exo-metabolomic analysis is both robust and flexible. Indeed, independently of the specific species and cultivation set-up, the relationship between the metabolic and physiological status of cell cultures progressively diluted cultivated accordingly to the dilution-resolved method is maintained. Parameters such as cultivation set-up, dilution factor, number of dilutions, inoculation density and incubation time can be tuned to the specific metabolic dynamics of the cells or to specific needs of the operator, providing flexibility and optimal solutions for customization. This method can easily become integrated in automated workflows using liquid-handling robots with applications that include biotechnology platform strains such as *P. putida* but also clinically relevant isolates as *P. aeruginosa*. The method can be used for both high-resolution investigations by increasing the number of dilutions per strain/condition, and for large-scale high-throughput investigations by increasing the dilution factor and reducing the number of dilutions per strain/condition. Moreover, by modifying either the dilution factor or the inoculum density, the cultivation can be carried out using both short and long incubation times which allows even more flexibility. While scalability using the time-resolved method depends on the availability of the laboratory resources (flasks, incubators, etc.), the dilution-resolved method can be easily scaled up to 96 samples using multi-well plates and a single laboratory set-up. Since the set-up of bacterial cultivation has an impact on the exo-metabolite dynamics as a consequence of the different cellular physiology, it should be considered when planning high-throughput experiments using the dilution-resolved method. OTR, indeed, varies between cultivation vessels and setups and it should, therefore, be specifically selected in relationship to the oxygen requirement for the cultivation. Matching the metabolic profiles of bacteria growing in microtiter plates in simple carbon sources to the flask condition, therefore, requires further optimization. Scalability of microtiter plates to larger fermenters indeed poses several challenges which have been previously investigated (Duetz, 2007). However, overall in our experiments with Pseudomonads, deep-well plates provided the best cultivation conditions which are comparable to Erlenmeyer flasks and which permit analysis of large numbers of strains and/or culture conditions in a high-throughput manner. Further validation and optimization are required for other industrially or biologically relevant species. Although the dilution-resolved method in the present study was only applied for high-throughput sampling for dynamic sugar quantification and for targeted exo-metabolomic analyses, it can also be optimized for endo-metabolomic analysis and for transcriptomic, fluxomic or proteomic analyses with relatively few adjustments. Whether the dilution-resolved data are in agreement with the time-resolved data, however, merits further investigations. Still, the method has been successfully used for quantification of rhamnolipids in *P. aeruginosa* and production of biofilm in *P. putida* (van Ditmarsch and Xavier, 2011; López-Sánchez *et al*., 2013). Importantly, the relationship between the diluted cell cultures is linear between different wells, indicating that the metabolic processes, controlled by several global and local regulators, are maintained independent of the initial inoculum. In conclusion, the dilution-resolved method can be combined with exo-metabolomics as a powerful tool for high-resolution and/or high-throughput metabolic footprinting investigations of bacteria with complex metabolic dynamics.

Experimental procedures

Bacterial strains and media composition

Pseudomonas putida KT2440 was cultivated in de Bont minimal medium (containing, per litre of final medium,

1.55 g K_2HPO_4, 0.85 g NaH_2PO_4, 2.0 g $(NH_4)_2SO_4$, 0.1 g $MgCl_2$, 10 mg EDTA, 2 mg $ZnSO_4$, 1 mg $CaCl_2$, 5 mg $FeSO_4$, 0.2 mg Na_2MoO_4, 0.2 mg $CuSO_4$, 0.4 mg $CoCl_2$, and 1 mg $MnCl_2$) containing 5 g/L (27.7 mM) of glucose as sole carbon source. de Bont minimal medium was prepared according to (Hartmans *et al*., 1989) and a single medium batch was used for all the experiments to avoid any differences that could arise from medium composition. *Pseudomonas aeruginosa* PAO1 was cultivated in the defined rich medium Synthetic Cystic Fibrosis Medium (SCFM), designed to mimic the conditions of the airways in patients with cystic fibrosis and containing amino acids, glucose and lactate as carbon sources (Turner *et al*., 2015). We excluded DNA and mucins to reduce viscosity and allow HPLC analysis of the samples (Deschamps *et al*., 2021). Two different batches of SCFM were used for the cultivation experiments in deep-well plates and Erlenmeyer flasks, respectively, and some variation in the concentration of specific metabolites was determined by HPLC analysis. These differences are listed in Table S1. *P. putida* was cultivated in baffled Erlenmeyer flasks, 96-well deep plates (Cat. No. 0030502302; Eppendorf, Hamburg, Germany) and 96-well clear bottom microtiter plates (Cat. No. 650001; Greiner Bio-One, Kremsmünster, Austria) while *P. aeruginosa* in baffled Erlenmeyer flasks and 96-well deep plates. In all cases, both precultures and cultures were incubated in the same culture medium to avoid changes in media composition and extended lag phase. *P. putida* precultures were carried out overnight in 50-ml Falcon tubes containing 10 ml of de Bont medium containing 5 g/L (27.7 mM) of glucose as sole carbon source at 250 rpm at 30°C. *P. aeruginosa* precultures were carried out overnight in 15-ml Falcon tubes containing 6 ml of SCFM at 250 rpm and at 37°C. For both species, a shaker incubator with an orbit diameter of 2.5 cm (1 in) was used.

Time-resolved cultivation method

For the time-resolved method, bacteria were cultivated in Erlenmeyer flasks in three independent biological replicates. Precultures of *P. putida* were grown for 18 h, centrifuged at 10 000*g* for 5 min, washed twice in 1-ml de Bont medium without glucose and used to inoculate at OD_{600} of 0.05, 250-ml Erlenmeyer flasks containing 50 ml (1:5 media to air volume ratio), 125 ml (1:1 media to air volume ratio) or 166.7 ml (2:1 media to air volume ratio) of glucose de Bont medium. During cultivation at 30°C and 200 rpm, 0.5 ml of bacterial culture was harvested after 2, 3, 4, 5, 6, 7, 8, 9, 10 and 12 h, the OD_{600} recorded, and the supernatant collected by centrifugation at 21 000*g* for 5 min at 4°C. Samples were stored at −20°C until further analysis. Precultures of *P. aeruginosa* were grown overnight and directly used, without washing, to inoculate at 0.05 of OD_{600}, 100-ml Erlenmeyer flasks containing 50 ml of SCFM. During cultivation at 37°C and 250 rpm, 1 ml of bacterial culture was harvested after 2, 3, 4, 4.75, 5.75, 7.5 and 9.5 h of incubation, the OD_{600} recorded, and the supernatant collected by centrifugation at 21 000*g* for 7 min at 4°C. Samples were stored at −80°C until further analysis. For both species, a shaker incubator with an orbit diameter of 2.5 cm (1 in) was used.

Dilution-resolved cultivation method

For *P. putida*, three independent overnight cultures were washed as for the time-resolved method and inoculated at OD_{600} of 0.05 in a 96-well deep plate containing 1 ml of de Bont medium in rows B, C and D of column 2 and diluted sequentially 1:2 until column 11, and again from rows E, F and G of columns 2 till column 11. This way an array of 20 dilutions was established for each biological replicate. Columns 1 and 12 were used as contamination control and contained de Bont medium with glucose. 96-well microtiter plates were set up similarly to the deep-well plates with few differences. The volume of cultivation was set to 200 μl and since growth was performed without the plate lid to avoid condensation, the remaining external wells were filled with 280 μl of water to reduce evaporation which in all cases was on average 9.7 ± 3.7%. For *P. aeruginosa*, a different approach was used. Three independent overnight cultures were used directly without washing to prepare two master culture dilutions at the OD_{600} of 0.25 and 0.00625 and used to inoculate wells from columns 1 to 6 and 7 to 11 respectively. In this way, specific volumes of each master dilution (960, 480, 240, 120, 60 and 30 μl from dilution 1 and 600, 300, 150, 75 and 38 μl from dilution 2 respectively) were used to inoculate each well of a deep-well plate, after which the corresponding volume of SCFM was added to reach a final volume of 1.2 ml. On average, the amount of carry-over of preculture medium was 1.7% ± 3.4%. However, no amino acids, sugars or organic acids were identified in the overnight precultures. Column 1 was inoculated at an initial OD_{600} of 0.2 and the following columns corresponded to 1:2 dilutions. Column 12 was used as contamination control and contained pure SCFM. In both cases, deep-well plates were incubated at 30°C (*P. putida*) or 37°C (*P. aeruginosa*) in an orbital shaker with an orbital diameter of 2.5 cm (1 in) at 250 rpm. After 22 h (*P. putida*) and 5.5-6.5 h (*P. aeruginosa*), when the wells of the second-lowest dilution showed signs of growth, 40 μl of cell suspensions were transferred to a new 96-well microtiter plate to measure the OD_{600} in a Synergy™ MX microtiter plate reader (BioTek Instruments Inc., Winooski, VT, USA).

The remaining volume was centrifuged at 1740*g* at 4°C for 30 min to separate the biomass from the supernatant (250 μl) which was stored at −20°C (*P. putida*) or −80°C (*P. aeruginosa*) until further analysis. 96-well microtiter plates for *P. putida* cultivation were incubated at 30°C in a BioTek® ELx808 Absorbance Microtiter Reader (BioTek Instruments Inc., Winooski, VT, USA) where the shake movement is a repeated 0.021 inch (0.05334 cm) movement from the shake position and back. The shaking mode was set to 'medium' mode which corresponds to 18 Hz or approximately 1080 rpm. The bacterial growth was followed by measuring the OD_{630} every 15 min. After 22 h of growth, 150 μl of each well was transferred to a 96-filter plate ($MultiScreen_{HTS}$, HV Filter Plate 0.45 μm, hydrophilic, clear, non-sterile, Millipore, Catalogue number MSHVN45) to filter out the bacteria and collect the supernatants. Plates were centrifuged at 1000*g* for 3 min and the supernatants stored at −20°C until further analysis. For each experiment, 16 to 20 samples/time points for *P. putida* and 6 to 8 samples/time points for *P. aeruginosa* were selected for HPLC analysis based on the following criteria: (i) the OD reflected the dilution relative to the other samples; and (ii) the total samples provided the highest variance of ODs.

High-performance liquid chromatography for sugars quantification and targeted exo-metabolomic analysis

For sugars analyses and targeted exo-metabolomic analyses, frozen samples were thawed at 4°C and further processed for high-performance liquid chromatography (HPLC). Glucose, gluconate and 2-ketogluconate concentration, for the *P. putida* experiments, were quantified on a Dionex Ultimate 3000 system (Thermo Scientific, Waltham, USA) with a HPx87H ion exclusion column (125-0140, Aminex, Dublin, Ireland), equipped with a guard column (125-0129, Bio-Rad, Hercules, California, USA) and guard column holder (125-0131, Bio-Rad, Hercules, California, USA) and eluted with 5 mM H_2SO_4 at an isocratic flow of 0.6 ml min^{-1} at 30°C for 30 min. Glucose and 2-ketogluconate were analysed by RI detection using a Smartline RI detector 2300 (KNAUER Wissenschaftliche Geräte, Berlin, Germany), whereas gluconate was analysed by UV detection at a wavelength of 210 nm using a System Gold 166 UV detector (Beckman Coulter, Brea, USA). Metabolites for the *P. aeruginosa* experiments were quantified using two separate HPLC methods. Organic acids and sugars (glucose, gluconate, succinate, lactate, formate, acetate and pyruvate) were analysed by the same methodology and instrument as for *P. putida*, but at 45°C instead of 30°C. Pyruvate was analysed by UV detection while all other organic acids and sugars were analysed by RI detection.

For amino acids quantification (aspartic acid, glutamic acid, cysteine, asparagine, serine, glutamine, histidine, glycine, threonine, arginine, alanine, tyrosine, valine, methionine, tryptophan, phenylalanine, isoleucine, leucine, lysine and proline), 20 μl of supernatant sample was diluted 1:10 in Ultrapure MilliQ water and mixed with 100 μl of internal standard (20 μg/ml 2-aminobutyric acid and sarcosine). Derivatization was performed directly in the HPLC-instrument prior to injection by automatic mixing with the following eluents: (i) 0.5% (v/v) 3-mercaptopropionic acid in borate buffer 0.4 M at pH 10.2; (ii) 120 mM iodoacetic acid in 140 mM NaOH; (iii) OPA reagent (10 mg/mL *o*-phthalaldehyde and 3-mercaptopropionic acid in 0.4 M borate buffer); (iv) FMOC reagent (2.5 mg/ml 9-fluorenylmethyl chloroformate in acetonitrile); and (v) buffer A (40 mM Na_2HPO_4, 0.02% (w/v) NaN_3 at pH 7). After derivatization, samples were separated isocratically on a Dionex UltiMate 3000 HPLC with fluorescence detector (Thermo Scientific, Waltham, USA) through a Gemini C18 column (00F-4439-E0, Phenomenex, Værløse, Denmark) equipped with a SecurityGuard Gemini C18 guard column (AJ0-7597, Phenomenex, Værløse, Denmark) with a flowrate of 1 ml/min at 37°C using a 5 mM sulfuric acid mobile phase. Metabolites were detected using an UltiMate™ 3000 Fluorescence variable wavelength UV detector (FLD-3400RS, Waltham, Massachusetts, USA). Standard curves for each metabolite were used for absolute quantification. All chromatograms were analysed using the software Chromeleon v7.2.9.

Data analysis

Compounds which signal was undetectable (pyruvate, gluconate, formate, succinate and acetate), near the detection limit in all samples (asparagine and glutamine), if a reliable calibration was not possible due to instability of the metabolite (cysteine) or if signal appeared in blanks (tryptophan and methionine) were excluded from the analysis. Missing values were replaced with 20% of lowest detected concentration (mM). Since different batches of SCFM were used for cultivation in flasks and deep-well plates with slight variations in the specific metabolites concentration, they were normalized to percentage and then recalculated setting as 100% of the metabolite concentration of the SCFM standard formulation (see Table S1). For principal component analysis (PCA) and hierarchical clustering analysis (HCA), the metabolite concentration was normalized by $\log_{10}$ transformation. PCA was calculated on the covariance of each metabolome (sample/time point). HCA was calculated using Ward's method on the variance of the concentration of each metabolite, which shows how much the concentration of each metabolite varies across

samples. To calculate the metabolites OD_{50}, which represent the OD at which 50% of the metabolite has been assimilated (metabolite half-life), the concentrations were plotted against the $\log_{10}$(OD) and several sigmoidal models (Gompertz 3P and 4P, Logistic 4P, 4P Hill and 5P, Probit 4P and Mechanistic Growth) and exponential models were fit to the assimilation profiles. The mechanistic growth model (Equation: $a(1-b\text{Exp}(-cx))$ where a = asymptote, b = scale and c = rate) was selected because it provided the best fit across AICc, AICc Weight, BIC, SSE, MSE, RMSE and R^2 parameters, as well as producing the lowest standard error for OD_{50} across metabolites. The hierarchy of assimilation for *P. aeruginosa* was identified by ordering the assimilated compounds by their OD_{50}. The assimilation rate was calculated from a minimum of five points by linear regression, and it was limited to samples in the OD range that produced the highest rate. Statistical significance between OD_{50} values and assimilation rates was determined by Unpaired Welch *t*-test. Data analyses were carried out using the software JMP® version 15, except for Welch *t*-test, which was computed in GraphPad Prism 9.0. Time-resolved growth curves were inferred by fitting a spline/LOWESS curve with 9 knots for *P. putida* and 8 knots for *P. aeruginosa* to the OD and time data using GraphPad Prism 9.0. Bar charts were created in GraphPad Prism 9.0 and the schematic in Fig. 1 was drawn in Biorender (https://biorender.com/). Assimilation plots, PCA and HCA were created in JMP® version 15. All figures were finalized in Adobe Illustrator.

Acknowledgements

This research was funded by the Cystic Fibrosis Foundation (CFF), grant number MOLIN18G0, the Cystic Fibrosis Trust, Strategic Research Centre Award – 2019 – SRC 017, and the Novo Nordisk Foundation Center for Biosustainability, grant number NNF10CC1016517. H.K.J. was supported by The Novo Nordisk Foundation as a clinical research stipend (NNF12OC1015920), by Rigshospitalets Rammebevilling 2015–17 (R88-A3537), by Lundbeckfonden (R167-2013-15229), by Novo Nordisk Foundation (NNF15OC0017444), by RegionH Rammebevilling (R144-A5287), by Independent Research Fund Denmark/Medical and Health Sciences (FTP-4183-00051) and by 'Savværksejer Jeppe Juhl og Hustru Ovita Juhls mindelegat'. The financial support from The Novo Nordisk Foundation (grants NNF20CC0035580 and LiFe, NNF18OC0034818), the Danish Council for Independent Research (*SWEET*, DFF-Research Project 8021-00039B) and the European Union's Horizon 2020 Research and Innovation Programme under grant agreement No. 814418 (*SinFonia*) to P.I.N. is also gratefully acknowledged. We are grateful to Lars Boje Petersen and Mette Kristensen at the Analytics Core for their assistance with HPLC measurements, to Douglas McCloskey at the Computational Biology group and Daniel Christoph Volke and Systems Environmental Microbiology group for inputs on the implementation of the dilution-resolved method.

Conflicts of interest

The authors declare no competing or financial interests.

Data availability

The data that support the findings of this study are openly available in the Table S1.

References

Arce-Rodríguez, A., Nikel, P.I., Calles, B., Chavarría, M., Platero, R., Krell, T., and de Lorenzo, V. (2021) Low CyaA expression and anti-cooperative binding of cAMP to CRP frames the scope of the cognate regulon of *Pseudomonas putida*. *Environ Microbiol* **23:** 1732–1749.

Bartell, J.A., Sommer, L.M., Haagensen, J.A.J., Loch, A., Espinosa, R., Molin, S., and Johansen, H.K. (2019) Evolutionary highways to persistent bacterial infection. *Nat Commun* **10:** 629.

Behrends, V., Ebbels, T.M.D., Williams, H.D., and Bundy, J.G. (2009) Time-resolved metabolic footprinting for nonlinear modeling of bacterial substrate utilization. *Appl Environ Microbiol* **75:** 2453–2463.

Behrends, V., Geier, B., Williams, H.D., and Bundy, J.G. (2013) Direct assessment of metabolite utilization by *Pseudomonas aeruginosa* during growth on artificial sputum medium. *Appl Environ Microbiol* **79:** 2467–2470.

Behrends, V., Williams, H.D., and Bundy, J.G.. (2014) Metabolic footprinting: extracellular metabolomic analysis. In *Pseudomonas Methods and Protocols*. Filloux, A.. and Ramos, J.-L.. (eds). New York, NY: Springer, pp. 281–292.

del Castillo, T., Ramos, J.L., Rodríguez-Herva, J.J., Fuhrer, T., Sauer, U., and Duque, E. (2007) Convergent peripheral pathways catalyze initial glucose catabolism in *Pseudomonas putida*: genomic and flux analysis. *J Bacteriol* **189:** 5142–5152.

Chubukov, V., Gerosa, L., Kochanowski, K., and Sauer, U. (2014) Coordination of microbial metabolism. *Nat Rev Microbiol* **12:** 327–340.

Crone, S., Vives-Flórez, M., Kvich, L., Saunders, A.M., Malone, M., Nicolaisen, M.H., *et al*. (2020) The environmental occurrence of *Pseudomonas aeruginosa*. *Apmis* **128:** 220–231.

Davis, R., Duane, G., Kenny, S.T., Cerrone, F., Guzik, M.W., Babu, R.P., *et al*. (2015) High cell density cultivation of *Pseudomonas putida* KT2440 using glucose without the need for oxygen enriched air supply. *Biotechnol Bioeng* **112:** 725–733.

Deschamps, E., Schaumann, A., Schmitz-Afonso, I., Afonso, C., Dé, E., Loutelier-Bourhis, C., and Alexandre, S.

(2021) Membrane phospholipid composition of *Pseudomonas aeruginosa* grown in a cystic fibrosis mucus-mimicking medium. *Biochim Biophys Acta - Biomembr* **1863:** 183482.

Deutschbauer, A., Price, M.N., Wetmore, K.M., Tarjan, D.R., Xu, Z., Shao, W., *et al*. (2014) Towards an informative mutant phenotype for every bacterial gene. *J Bacteriol* **196(20):** 3643–3655.

van Ditmarsch, D., and Xavier, J.B. (2011) High-resolution time series of *Pseudomonas aeruginosa* gene expression and rhamnolipid secretion through growth curve synchronization. *BMC Microbiol* **11:** 140.

Dolan, S.K., Kohlstedt, M., Trigg, S., Vallejo Ramirez, P., Kaminski, C.F., Wittmann, C., and Welch, M. (2020) Contextual flexibility in *Pseudomonas aeruginosa* central carbon metabolism during growth in single carbon sources. *MBio* **11:** e02684-19.

Duetz, W.A. (2007) Microtiter plates as mini-bioreactors: miniaturization of fermentation methods. *Trends Microbiol* **15:** 469–475.

Duetz, W.A., and Witholt, B. (2004) Oxygen transfer by orbital shaking of square vessels and deepwell microtiter plates of various dimensions. *Biochem Eng J* **17:** 181–185.

Govantes, F. (2018) Serial dilution-based growth curves and growth curve synchronization for high-resolution time series of bacterial biofilm growth. In *Host-Pathogen Interactions: Methods and Protocols*. Medina, C., and López-Baena, F.J. (eds). New York, NY: Springer, pp. 159–169.

Hartmans, S., Smits, J.P., Van der Werf, M.J., Volkering, F., and De Bont, J.A.M. (1989) Metabolism of styrene oxide and 2-phenylethanol in the styrene-degrading Xanthobacter strain 124X. *Appl Environ Microbiol* **55:** 2850–2855.

Henriques, I.D.S., Aga, D.S., Mendes, P., O'Connor, S.K., and Love, N.G. (2007) Metabolic footprinting: a new approach to identify physiological changes in complex microbial communities upon exposure to toxic chemicals. *Environ Sci Technol* **41:** 3945–3951.

Howell, K.S., Cozzolino, D., Bartowsky, E.J., Fleet, G.H., and Henschke, P.A. (2006) Metabolic profiling as a tool for revealing Saccharomyces interactions during wine fermentation. *FEMS Yeast Res* **6:** 91–101.

Jiménez-Fernández, A., Lopez-Sanchez, A., Calero, P., and Govantes, F. (2015) The c-di-GMP phosphodiesterase BifA regulates biofilm development in *Pseudomonas putida*. *Environ Microbiol Rep* **7:** 78–84.

Jiménez-Fernández, A., López-Sánchez, A., Jiménez-Díaz, L., Navarrete, B., Calero, P., Platero, A.I., and Govantes, F. (2016) Complex Interplay between FleQ, cyclic diguanylate and multiple σ factors coordinately regulates flagellar motility and biofilm development in *Pseudomonas putida*. *PLoS One* **11:** e016314.

Kaderbhai, N.N., Broadhurst, D.I., Ellis, D.I., Goodacre, R., and Kell, D.B. (2003) Functional genomics via metabolic footprinting: monitoring metabolite secretion by *Escherichia coli* tryptophan metabolism mutants using FT-IR and direct injection electrospray mass spectrometry. *Comp Funct Genomics* **4:** 376–391.

Kragh, K.N., Alhede, M., Rybtke, M., Stavnsberg, C., Jensen, P.Ø., Tolker-Nielsen, T., *et al*. (2018) The inoculation method could impact the outcome of microbiological experiments. *Appl Environ Microbiol* **84:** 1–14.

La Rosa, R., Behrends, V., Williams, H.D., Bundy, J.G., and Rojo, F. (2016) Influence of the Crc regulator on the hierarchical use of carbon sources from a complete medium in *P. seudomonas*. *Environ Microbiol* **18:** 807–818.

La Rosa, R., Johansen, H.K., and Molin, S. (2018) Convergent Metabolic specialization through distinct evolutionary paths in *Pseudomonas aeruginosa*. *MBio* **9:** e00269-18.

La Rosa, R., Johansen, H.K., and Molin, S. (2019) Adapting to the airways: metabolic requirements of *Pseudomonas aeruginosa* during the Infection of cystic fibrosis patients. *Metabolites* **9:** 234.

López-Sánchez, A., Jiménez-Fernández, A., Calero, P., Gallego, L.D., and Govantes, F. (2013) New methods for the isolation and characterization of biofilm-persistent mutants in *Pseudomonas putida*. *Environ Microbiol Rep* **5:** 679–685.

López-Sánchez, A., Leal-Morales, A., Jiménez-Díaz, L., Platero, A.I., Bardallo-Pérez, J., Díaz-Romero, A., *et al*. (2016) Biofilm formation-defective mutants in *Pseudomonas putida*. *FEMS Microbiol Lett* **363:** fnw127

Mapelli, V., Olsson, L., and Nielsen, J. (2008) Metabolic footprinting in microbiology: methods and applications in functional genomics and biotechnology. *Trends Biotechnol* **26:** 490–497.

McGill, S.L., Yung, Y., Hunt, K.A., Henson, M.A., Hanley, L., and Carlson, R.P. (2021) *Pseudomonas aeruginosa* reverse diauxie is a multidimensional, optimized, resource utilization strategy. *Sci Rep* **11:** 1–16.

Molina, L., La Rosa, R., Nogales, J., and Rojo, F. (2019a) Influence of the Crc global regulator on substrate uptake rates and the distribution of metabolic fluxes in *Pseudomonas putida* KT2440 growing in a complete medium. *Environ Microbiol* **21:** 4446–4459.

Molina, L., La Rosa, R., Nogales, J., and Rojo, F. (2019b) *Pseudomonas putida* KT2440 metabolism undergoes sequential modifications during exponential growth in a complete medium as compounds are gradually consumed. *Environ Microbiol* **21:** 2375–2390.

Nikel, P.I., Chavarría, M., Fuhrer, T., Sauer, U., and de Lorenzo, V. (2015) *Pseudomonas putida* KT2440 strain metabolizes glucose through a cycle formed by enzymes of the Entner-Doudoroff, Embden-Meyerhof-Parnas, and Pentose Phosphate pathways. *J Biol Chem* **290:** 25920–25932.

Nikel, P.I., Fuhrer, T., Chavarría, M., Sánchez-Pascuala, A., Sauer, U., and de Lorenzo, V. (2021) Reconfiguration of metabolic fluxes in *Pseudomonas Putida* as a response to sub-lethal oxidative stress. *ISME J* **15:** 1751–1766.

Nikel, P.I., Martínez-García, E., and de Lorenzo, V. (2014) Biotechnological domestication of pseudomonads using synthetic biology. *Nat Rev Microbiol* **12:** 368–379.

O'Brien, E.J., Monk, J.M., and Palsson, B.O. (2015) Using genome-scale models to predict biological capabilities. *Cell* **161:** 971–987.

Paczia, N., Nilgen, A., Lehmann, T., Gätgens, J., Wiechert, W., and Noack, S. (2012) Extensive exometabolome analysis reveals extended overflow metabolism in various microorganisms. *Microb Cell Fact* **11:** 1–14.

Palmer, K.L., Aye, L.M., and Whiteley, M. (2007) Nutritional cues control *Pseudomonas aeruginosa* multicellular behavior in cystic fibrosis sputum. *J Bacteriol* **189:** 8079–8087.

Rojo, F. (2010) Carbon catabolite repression in Pseudomonas: optimizing metabolic versatility and interactions with the environment. *FEMS Microbiol Rev* **34:** 658–684.

Rossi, E., La Rosa, R., Bartell, J.A., Marvig, R.L., Haagensen, J.A.J., Sommer, L.M., *et al*. (2021) *Pseudomonas aeruginosa* adaptation and evolution in patients with cystic fibrosis. *Nat Rev Microbiol* **19:** 331–342.

Sezonov, G., Joseleau-Petit, D., and D'Ari, R. (2007) *Escherichia coli* physiology in Luria-Bertani broth. *J Bacteriol* **189:** 8746–8749.

Turner, K.H., Wessel, A.K., Palmer, G.C., Murray, J.L., and Whiteley, M. (2015) Essential genome of *Pseudomonas aeruginosa* in cystic fibrosis sputum. *Proc Natl Acad Sci USA* **112:** 4110–4115.

Weimer, A., Kohlstedt, M., Volke, D.C., Nikel, P.I., and Wittmann, C. (2020) Industrial biotechnology of *Pseudomonas putida*: advances and prospects. *Appl Microbiol Biotechnol* **104:** 7745–7766.

Wewetzer, S.J., Kunze, M., Ladner, T., Luchterhand, B., Roth, S., Rahmen, N., *et al*. (2015) Parallel use of shake flask and microtiter plate online measuring devices (RAMOS and BioLector) reduces the number of experiments in laboratory-scale stirred tank bioreactors. *J Biol Eng* **9.** https://doi.org/10.1186/s13036-015-0005-0

Yung, Y.P., McGill, S.L., Chen, H., Park, H., Carlson, R.P., and Hanley, L. (2019) Reverse diauxie phenotype in *Pseudomonas aeruginosa* biofilm revealed by exometabolomics and label-free proteomics. *NPJ Biofilms Microbiomes* **5:** 31.

Zampieri, M., Sekar, K., Zamboni, N., and Sauer, U. (2017) Frontiers of high-throughput metabolomics. *Curr Opin Chem Biol* **36:** 15–23.

Supporting information

Additional supporting information may be found online in the Supporting Information section at the end of the article.

Fig. S1. Assimilation plots of all quantified metabolites for *Pseudomonas aeruginosa* PAO1 cultivated in SCFM. The concentration of each metabolite in Erlenmeyer flasks (blue symbols and lines), and deep-well plates (red symbols and lines) is shown relative to the OD at which supernatant samples were collected. Shaded areas indicate the 95% confidence intervals of the curves (cubic spline fitting).

Fig. S2. Assimilation hierarchy (A and B) and assimilation rate (C and D) determined using the data from three (blue bars) or two (red bars) biological replicates for the dilution-resolved (A and C) and time-resolved (B and D) methods. The error bar indicates the SEM (Standard Error of the Mean). Differences between rates were evaluated by Unpaired Welch *t*-test with significance indicated as 'ns' where $P > 0.05$ and '**' where $P < 0.01$.

Table S1. Data tables of metabolomics data for *Pseudomonas putida* and *Pseudomonas aeruginosa*; hierarchy and rate of assimilation; SCFM composition.

Chapter 3: Metabolic specialization drives reduced pathogenicity in *Pseudomonas aeruginosa* infections in cystic fibrosis patients

3.1 Previous exo-metabolomic studies of *P. aeruginosa* in CF airways

Exo-metabolomics has also been applied for studying infection dynamics. In the context of *P. aeruginosa*, it has been used to study the relationship between media composition and assimilation hierarchies [182], production of the virulence factor PrmC [183] and the role of carbon catabolite repression in biofilms compared to free planktonic cells [184].

One study by Behrends et al., (2013) used single time-point exo-metabolomic analysis of overnight cultures from 179 clinical isolates of *P. aeruginosa* across 18 patients with CF to study the changes in metabolism as a function of infection age and specific patient environments. Figure 8 below shows the clinical data, metabolomic data and dependence of metabolite concentrations on either infection age or patient environment respectively.

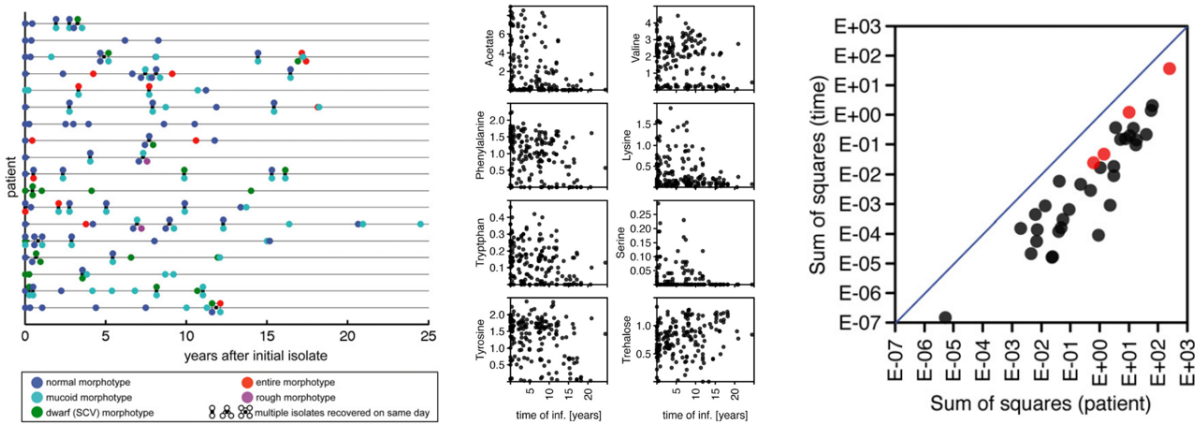

Figure 8: Figures 1, 3 and 4 from Behrends et al., (2013) showing years of infection, stationary phase metabolite concentrations and sum of squares by time compared with by patient.

While they found some trends e.g. a tendency toward reduced acetate production and trehalose utilization as a function of infection age, they also found that the most important factor determining the metabolic state was not the time spent adapting to the airways, but the specific patient environment the isolate was sampled from – as illustrated by all points representing metabolites being below the blue line in the sum of squares comparison plot.

However, metabolism is a highly dynamic process, and a lot of information is lost when looking only at a single time-point. Dynamic exo-metabolomics instead aim to capture the innate dynamicity of metabolism, by taking several time-resolved samples along the growth

curve and analyzing them together. Using this method for six clinical isolates of *P. aeruginosa*, representing different stages of adaptation in one patient, La Rosa et al., (2018) instead looked at changes in assimilation and secretion *profiles* and the overall shift in nutrient preferences, i.e. the order of assimilation of the various metabolites, to identify convergence toward an adapted metabotype. This adapted metabotype was characterized e.g. by increased secretion of pyruvate, lactate and glycine and reduced secretion of ornithine at late growth stage, as well as an assimilation hierarchy tailored to the CF sputum – see Figure 9 below.

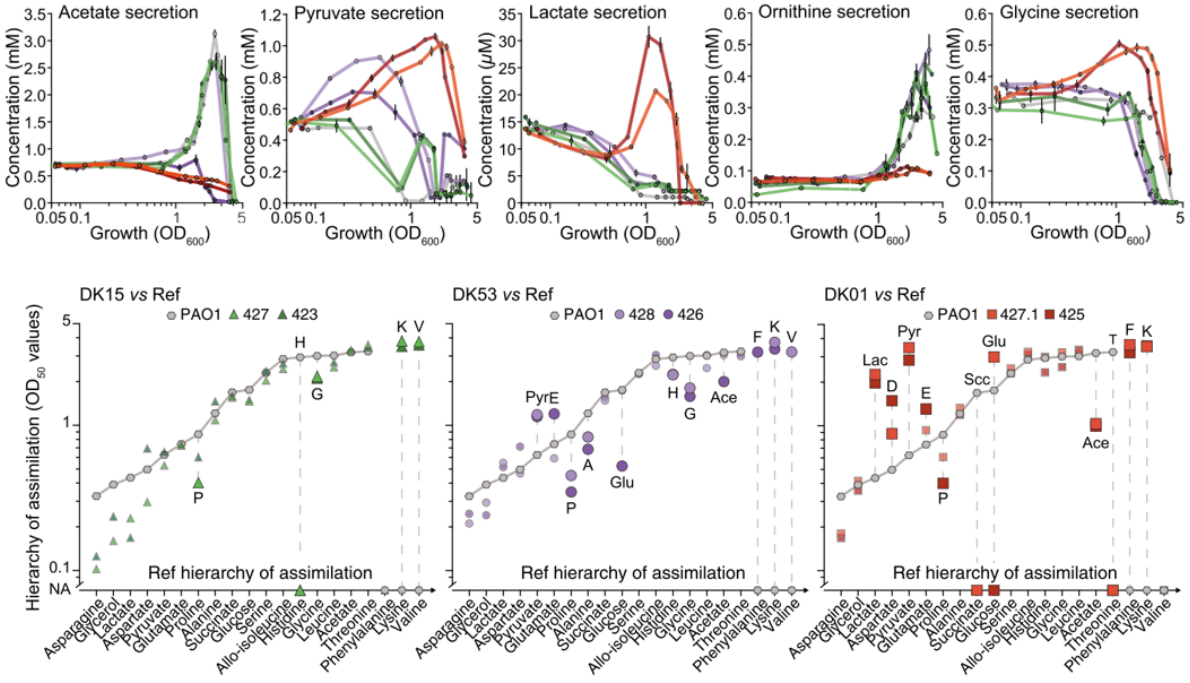

Figure 9: Figures 4-5 from La Rosa et al., (2018) showing assimilation and secretion profiles of specific metabolites and shift in overall assimilation hierarchy of metabolites for highly adapted clinical isolates. Red indicates highly adapted isolates; purple indicates intermediate adapted and green indicates naïve isolates.

All of the metabolite profiles seen on Figure 9 show differential secretion and subsequent reassimilation in different strains, which is an example of something that would be missed or misinterpreted by looking only at single time-point snapshots of the exo-metabolome – especially in late-stationary phase. This highlights the importance of time-resolved data when studying metabolism.

Due to feasibility, the study by La Rosa et al., (2018) only looked at isolates from one patient and as we see from Behrends et al., (2013), the specific patient environment plays a major role in metabolic adaptation. Thus, in order to obtain conclusive and more generalized results

on the metabolic adaptation related to CF airway infections, there is a need to look for convergence in adapted metabotypes between patients. To this end, the high-throughput method described in Chapter 2 was applied to a collection of 16 clinical isolates from 8 different CF patients. The following section encloses the manuscript, in preparation for publication, containing and building on these findings.

3.2 "Metabolic specialization drives reduced pathogenicity in *Pseudomonas aeruginosa* infections in cystic fibrosis patients", In preparation (2023)

Metabolic specialization drives reduced pathogenicity in *Pseudomonas aeruginosa* clinical isolates

Bjarke H. Pedersen [1], Filipa B. Simões [2], Ivan Pogrebnyakov [1], Martin Welch [3], Helle Krogh Johansen [1,2,4], Søren Molin [1] and Ruggero La Rosa [1#]

[1] The Novo Nordisk Foundation Center for Biosustainability, Technical University of Denmark, 2800 Kgs. Lyngby, Denmark

[2] Department of Clinical Microbiology 9301, Rigshospitalet, 2100 Copenhagen, Denmark

[3] Department of Biochemistry, University of Cambridge, CB2 1TN Cambridge, United Kingdom

[4] Department of Clinical Medicine, Faculty of Health and Medical Sciences, University of Copenhagen, 2200 Copenhagen, Denmark

Address correspondence to Ruggero La Rosa, rugros@biosustain.dtu.dk

Abstract

Metabolism provides the foundation for all cell functions. In pathogenic bacteria carrying-out persistent infections, metabolism functions radically differently compared to more naïve strains of the same species. However, whether this is simply a consequence of necessary accommodations to the persistence phenotype or if metabolism plays a direct role in achieving persistence in the host is still unclear. Here, we characterize the change in metabolome and proteome of eight infection scenarios of *Pseudomonas aeruginosa* in people with cystic fibrosis that show a shift in metabolic functions aligned with a persistence phenotype. We identify clinical mutations in the key metabolic enzyme pyruvate dehydrogenase leading to a host specialized metabolism. When tested in an air-liquid-interface airway infection model system, recombinant laboratory strains harboring pyruvate dehydrogenase mutations exhibit reduced virulence and immunogenicity recapitulating the persistence phenotype of clinical isolates. Altogether, these results provide evidence for the direct adaptiveness of metabolism during a persistent infection and the intrinsic role of metabolism in supporting pathogenicity. Moreover, it confirms the role of the pyruvate dehydrogenase as pathoadaptive gene.

Introduction

Metabolism of bacterial pathogens is a central process involved both in cell duplication but also in pathogenicity and virulence. Accordingly, nutrient availability in the host microenvironment guides the bacterial phenotype to trigger specific responses [186]. Nutritional restriction as consequence of a change in environment, for instance, can prompt the activation of specific virulence factors required to carry out an infection and succeed in the host. One example is the activation of the type III secretion system (T3SS) in response to acidic pH and nutrient limitation such as that found in the lumen of the *Salmonella*-containing vacuole during *S. enterica* infections [187,188]. Similarly, abnormalities in calcium homeostasis, as occurring in several host microenvironments or diseases, signals the activation of the T3SS cascade in *Pseudomonas aeruginosa* and *Vibrio parahaemolyticus* providing an environmental cue for bacterial pathogens to activate their virulence repertoire [189,190].

However, metabolism is not a static process but can dynamically change and specialize accordingly to the specific nature of the host environment. In *P. aeruginosa* clinical strains infecting people with cystic fibrosis (CF), for example, it has been observed that bacteria modify their metabolic preference to accommodate the specific needs of the infection [191,192]. The development of antibiotic resistance and bacterial adaptive evolution, moreover, provide the ground for chronic persistent infections lasting for decades [193]. Auxotrophy, specialized assimilation of carbon sources, secretion of high value metabolites and differential oxygen requirements of adapted clinical strains suggest a specific bacterial strategy to properly support the phenotype requirements in the host and contemporarily ensure the appropriate functionality of the cell [194]. The nutrient-rich mucus present in the airways of CF patients provides ample possibility of metabolic specialization with the aim of properly supporting the evolutionary events required for the establishment of a successful infection [195].

In persistent infections, adaptive evolution plays a fundamental role in improving the bacterial phenotype to overcome antibiotic treatment and other stresses, to hide from the host immune system, and to endure in the host long term [196,197]. Specific pathoadaptive mutations are selected for during within-patient evolution, providing the genetic foundation for increased persistence in the patient [198,199]. While antibiotic resistance mutations are specifically accumulated as consequence of the antibiotic treatment, it is still unclear how other mechanisms such as reduced growth rate or metabolic specialization contribute to persistence [191,200]. Laboratory studies in *P. aeruginosa* and *E. coli* have shown the involvement of specific metabolic mutations associated with changes in antibiotic susceptibility and virulence [201–205]. However, limited knowledge is available on their relevance and purpose in clinical isolates of *P. aeruginosa* during an infection. Moreover, the extent to which metabolic specialization provides *per se* a specific fitness advantages or if it is merely a fitness associated cost of other required phenotypes remains still unknown. Furthermore, the specific selective forces (for example antibiotic treatment or the immune system) leading to decreased growth rate and metabolic specialization are still unknown.

By analyzing in detail, the metabolic profiles of clinical strains of *P. aeruginosa* isolated from CF patients at different stages of evolution, we identified distinct metabolic configurations supported by changes in both assimilation and secretion of metabolites and by changes in proteome allocation. Moreover, we characterized a specific mechanism of metabolism

specialization involving the metabolic enzyme pyruvate dehydrogenase (PDH), which is essential for the processive fluxes through central carbon metabolism. Surprisingly, recombinant strains containing single mutations in PDH showed reduced infection capabilities and immunogenicity in an air-liquid-interface (ALI) infection model system. Such strains displayed a chronic-like phenotype as consequence of reduced expression of T3SS and increased T6SS determinants. Interestingly, such mutations occur frequently in clinical isolates of *P. aeruginosa*, suggesting that metabolic specialization as an adaptation to the host environment might be explicitly selected for at early stages of an infection to counterbalance the activity of the host. Altogether these results provide a rationale for metabolic specialization during CF airway infections.

Results

Growth rate reduction as proxy for within patient adaptation

To gain insight on the metabolic adaptation occurring in *P. aeruginosa* clinical isolates during the infection of CF patients, we selected 8 pairs of clinical isolates from different infection scenarios, i.e. 8 distinct clone types (> 10.000 unique SNPs) [18] isolated from different patients. Each pair was composed of one early (first *P. aeruginosa* isolated in the patient of that clone type) and one corresponding late clinical strain of the same clone type, longitudinally isolated from the same patient (Fig. 1A). Reduced growth rate was used as proxy for within-patient evolution of metabolism, allowing to assemble a diverse and variegated collection of clinical isolates spanning between 1.4 and 7 years of within-patient evolution. When grown in Synthetic Cystic Fibrosis Media (SCFM) designed to mimic the conditions of CF-mucus [54], early isolates present a high growth rate comparable to the reference strain PAO1 whereas the late isolates show a 2.2- to 5.1-fold reduction in addition to a halved maximal optical density (Paired t test, P = 0.002) (Fig. 1A-B). Moreover, some late isolates are unable to grow on minimal medium in presence of single carbon sources such as glucose, lactate or succinate, suggesting the development of some metabolic constraints (Fig. 1C).

Despite belonging to distinct clone types, a certain level of phylogenetic convergence is shown by the strains since, on the final branch of the phylogeny tree, early and late isolates tend to group closely within each group (early and late) rather than close to their clone type (Fig. 1D).

The distribution of mutations either accumulated or reverted during patient evolution differs between clone types, suggesting different evolutionary trajectories in each patient, including hypermutation events (Fig. 1E). However, mutated genes are similarly enriched between clone types (pyoverdine biosynthetic process for GO and bacterial secretion system and porphyrin metabolism for KEGG), suggesting conserved targets of within-patient evolution (Fig. 1F).

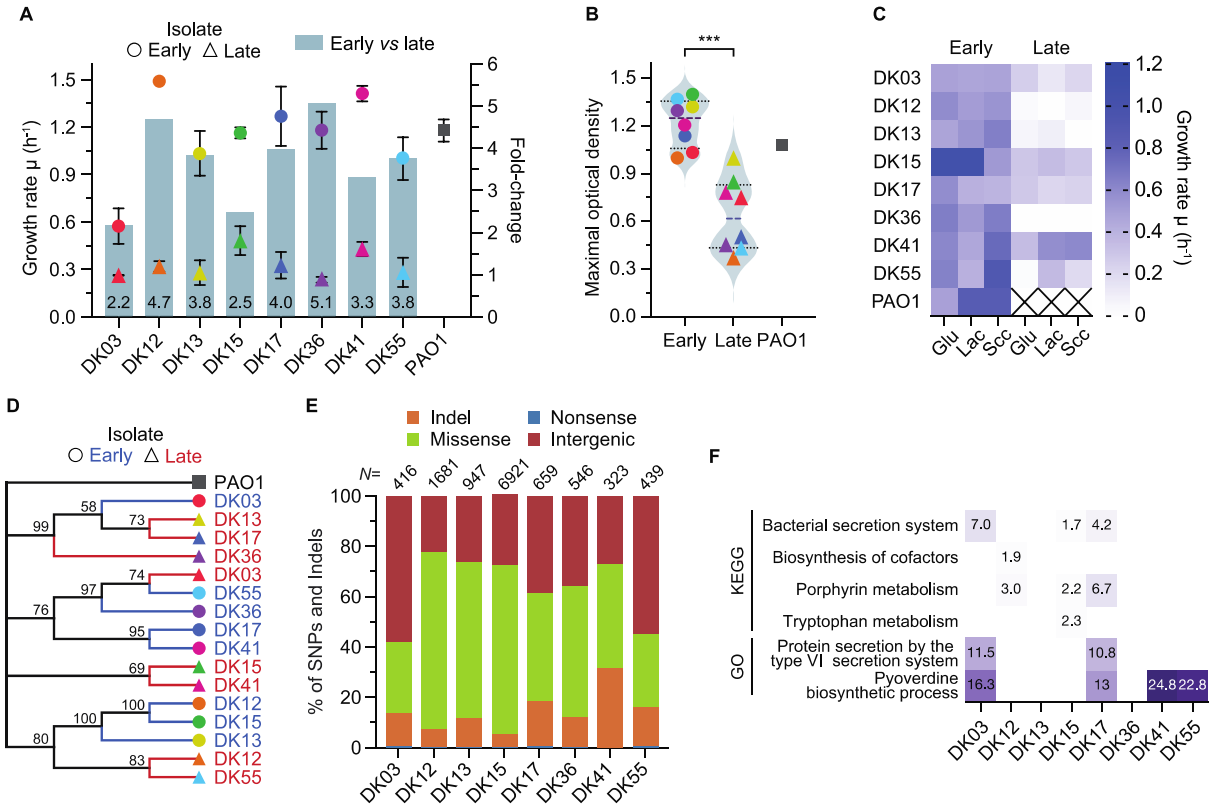

Fig. 1

Within patient evolution selects for specialized metabotypes

To evaluate the degree of metabolic specialization of the clinical isolate, dynamic exo-metabolomics was performed on cells growing in SCFM. PCA of the extracellular metabolomes reveals the presence of three distinct late specialized metabolic configurations, here defined “metabotypes” (DK15 and DK55 metabotype 1; DK12 metabotype 2; DK03, DK13 and DK36 metabotype 3). In these metabotypes, late isolates separate from each respective early isolate and from the rest of the non-adapted metabotypes (Fig. 2A). While PCA emphasizes the largest differences in the metabolome profiles, hierarchical cluster analysis clearly separates early from late strains, indicating a certain degree of metabolic

specialization in all late isolates (Fig. 2B). Indeed, both the hierarchy of assimilation (ordered by metabolite half-lives, OD_{50}) and the secretion of metabolites differ between early and late isolates (Fig. 2C-D). Specifically, metabotype 1 shows reduced assimilation of the amino acids Lys, Gly, Ile, Leu, Phe, Thr, Tyr and Val, as well as secretion of pyruvate by strain DK55 late; metabotype 2 shows increased assimilation of glucose, Ala, Asp, Glu, Gly, Pro, Ser, Arg and His, and rapid secretion of high concentrations of pyruvate; and metabotype 3 shows increased assimilation of glucose and lactate, differential assimilation of Ala, Asp, Glu, His and Pro, as well as secretion of pyruvate by strain DK36 late (Fig. 2C-D). Late DK13, DK36 and DK41 strains also secreted low concentration of formate. Notably, *all* late isolates secreted acetate, albeit at different concentration and with different profiles, whereas the early isolates did not (Fig. 2D). Unsurprisingly, the net balance between assimilated and secreted metabolites (total mM) varies between early and late strains (Fig. 2E), which positively correlates with the lower max OD of the late isolates (Pearson's $r = 0.9$; $P = 0.0023$) (Fig. 1B and 2E). This suggests either a specific metabolic configuration for the late isolates, which objective is not biomass accumulation, or an apparent inefficient metabolism.

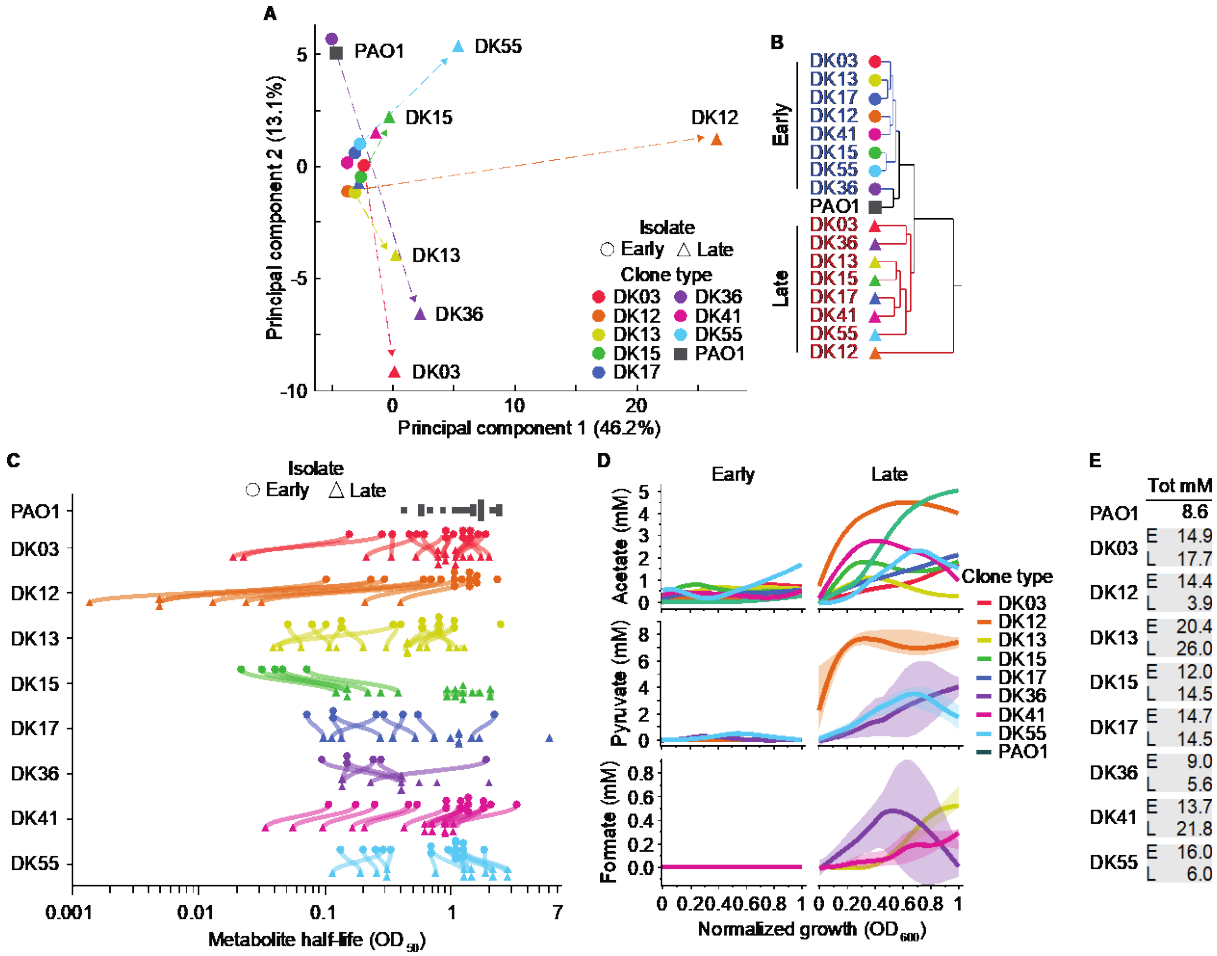

Fig. 2

Changes in proteome allocation support the metabolic specialization

To evaluate the contribution of the proteome composition to the metabolic specialization of clinical strains, we quantified 2061 proteins for all 17 strains by whole cell proteomics and identified 740 proteins as differentially expressed in at least one comparison of either clinical strains to PAO1 or late to corresponding early strains. Similarly to the metabolomic analysis, PCA separates late from early proteomes, suggesting that changes in metabolite profiles might be rooted in the proteome plasticity (Fig. 3A, B). Most of the early and some of the late proteomes co-localize with the reference strain PAO1, indicating little or no changes in proteome allocation (cluster 2) (Fig. 3A, B). However, proteomes of the late strains of DK03, DK12, DK17, DK36, DK55 lineages separate from the respective early strains, forming two clusters of adapted proteomes (DK03 cluster 1; DK12, DK17, DK36, DK55 cluster 3) (Fig. 3A, B). Notably, the early and late DK03 strains form an independent cluster, indicating a lineage

specific proteome signature which may explain the already reduced growth rate of the early isolate (Fig. 1A and 3A, B).

A similar result is obtained when performing hierarchical clustering analysis specifically on the 235 proteins differentially expressed between late and early strains belonging to the Clusters of Orthologous Groups (COG) categories involved in metabolism. The adapted metabotypes DK12, DK36 and DK55 and DK17 (cluster B) separate from the naïve metabotypes (cluster A), supporting the hypothesis that metabolic specialization is likely rooted in changes in expression of proteins involved in cellular metabolism (Fig. 3C). Notably, cluster B is characterized by a higher number of differentially expressed proteins in the categories of amino acids and lipid metabolism, as well as energy production and conversion relative to cluster A (Fig. 3D and Fig. S1A). Similarly, several categories of proteins involved in the metabolism of amino acids, fatty acid and sugars are differentially enriched in naïve and adapted clone types (Fig. S1B), providing an explanation for the altered hierarchy of assimilation of the amino acids and the reduced growth rate of the late adapted metabotypes (Fig. 2C, D).

Although late strains of DK12, DK36, DK55 belong to different metabotypes, their proteomes move in the same direction (Fig. 3A-C). This indicates that similar proteomes can sustain distinct metabolic configurations which ultimately depends on the specific metabolic fluxes and on metabolic regulation. Moreover, proteome adaptation can be achieved without rewiring of metabolism, as shown by DK17 which belongs to cluster 3 (late strain) and cluster B (Fig. 3A-C), but do not present any major metabolic rewiring (Fig. 2A, B).

Interestingly, several enzymes belonging to the Entner-Doudoroff (EDP), Embden-Meyerhof-Parnas (EMPP), glycolysis and Tricarboxylic Acid Cycle (TCA) pathways are upregulated in the early and late strains relative to PAO1, indicating a specific and convergent configuration of central carbon metabolism enzymes which is optimal for the resources available in the airways (Fig. 3E and S2). For example, our metabolomic data show that several late strains (metabotypes 2 and 3) exhibit increased glucose assimilation which is in agreement with the increased expression of pathways involved in glucose assimilation (enzymes 3, 11, 12, 18) (Fig. 3E). Similarly, fumarate hydratase (enzyme 33) together with the enzymes involved in Trp, Phe and Tyr catabolism (enzymes 65 and 66) show increased expression likely to better

accommodate the increased assimilation of amino acids that are catabolized through the TCA cycle (Fig. 3E). This hypothesis is corroborated by the changes in expression (both increased and decreased) in late vs early strains of several enzymes involved in amino acids, glucose, and lactate catabolism and of their respective transporters (Fig. 3E). This proteome configuration supports the overflow of amino acids through central carbon metabolism which leads to the secretion of pyruvate in late strains of DK12, DK36 and DK55 (Fig. 2D and 3E).

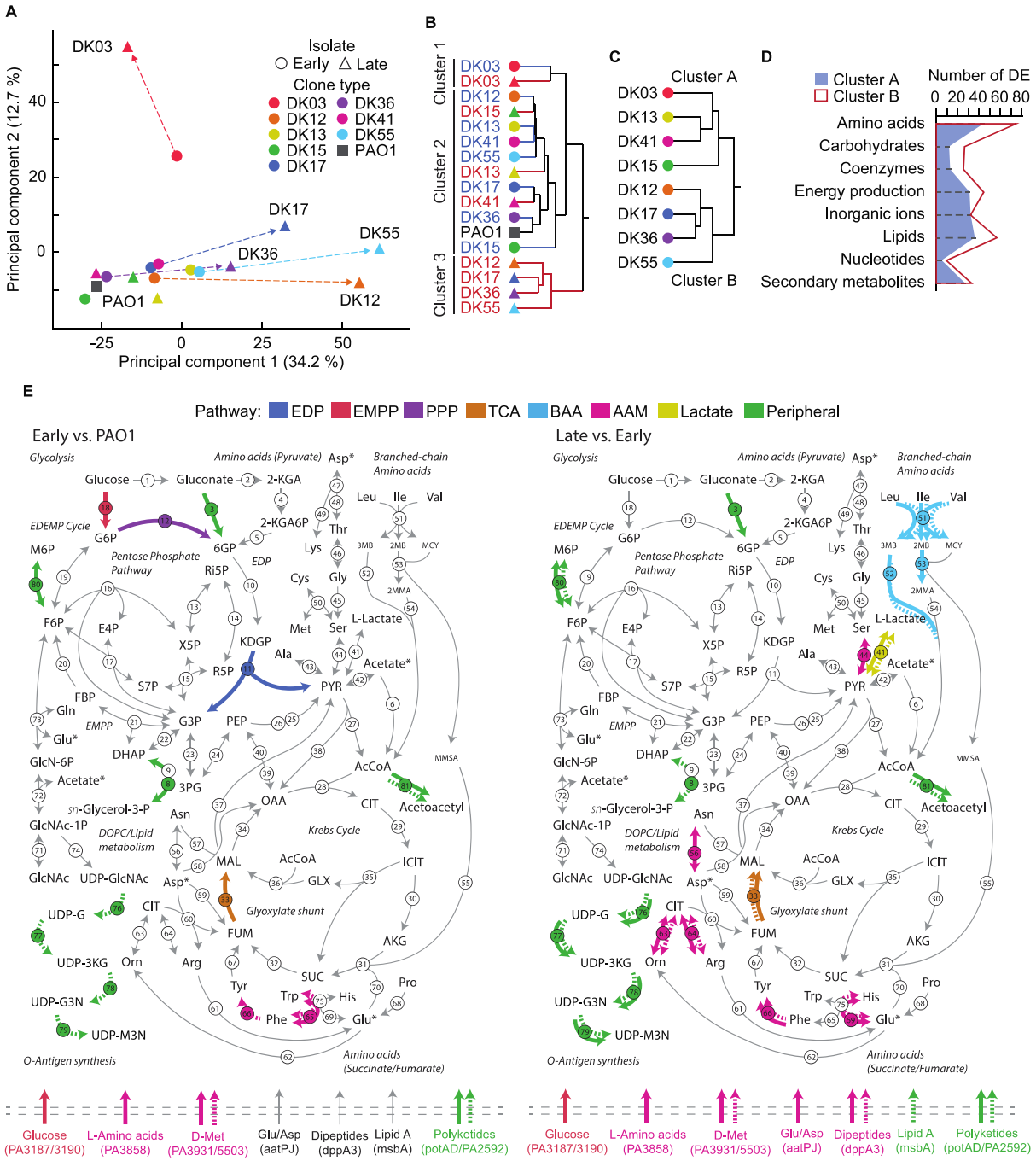

Fig. 3

Changes in virulence traits during within-patient evolution

Analysis of the differentially expressed proteins enriched when comparing late *vs* early isolates shows that most of the changes are rooted in adaptation to the infection environment, specifically in the redox balance and virulence of strains (Fig. 4A and S1B). Indeed, the categories of proteins for which expression changes in most of the lineages are phenazine biosynthesis (KEGG) and secondary metabolites biosynthetic process (GO) which are both deeply connected with the cell homeostasis, metabolism and virulence [206,207]. Not surprisingly, several clone types contain mutations in genes belonging to the pyoverdine biosynthetic process (GO) category (Fig. 1F), and several mutated genes shared between metabotypes belong to the COG category of secondary metabolites biosynthesis, transport and catabolism (Fig. S1B). Interestingly, several changes in protein expression are already shown by early strains relative to PAO1, indicating a different response of the clinical strains to the airway-like conditions of the SCFM (Fig. 4A). Specifically, early strains show increased expression of proteins involved in alginate production, hydrogen cyanide (HCN), phenazine biosynthesis and PQS (*Pseudomonas* quinolone signal), and decreased expression of proteins involved in flagella biogenesis, lipopolysaccharide (LPS) O-antigen metabolism and pyoverdine production (Fig. 4B). The adapted metabotypes, specifically strains belonging to cluster B, show convergent upregulation of proteins related to alginate and phenazine production, PQS and type VI secretion system (T6SS), suggesting an active role of metabolism in virulence regulation (Fig. 4C and S3). Interestingly, the DK12 late strain also shows a reduced expression (-1.5-fold reduction) of the type III secretion system (T3SS) secreted factor ExoT, which induces apoptosis in the host cells [208]. Overall, the identified pattern suggests a reduced immunogenicity of the clinical strains relative to PAO1, which is in line with their persistence during the infections.

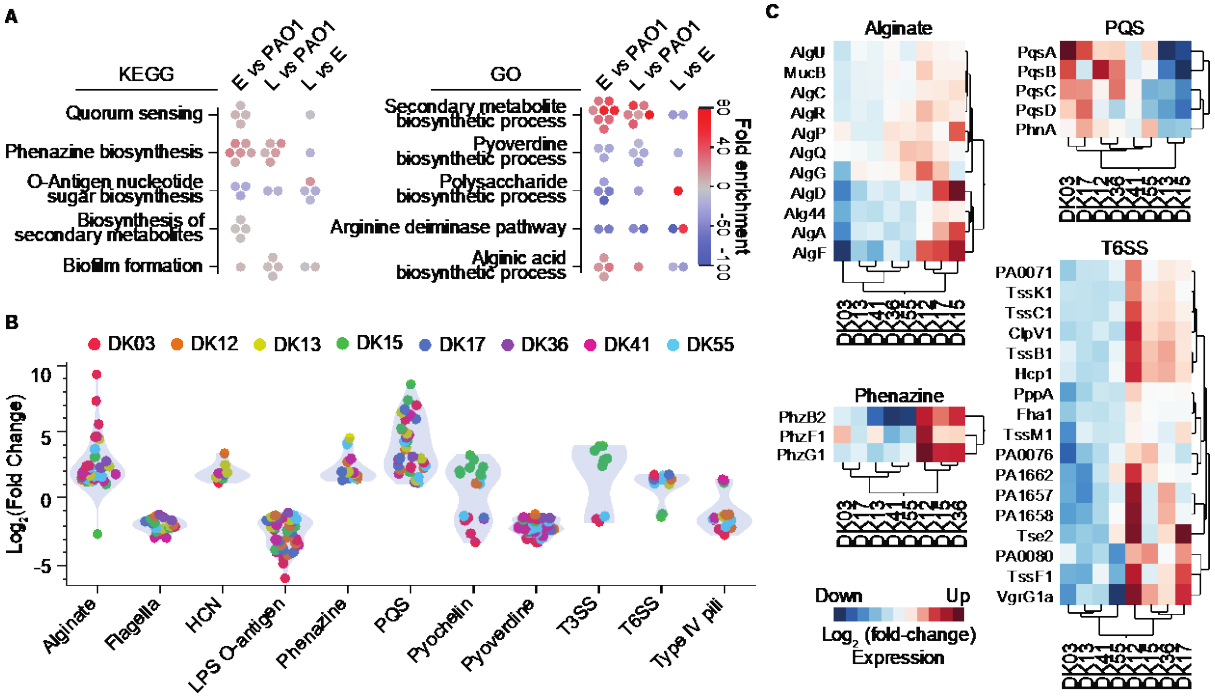

Fig. 4

Pyruvate dehydrogenase mutations modulate virulence in ALI infections

Screening for mutations which could explain the metabolic specialization of the late isolates led to the identification of mutations in the pyruvate dehydrogenase complex (PDHc) encoding genes *aceEF* in late strains of DK12 and DK36. The PDHc catalyses the conversion of pyruvate into acetyl-CoA connecting sugar metabolism to the TCA cycle. Interestingly, the *aceEF* genes are defined as candidate pathoadaptive due to frequent mutation during CF airway infections [18] and their *in-situ* expression is reduced in clinical strains, as evidenced by meta-transcriptomic analysis of sputum samples collected from chronically infected patients [67]. This indicates an undescribed role of the PDHc during infection. To evaluate their contribution to the bacterial phenotype, independently of the underlining historical contingency, we generated recombinant PAO1 derivatives containing the +TCCC duplication (position 813) in the *aceF* gene from the late DK12 strain, and the T>C SNP (position 551) in the *aceE* gene from the late DK36 strain (Fig. 5A). The *aceF* mutation leads to a frameshift of translation while the *aceE* mutation leads to a Phe to Ser change. The recombinant *aceE* and *aceF* mutant strains show a reduction in growth rate and an increased secretion of pyruvate similar to that of the late DK12 and DK36 strains respectively (Fig. 1A, 2D and 5B-C). The *aceE* mutant strain shows a milder phenotype (lower growth rate reduction and lower pyruvate

secretion) compared to the *aceF* mutant strain, suggesting a partial functionality of the PDH complex. Indeed, supplementing acetate to the bacterial culture to replenish the pool of acetyl-CoA fully restores the growth phenotype of the *aceE* strain, while it restores it only partially in the *aceF* strain, confirming a much more significant effect of the *aceF* mutation. A similar effect is seen when supplementing the clinical strains with acetate (Fig. 5B). Screening for other *aceEF* mutations in our strain collection, showed the presence of 18 different mutations including 4 indels which support the idea that modulation of the PHDc might be selected for specifically during airway infections (Fig. S4). Surprisingly, when testing phenotypes such as biofilm formation, motility, redox susceptibility, pyoverdine production and antibiotic susceptibility, no differences are shown, except for a slight decrease in twitching motility and tobramycin susceptibility, between the PAO1 wild type strain and the *aceE* and *aceF* mutant strains (Fig. S5).

To characterize the effect of the *aceE* and *aceF* mutations more broadly, we performed whole cell proteomics of the recombinant strains including the PAO1 reference strain in presence and absence of acetate. In total, we quantified 3246 proteins and identified 449 as differentially expressed in at least one comparison of either mutant *vs* wild type strain or of mutant strain in presence *vs* absence of acetate. In absence of acetate, the proteomes of the mutant strains *aceE* and *aceF* cluster in different quadrant than that of PAO1. More than 50% of variance on PC1 separates the *aceF* strain proteome from that of PAO1, while only less than 20% variance on PC2 separates the proteome of the *aceE* strain from that of PAO1 (Fig. 5D). As previously reported, the supplementation of acetate benefits both the *aceE* and *aceF* strains which proteomes move closer to that of PAO1 (Fig. 5D). This effect is accentuated in the *aceF* mutant strains where the supplementation of acetate decreases the number of differentially expressed proteins by more than half (from 301 to 126) (Fig. 5E). Unsurprisingly, several enzymes involved in central carbon metabolism, amino acid catabolism and specifically those involved in pyruvate and acetyl-CoA metabolism (lactate dehydrogenase (41), acetyl-coenzyme A synthetase (6), citrate synthase (28)) were upregulated in the *aceF* mutant strain, while expression returned to physiological levels by the addition of acetate (Fig. 5F and S6A). As shown for the clinical isolates DK12_L and DK36_L, the categories of proteins involved in amino acid and lipid metabolism, and energy conversion were the most dysregulated ones (Fig. S6B). Similarly, proteins involved in terpene, propionate, isoprenoid

and branched-chain amino acids which are directly connected to pyruvate and acetyl-CoA metabolism were statistically enriched in the *aceF* mutant strain indicating a reorganization of both central and peripherical pathways to cope with the lack of acetyl-CoA (Fig. S6C). Importantly, the *aceE* and *aceF* mutant strains show increased expression of proteins involved in alginate production and T6SS and reduced expression of proteins involved in the T3SS, including the secreted factor ExoT, similar to the profiles shown by the late clinical isolates of DK12 and DK36 (Fig. 4 and 5G).

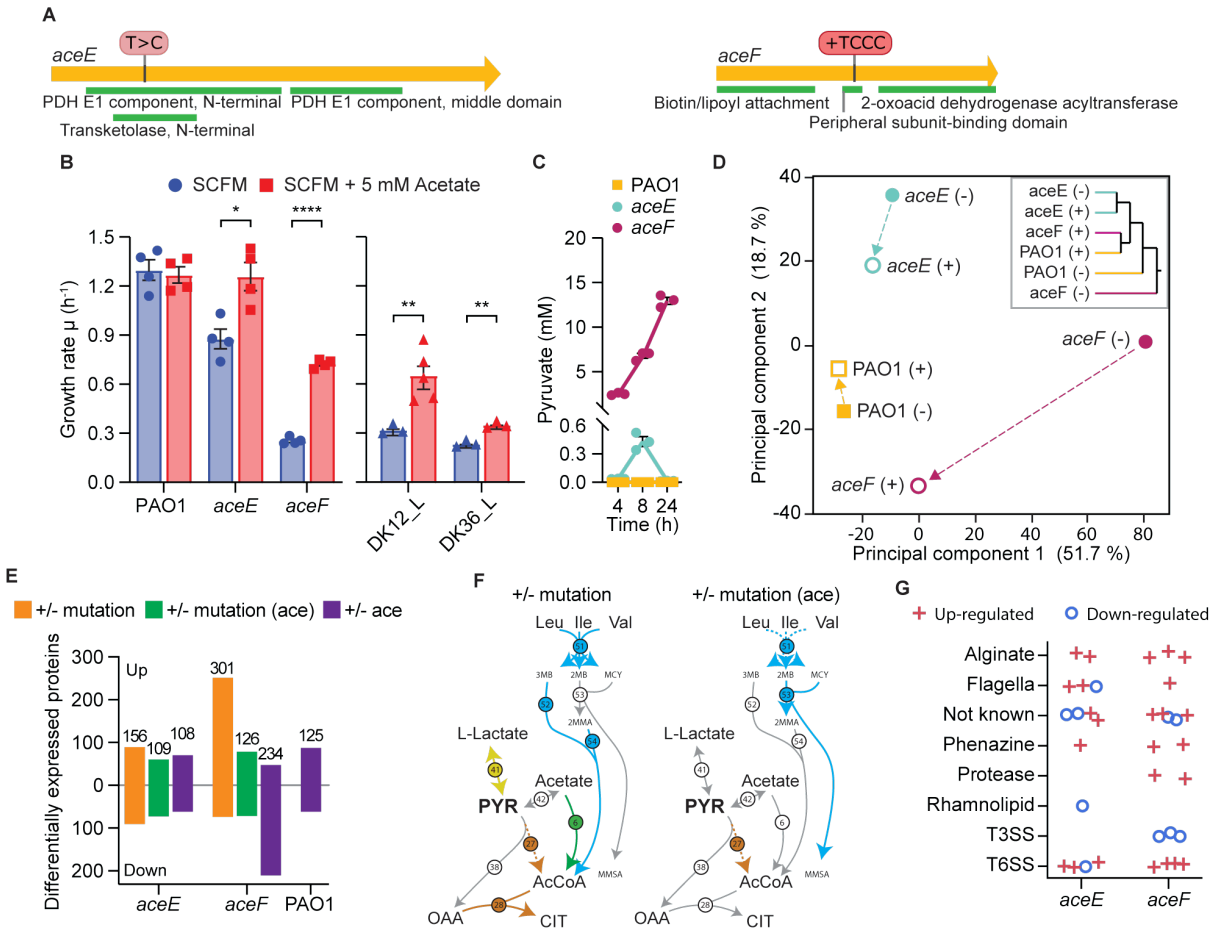

Fig. 5

In *P. aeruginosa* infections, the activity of the type III secretion system (T3SS) influences the degree of virulence of *P. aeruginosa* strains by injecting host cells with effector proteins that promote colonisation [209]. Since the *aceF* and *aceE* mutant strains show a different virulence expression profile than that of the PAO1 laboratory strain, we performed host-bacteria infection using an air-liquid-interface (ALI) infection model system composed of differentiated airway epithelial cells and the recombinant *aceF* and *aceE* mutant strains. Interestingly, the

aceF mutant strain shows a broad suppression of virulence including reduced epithelium damage and immune recognition during the infection (Fig. 6). The transepithelial electrical resistance (TEER) which quantifies the tightness of the tight junctions between epithelial cells, the LDH release which serves as a biomarker of cytotoxicity and the bacterial count, which quantifies the growth and penetration of the bacteria through the epithelium to the basolateral side of the ALI transwells all show reduced values after 14 hours of infection when compared to the PAO1 wild type strain (Fig. 6A). This is in line with the *ΔpscC* mutant strain defective in T3SS which shows a severely reduced virulence. The *aceE* strain instead shows a profile similar to that of PAO1, indicating that this mutation does not influence the bacterial penetration (Fig. 6A). However, it does show a reduced IL-8 release relative to PAO1, suggesting a lower degree of immune-recognition from the epithelial layer and consequent recruitment of the immune system at the site of infection, although still at an intermediary level compared with the *aceF* and *ΔpscC* strains (Fig. 6B). These results are corroborated by the confocal microscopy images, which show a similar degree of co-localization of bacterial cells on the airway epithelium for the PAO1 and *aceE* strains and of the *aceF* and *ΔpscC* respectively. It is also worth noting that only the PAO1 wild type strain appears to cause nuclei shedding in the epithelial cells, as seen from the nuclei in blue situated above the epithelial layer in red (Fig. 6C). This mechanism of reduced cellular damage and immunogenicity is not dependent on the growth defect of the *aceF* strain, since the *ΔpscC* strain shows similar virulence of the *aceF* mutant strain but a wild type-like growth rate.

Interestingly, the DK12 late strain has a reduced expression of the exoenzyme T (ExoT) and no impactful mutation in the T3SS, supporting the hypothesis that the *aceF* mutation contributes to the virulence phenotype of the clinical strain. Similarly, the DK15 late strain shows a reduced ExoT expression and a reduced expression of isocitrate lyase, which has also been associated with reduced T3SS activity [203]. In our longitudinal collection of clinical strains of *P. aeruginosa*, 12 clone types (89 isolates) harbour mutations in the *aceEF* genes and additional mutations in one or more genes encoding either the secreted factors or parts of the T3SS injectosome. In 9 lineages (clone types in specific patient), the PDHc mutations are present without or have been accumulated before the accumulation of mutations in the T3SS injectosome. The T3SS mutations occur before the PDHc mutations in 7 lineages and concurrently in 4 lineages, already at the start of infection (Fig. S7). These results suggest a

role for the *aceEF* mutations prior of those on the T3SS. Moreover, they provide direct evidence of the contribution of metabolism to the bacterial virulence and transition to the persistence phenotype.

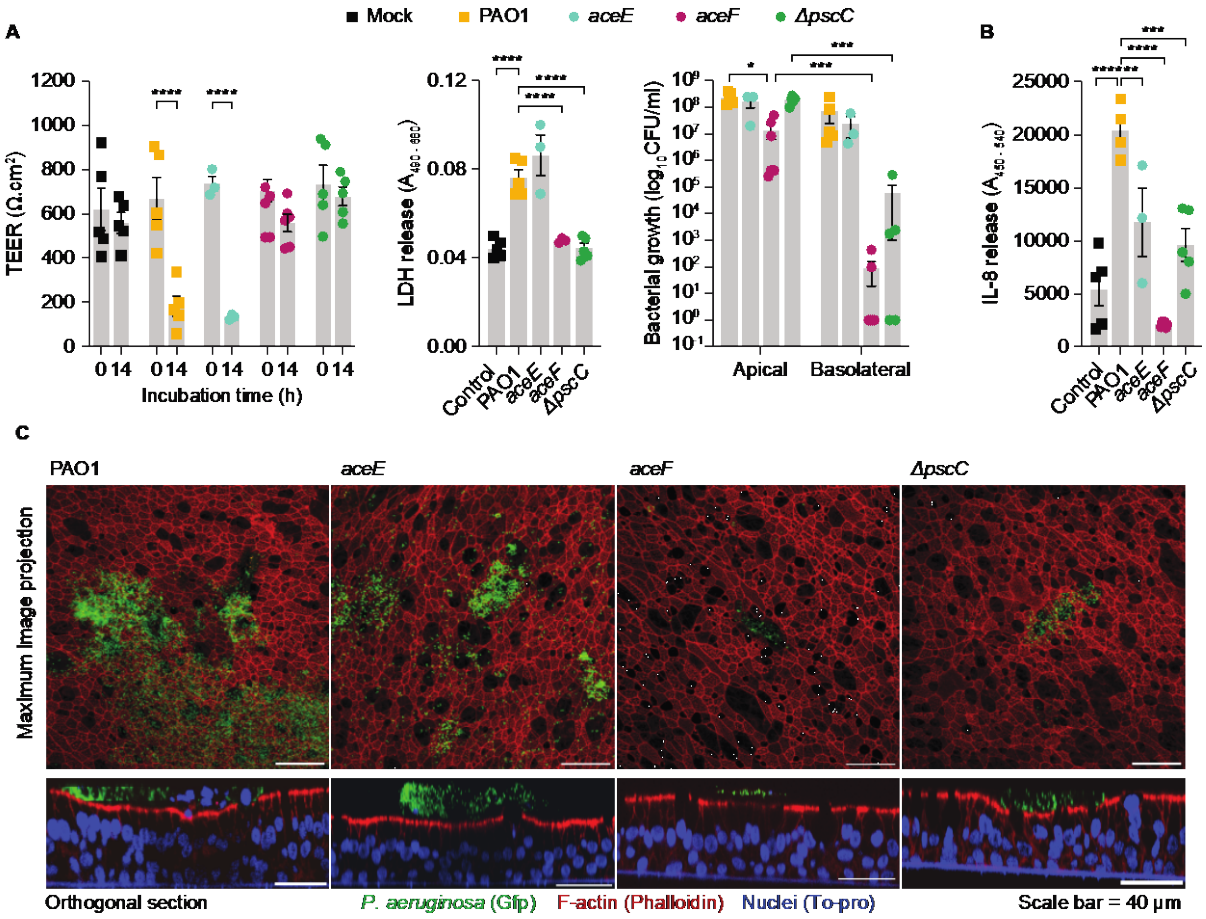

Fig. 6

Discussion

Metabolism constitutes a central process of the cell and, in long-term infections, requires optimization and specialization to account both for the nutritional resources presents in the environment and the phenotype requirements of the cell. Several studies have shown that metabolic specialization occurs in clinical isolates of *P. aeruginosa* [43,185,210]. However, little is known if metabolic specialization is convergently selected for and if specific metabolic configurations provide selective advantages during an infection. The CF environment is a complex and stressful environment where different selective forces including antibiotics, the immune system and specifically macrophages and dendritic cells together with their secreted

cytokines and ROS, push evolution of the infecting bacteria [23]. Most of the bacterial adaptation occurs during the first years of infection but surprisingly, antibiotic treatment is not the main driver of adaptation since during this period bacteria retain their susceptibility while still persisting in the host despite the treatment [164]. This may suggest that metabolic specialization is not simply a consequence of other more important fitness gains but could be specifically selected for, providing increased fitness in the host environment.

By analysing the metabolic profiles of different lineages of *P. aeruginosa* adapted to the airway environment, we show that all infection lineages underwent a substantial metabolic rewiring during adaptation in CF patients, moving toward a seeming overflow metabolism characterized by increased rate and amount of assimilation of nutrients such as amino acids and secretion of acetate by all late strains [71,211–215]. Such metabolic rewiring is associated with a change in proteome allocation which, together with the accumulated mutations in metabolic genes, provide the ground for the metabolic specialization of the bacteria. Some adapted strains are characterized by the secretion of high amounts of the metabolite pyruvate, due to mutations in the genes *aceE* (SNP) and *aceF* (Indel) encoding pyruvate dehydrogenase, which is a central enzyme involved in carbon metabolism. Insertion of the *aceE* and *aceF* mutations in the laboratory background of *P. aeruginosa* PAO1 recapitulates the metabolic profile (pyruvate secretion) and the chronic-like phenotype (T3SS downregulation, upregulation of T6SS, phenazines and alginate biosynthetic pathway and slow growth) of the late clinical isolates. Testing the aggressiveness of the recombinant strains in an ALI culture infection model system confirmed that the *aceE* and *aceF* mutant strains show reduced penetration and stimulation of the immune system when compared to the control strain.

Interestingly, the *aceE* and *aceF* mutant strains show upregulation of the T6SS and specifically the Tse2 effector together with the H2-T6SS locus involved in the growth arrest of both prokaryotic and eukaryotic cells [76,105,106], and in the internalization of *P. aeruginosa* in epithelial cells to evade the immune system [108]. Furthermore, the strains containing mutations in the *aceF* gene show reduced expression of the T3SS and specifically the ExoT effector, which can explain the reduced virulence during infections in the ALI infection model system. This expression profile might provide protection from other invading bacteria and alter the relationship with the host and its immune system. These results are consistent with

previous knowledge showing that mutations in the PDHc leads to repression of T3SS in *P. aeruginosa* [216,217]. Importantly, *aceE* and *aceF* mutations predominantly precede the also frequent T3SS mutations in our collection, indicating a fundamental and broader role of the PDHc mutations during evolution within the host. The fact that 63% of *aceE* and *aceF* mutations are SNPs compared to 27% of Indels suggests that the activity of PDHc can be modulated to balance the fitness costs and gains according to the specific host. Thus, distinct PDHc mutations may lead to different outcomes such as reduced immunogenicity and/or reduced disruption of the epithelial layer based on the specific effect of the mutation. Subsequent mutations on other virulence-related factors may fine-tune the phenotype by stabilizing or augmenting the effect of the PDHc mutations.

Pyruvate is an essential substrate for *P. aeruginosa* since it allows long-term survival without growth through pyruvate fermentation, which may be done in parallel with arginine fermentation to help stabilize extracellular pH [71]. In PAO1, this occurs only when TCA activity is inhibited by the depletion of both oxygen and nitrate [71], whereas PDHc-mutations may serve as an alternative mechanism for ensuring consistent TCA-inhibition in clinical strains. Moreover, pyruvate fermentation is key for the formation of microcolonies of biofilm, while its depletion leads to biofilm dispersal and enhanced antibiotic killing, both *in vitro* and in an *in vivo* porcine burn wound model [218,219]. These results have led some to suggest pyruvate-depletion by treatment with active PDH as an effective anti-biofilm therapy [219]. Conversely, inhibition of the PDHc and redirection of the pyruvate flux has been suggested both as a potential anti-inflammation therapy for chronic metabolic diseases [220] and as a cancer treatment [221].

It is important to note that fine-tuning of the flux through the mitochondrial PDHc in macrophages, dendritic cells and other immune cells is crucial for regulating their polarization and thus the balancing between pro- and anti-inflammatory responses [220,222–234]. Indeed, LPS-induced polarization of macrophages is prevented by pharmacological inhibition of pyruvate import into the mitochondria [231]. Moreover, flux through the PDHc controls the production of the antibacterial cytokine Itaconate [223,224,227,230,231]. Indeed, secretion of pyruvate by the PDHc mutant strains, might influence the distribution and activity of macrophages and dendritic cells present in the airways by a mechanism of cross-feeding. Thus, the PDHc dysregulation seen in the clinical isolates may serve as a mechanism for ensuring consistent

TCA inhibition and pyruvate fermentation, active pyruvate secretion, increased biofilm production and finally reduced immunogenicity. These combined mechanisms can explain the reduced aggressiveness shown by the *aceE* and *aceF* mutant strains in the ALI culture infection system and provide a rationale for the broad accumulation and maintenance of PDHc-mutations in our collection of *P. aeruginosa* clinical isolates. Moreover, it suggests a highly complex and near universal role of pyruvate in regulation of a diverse set of cells (pathogen and host) and their respective functions *in vivo* through a conserved central metabolite.

Altogether our results strongly indicate that metabolic specialization, especially within the pyruvate node, is specifically selected for in the CF airway environment. For this reason, the *aceE* and *aceF* genes are under high selective pressure and considered pathoadaptive genes [18]. Moreover, the expression of the PDHc is kept at a low level in the airways, as shown by the analysis of the transcriptional profile of *in situ* sputum samples [67], indicating that modulation of pyruvate metabolism is evolutionarily beneficial. Importantly, *aceE* and *aceF* mutations not only change the bacterial phenotype, but they reduce the activity of the immune system to provide immune escape and successfully establish persistent infections. Such a mechanism might be used years before the development of antibiotic resistance and therefore be of high relevance for the establishment of a chronic phenotype. Understanding specific mechanisms linking metabolism, energy balance and virulence and most importantly how the relationship between the host and the pathogen changes during an infection could therefore provide new opportunities for improved and more efficient treatments which go beyond the classical antibiotic regimens.

Methods

Media preparation

Synthetic Cystic Fibrosis Media 2 (SCFM2) is a defined rich medium that mimics the nutrient conditions of the CF airways to provide a more accurate model of the conditions during infection. SCFM2 was prepared according to the protocol described in Turner et al., (2015). To reduce viscosity and allow for HPLC analysis, DNA and mucins were excluded [235]. The main carbon sources in the media are lactate (9.3 mM) and glucose (3.0 mM), but it also contains several amino acids, as well as the amino sugar N-acetylglucosamine and the lipid 1,2-

dioleoyl-sn-glycero-3-phosphocholine (DOPC). For a full description of the composition, see Turner et al., (2015).

M9 minimal media was prepared from a 10x stock of salts and supplemented with either lactate, glucose or succinate respectively to a final concentration of 20 mM, as well as with vitamins and trace elements (33.7 mM Na_2HPO_4; 22.0 mM KH_2PO_4; 8.55 mM NaCl; 9.35 mM NH_4Cl; 1 mM $MgSO_4$; 0.3 mM $CaCl_2$; 1 μg/mL biotin; 1 μg/mL thiamine; 134 μM EDTA; 31 μM $FeCl_3$; 6.2 μM $ZnCl_2$; 0.76 μM $CuCl_2$; 0.42 μM $CoCl_2$; 1.62 μM H_3BO_3; 0.081 μM $MnCl_2$; pH = 7.2).

Pseudomonas isolation agar (PIA) plates were prepared by dissolving 11.26 g of PIA powder (Sigma Aldrich) and 10 mL of 50 % glycerol in 240 mL tap water and autoclaving for 15 min. at 121 C. After cooling to 60 C, PIA was supplemented to a final concentration of 5 mM acetate and 30 μg/mL gentamycin, before adding 20 mL per plate and incubating the plates at room temperature overnight.

Luria Broth (LB) media was prepared by dissolving 25 g of LB powder (Sigma Aldrich) in 1 L of distilled water and autoclaving for 15 min. at 121 C. King's B media was prepared for the pyoverdine assay (20 g/L proteose peptone; 8.61 mM K_2HPO_4; 12.46 mM $MgSO_4$; 10 % Glycerol; pH = 7.2).

Growth rate determination

Growth rates were determined from growth curves by inoculating 1 μL of ON culture in 149 μL of media in 96-well microtiter plates (Cat. No. 650001; Greiner Bio-One, Kremsmünster, Austria), covered with plate seals (Ref. 4306311, Thermo Fisher Scientific, United Kingdom) and incubated at 37 C and 250 rpm in a BioTek ELx808 Absorbance Microtiter Reader (BioTek Instruments Inc., Winooski, VT, USA) for 24 – 48 hours, depending on when stationary phase is reached. To avoid extended lag phase from changes in media composition, precultures were done in the same media as the cultivation experiment. Blanks were subtracted from OD_{600}-measurements and values converted to cm^{-1} (using Greiner dimensions for pathlength), then imported to the software JMP version 15.0.0. The stationary phase was excluded, and growth

rates were calculated by fitting the Exponential 3P model to the exponential phase ($r^2 > 0.99$). Mean ± sd was calculated from biological replicates.

Dynamic exometabolomics

Sampling

High-throughput sampling for dynamic exometabolomic analysis of clinical isolates was carried out in 96-well deep well plates (Cat. No. 0030502302; Eppendorf, Hamburg, Germany) with an air:liquid ratio of 1:1, as described in [236]. Both cultures and precultures were done in SCFM and incubated in an orbital shaker at 37 C and 250 rpm. Immediately before sampling, OD_{600} of the cultures were measured from 40 μL in a Synergy™ MX microtiter plate reader (BioTek Instruments Inc., Winooski, VT, USA). The remaining culture was sampled by centrifugation of deep well plates at 4 °C and 1740 G for 30 min. and supernatants were stored at -80 C until HPLC-analysis.

HPLC

Samples were thawed at 4 °C and analysed by two different methods: one for quantification of organic acids and sugars and one for quantification of amino acids. For organic acids and sugars (glucose, lactate, formate, acetate and pyruvate), a Dionex Ultimate 3000 system (Thermo Scientific,Waltham, United States) with a HPx87H ion exclusion column (125-0140, Aminex, Dublin, Ireland), equipped with a guard column (125-0129, BioRad, Hercules, California, United States) and guard column holder (125-0131, BioRad, Hercules, California, United States) was used. Samples were injected with an injection volume of 20 μL and eluted, using a 5 mM H_2SO_4 mobile phase, at an isocratic flow of 0.6 mL min^{-1} at 45°C for 30 min. Pyruvate was analysed by UV detection at a wavelength of 210 nm, using a System Gold 166 UV-detector (Beckman Coulter, Brea, United States), while the rest were analysed by RI detection, using a Smartline RI detector 2300 (KNAUER Wissenschaftliche Geräte, Berlin, Germany).

For amino acids (aspartic acid, glutamic acid, serine, histidine, glycine, threonine, arginine, alanine, tyrosine, valine, phenylalanine, isoleucine, leucine, lysine and proline), 20 μL of the thawed sample was diluted 1:10 by mixing with 80 μL Ultrapure MilliQ water and 100 μL of

internal standard (20 μg/mL 2-aminobutyric acid and sarcosine) before injection of 56.5 μL into the instrument. Prior to injection into the column, derivatization of amino acids was performed in the HPLC-instrument by automatic mixing with the following eluents: (i) 0.5% (v/v) 3-mercaptopropionic acid in borate buffer 0.4 M at pH 10.2; (ii) 120 mM iodoacetic acid in 140 mM NaOH; (iii) OPA reagent (10 mg/mL *o*-phtalaldehyde and 3-mercaptopropionic acid in 0.4 M borate buffer); (iv) FMOC reagent (2.5 mg/mL 9-fluorenylmethyl chloroformate in acetonitrile); and (v) buffer A (40 mM Na_2HPO_4, 0.02% (w/v) NaN_3 at pH = 7). Following derivatization, the samples were separated isocratically on a Dionex Ultimater 3000 HPLC with fluorescence detector (Thermo Scientific, Waltham, United States) through a Gemini C18 column (00F-4439-E0, Phenomenex, Værløse, Denmark) equipped with a SecurityGuard Gemini C18 guard column (AJ0-7597, Phenomenex, Værløse, Denmark) with 5 mM H_2SO_4 at a flowrate of 1 mL min^{-1} at 37°C for 31 min. Amino acids were detected using an UltiMate™ 3000 Fluorescence variable wavelength UV detector (FLD-3400RS, Waltham, Massachusetts, United States). Standard curves for each metabolite were used to quantify absolute concentrations for a total of 20 metabolites. All chromatograms were analysed with the software Chromeleon v7.2.9.

Data analysis

To compare assimilation and secretion dynamics between clinical isolates with radically different growth-curves, metabolite concentration (mM) was plotted against "Relative growth" – defined as $Sample_{OD}$ / $Final_{OD}$ for each strain. Small variations in specific metabolite concentrations between different batches of SCFM were observed and concentrations were standardized by dividing specific metabolite concentrations in each sample with the specific concentration in the relevant batch and multiplying by the standard concentration for SCFM. To allow for log-transformation of concentrations, missing values were replaced with 20% of the lowest concentration detected for any metabolite in any sample. Principal component analysis (PCA) and hierarchical cluster analysis (HCA) were done on $C_{metabolite}$ of all quantified metabolites for 16 samples (8 time-points from biological duplicates) of each strain. PCA was done on covariance and HCA using Ward's method for cluster analysis, based on the specific metabolomes (time-resolved samples) of each strain.

The assimilation hierarchy of each isolate was determined by ordering metabolites by their half-life (OD_{50}), defined as the normalized OD_{600}-value, where 50 % of the starting concentration of a metabolite is present. For metabolites not assimilated past 50 % of initial concentration, no OD_{50} can be determined. To calculate the OD_{50} for each strain/metabolite, the concentration was plotted against OD_{600} and the fit of several sigmoidal models (Gompertz 3P and 4P, Logistic 4P, 4P Hill and 5P, Probit 4P and Mechanistic Growth) were analysed, using the "model fit" function in JMP version 15.0.0. The mechanistic growth model (Equation: a(1 – bExp(–cx)) where a = asymptote, b = scale and c = rate) had the best fit across AICc, AICc Weight, BIC, SSE, MSE, RMSE and R^2 and was selected as the general model for assimilation and secretion dynamics. OD_{50}-values were calculated from this model, using the inverse prediction formular with $Y = 0.5*Y_0$ in each case. The mechanistic growth model was also fit to concentration plotted against "relative growth" and used to calculate the total amount (mM) of metabolite assimilated during growth, using the prediction formular with "Relative growth" = 1. These were summed for all metabolites to calculate the total mM carbon sources assimilated by each strain. All figures were created in JMP version 15.0.0 and finalized in Adobe Illustrator.

Proteomics of clinical isolates

Sampling

To maintain a 1:1 air:liquid ratio, as in the metabolomic analysis, 25 mL SCFM cultures were inoculated in 50 mL Falcon tubes at OD_{600} = 0.05 from ON cultures, also done in SCFM, and incubated in an orbital shaker at 37 C and 250 rpm. Five biological replicates were inoculated from separate ON cultures and sampled at mid-exponential phase by centrifugation for 15 min. at 4 C and 4000 rpm. Pellets were washed twice with 1 mL PBS, transferred to 1.5 mL e. tubes and spun down for 15 min. at 4 C and 15000 rpm, before being stored at -80 C. Before sampling, growth curves of all strains were done under the same conditions and used to define a mid-exponential phase for sampling. For PAO1, as well as all early clinical isolates and the late isolates of clone types DK13, DK15, DK36 and DK41, stationary phase was reached within 18 hours with final ODs of 0.9 – 1. For these strains, mid-exponential phase was defined as OD = 0.5. The late clinical isolates of clone types DK03, DK12, DK17 and DK55 all showed

biphasic growth with a pseudo-stationary phase of OD = 0.3 – 0.5 within the first 18 hours, followed by a prolonged secondary growth phase that eventually would reach OD = 1 after 18 to 36 hours. For these strains, mid-exponential phase was defined as OD = 0.2, based on the first growth phase. To obtain comparable protein yields for these four strains, each replicate was prepared as 75 mL inoculum from one ON culture and split in three 50 mL Falcon tubes containing 25 mL culture each before incubation. When sampling, the OD of each culture was measured and used to calculate a mean ± sd of the sample OD. The three pellets from one replicate were combined during the resuspension in PBS of the first washing step.

Sample-preparation

Pellets were placed in an ice bath and thawed for 20 min. before being resuspended in 1 mL of Lysis buffer (100 mM Tris, 50 mM NaCl, 1 mM TCEP, 10 % glycerol, pH = 7.5) with *cOmplete Mini protease inhibitor* (Roche), 1 tablet pr. 25 mL Lysis buffer to avoid proteolytic activity. Cells were lysed, while on ice, by sonication at amplitude 10 for 3x 10s cycles with 20s cooling between. Cell debris was removed by centrifugation for 15 min. at 4 C and 15000 rpm and transfer of 800 μL supernatant protein extract to new e. tubes. The protein concentration in each sample was determined from three technical replicates measured by Bradford assay and protein extracts were stored at -80 C. To remove salt from the Lysis buffer, 100 μg protein pellets were prepared by acetone precipitation. Specific volumes of each protein extract were aliquoted, containing 100 μg protein each, and mixed with 5x volume of -20 C acetone, vortexed and incubated ON at -20 C to allow protein aggregation. Samples were then vortexed and centrifuged for 10 min. at 10 C at 15000 rpm. Supernatant was removed and pellets left to air-dry for 30 min. Pellets were then resuspended in 50 μL Guanidium HCl cell lysis buffer (6 M Guanidinium hydrochloride (GuHCl), 5 mM tris(2-carboxyethyl)phosphine (TCEP), 10 mM chloroacetamide (CAA), 100 mM Tris–HCl, pH = 8.5), placed in thermomixer for 30 min. at 60 C and 600 rpm and then stored at -20 C until the next day. Tryptic digestion was done at constant shaking for 8 hours at 400 rpm, followed by addition of 10 μL 10% TFA. StageTipping was carried out using C18 as resin (Empore, 3M, USA).

LC-MS/MS

LC-MS/MS was carried out using a CapLC system (Thermo Fisher Scientific Inc., Waltham, USA) coupled to an Orbitrap Q-exactive HF-X mass spectrometer (Thermo Fisher Scientific Inc.,

Waltham, USA). The first samples were captured at a flow of 10 μl/min on a precolumn (µ-precolumn C18 PepMap 100, 5 μm, 100 Å) and then at a flow of 1.2 μl/min. Peptides were separated on a 15 cm C18 easy spray column (PepMap RSLC C18 2µm, 100Å, 150 µmx15cm). The applied gradient went from 4% acetonitrile in water to 76% over a total of 60 minutes. MS-level scans were performed with Orbitrap resolution set to 60,000; AGC Target 3.0e6; maximum injection time 50 ms; intensity threshold 5.0e3; dynamic exclusion 25 sec. Data dependent MS2 selection was performed in Top 20 Speed mode with HCD collision energy set to 28% (AGC target 1.0e4, maximum injection time 22 ms, Isolation window 1.2 m/z). After acquisition, the raw data were analyzed using the Proteome discoverer 2.4 software with the following settings: Fixed modifications: Carbamidomethyl (C) and Variable modifications: oxidation of methionine residues. First search mass tolerance 20 ppm and a MS/MS tolerance of 20 ppm. Trypsin as enzyme and allowing one missed cleavage. FDR was set at 0.1%. The Match between runs window was set to 0.7 min. Quantification was only based on unique peptides and normalization between samples was based on total peptide amount. For the searches the *Pseudomonas aeruginosa* PAO1 reference proteome (UniProt Proteome ID UP000002438) was used.

Data analysis

Data was reduced from 3011 proteins quantified to 2061 by elimination of proteins that were either 1) Not listed as “High” confidence under “Protein FDR Confidence: Combined”, 2) Not identified as “OS=*Pseudomonas aeruginosa*” or 3) Not quantified in at least three of five biological replicates for all 17 strains included in the analysis. Missing value imputation was done for missing values, based on the abundances from three or more biological replicates of that strain. Abundances were log2-transformed and Principal Component Analysis (PCA) and hierarchical clustering analysis were performed using the software JMP Pro version 15.0.0.

Differential expression was determined by two-way ANOVA with Tukey’s multiple comparisons test, using the software GraphPad Prism 9.3.1, and defined as those protein-comparisons where Adjusted *P* value ≤ 0.05 and Log2(Fold-Change) ≥ |0.6|. Using the three comparisons “Late/Early”, “Late/Control” and “Early/Control” for each Clone Type (with Control being PAO1), 609 proteins were identified as differentially expressed in at least one of the relevant comparisons.

Enrichment analysis of functional categories was performed using the DAVID Functional Annotation Bioinformatics Microarray Analysis tool, with input being lists of the Locus Tags associated with proteins that were differentially expressed, separated into lists of upregulated and downregulated proteins, for each of the relevant strain-comparisons. The reference genome was set as *Pseudomonas aeruginosa*.

Proteomic analysis of aceEF mutants

Sample preparation

Cell pellets were collected and stored following the same protocol as clinical isolates for three biological replicates of PAO1, *aceE* and *aceF* in SCFM in presence and absence of 5 mM acetate with mid-exponential OD_{600} = 0.5. Pellets were thawed and then kept on ice. Two (3-mm zirconium oxide) beads were added to each sample. Then, Lysis Buffer (6 M Guanidinium hydrochloride, 5 mM TCEP, 10 mM Chloroacetamide, 100 mM Tris-HCl pH 8.5) was added at 99 °C and samples were incubated for 5 min. in Tissuelyzer (Retsch, MM 400) at 25 Hz. Because of large cell pellets, this was done twice, first in 150 μL and then repeated with an additional 100 μL of Lysis Buffer. Samples were then boiled, still at 99 °C, in heat block (Eppendorf Thermomixer C) for 10 min. while shaking/mixing at 2000 rpm and then centrifuged for 10 min. at 15000 G. Protein concentration was determined with micro BCA™ Protein Assay Kit (Thermo Scientific, prod #23235). Trypsin/Lys-C Buffer was prepared by dissolving 0.1 μg/μL trypsin in 50 mM AmBic (Ammonium Bicarbonate, Cas nr.: 1066-33-7) and used to dilute samples 1:12 for trypsin digest. Samples were then placed in thermomixer with 400 rpm shaking at 37 °C for 12 hours, then kept at 4 °C. Reaction was stopped by addition of 10 μL 10 % TFA and centrifuged for 10 min at 20 °C and 4000 rpm (Heraeus, Multifuge X1R, centrifuge, Thermo Scientific). Desalting was done by stagetipping with C18 filter (Solaμ HRP 2mg/1ml 96 well plate, Thermo Scientific) plugs activated with 1x 100 μL MeOH (1 min at 1000 G at 20 °C), 1x 100 μL buffer B (80 % CH_3CN, 0.1 % Formic acid) (1 min at 1000 G at 20 °C) and 2x 100 μL buffer A´ (3 % CH_3CN, 1 % TFA) (1 min at 1000 G at 20 °C). Samples were spun through C18 column at 1500 G for 2 min at 20 °C and washed twice with 100 μL buffer A (0.1 % Formic acid), then spun down at 1500 G for 1 min at 20 °C. Next, samples were eluted with 2x50 μL buffer B for 1 min at 1000 G and reduced to 5 μL by running

on Eppendorf concentrator plus, at room temperature for 6 hours. Finally, peptide samples were resuspended in 40 μL of 0.1 % Formic acid and kept at 4 °C until MS-analysis.

MS analysis

Peptides were loaded onto a 2cm C18 trap column (ThermoFisher 164946), connected in-line to a 15cm C18 reverse-phase analytical column (Thermo EasySpray ES904) using 100% Buffer A (0.1% Formic acid in water) at 750bar, using the Thermo EasyLC 1200 HPLC system, and the column oven operating at 30°C. Peptides were eluted over a 70 minute gradient ranging from 10% to 60% of 80% acetonitrile, 0.1% formic acid at 250 nl/min, and the Orbitrap Exploris instrument (Thermo Fisher Scientific) was run in DIA mode with FAIMS Pro™ Interface (ThermoFisher Scientific) with CV of -45 V. Full MS spectra were collected at a resolution of 120,000, with an AGC target of 300% or maximum injection time set to 'auto' and a scan range of 400–1000 m/z. The MS2 spectra were obtained in DIA mode in the orbitrap operating at a resolution of 60.000, with an AGC target 1000% or maximum injection time set to 'auto', and a normalised HCD collision energy of 32. The isolation window was set to 6 m/z with a 1 m/z overlap and window placement on. Each DIA experiment covered a range of 200 m/z resulting in three DIA experiments (400-600 m/z, 600-800 m/z and 800-1000 m/z). Between the DIA experiments a full MS scan is performed. MS performance was verified for consistency by running complex cell lysate quality control standards, and chromatography was monitored to check for reproducibility.

Data analysis

The raw files were analyzed using Spectronaut™ (version 16.2) spectra were matched against the Uniprot *Pseudomonas aeruginosa* PAO1 proteome. Dynamic modifications were set as Oxidation (M) and Acetyl on protein N-termini. Cysteine carbamidomethyl was set as a static modification. All results were filtered to a 1 % FDR, and protein quantitation done on the MS1 level. The data was normalized by RT dependent local regression model [237] and protein groups were inferred by IDPicker. Subsequent analyses and exclusion criteria were kept the same as for clinical isolates.

Construction of aceEF mutants

DNA cloning

Derivatives of pACRISPR were constructed with the Uracil Specific Excision Reagent (USER) cloning [238]. For this method, primers were designed to create matching short overlaps between the DNA fragments that should be stitched together in the final plasmid. At the edges of these overlaps in the primers thymines were replaced with uracils. The plasmids are listed in Table S1, and primers in Table S2. Briefly, target DNA fragments were amplified with the primers using Phusion U polymerase kit (Thermo Fisher Scientific, USA). The resulting PCR products were treated with FastDigest DpnI enzyme (Thermo Fisher Scientific, USA) for 30 minutes at 37˚C to remove the template plasmid. Afterwards, USER® Enzyme (New England Biolabs, USA) was added to the mixture, which was further treated for 15 minutes at 37˚C, followed by stepwise decrease of 2˚C per minute until the temperature reached 10˚C. The mixture was then placed on ice and added to the ice-cold chemically competent *Escherichia coli* DH5alpha cells. After 30 minutes of incubation on ice, the cells were treated at 42˚C for 30 seconds, followed by 5 minutes on ice. Afterwards, SOC medium was added, cells were recovered for 1 hour at 37˚C with shaking, and finally seeded on LB agar plates supplemented with 100 µg/ml ampicillin. On the next day, PCR was performed with the random colonies using OneTaq® 2X Master Mix (New England Biolabs, USA) to confirm the correct insertions. Selected colonies were grown in liquid LB, plasmids were extracted from them using NucleoSpin Plasmid kit (Macherey Nagel, Germany) and sequenced with Sanger method (Eurofins Scientific, Luxembourg).

Genome editing

Precise mutations in the genome of *P. aeruginosa* PAO1 were introduced using the previously developed CRISPR-Cas9 system [239]. The system consists of two plasmids, pCasPA and pACRISPR. The first one, pCasPA, carries the genes necessary for cleaving DNA at specific sites (*cas9*), subsequent repair *via* recombination (λ-Red) and a counterselection marker for plasmid curing (*sacB*). The template for the introduction of target mutations and single guide RNA (gRNA) gene were inserted in plasmid pACRISPR. *P. aeruginosa* genome editing generally followed the original protocol [240]. Briefly, the cells were transformed with pCasPA plasmid *via* electroporation, as previously described [241] and selected on LB agar plates with 50 *µ*g/ml tetracycline. The resulting strain was further transformed with the appropriate derivative of

pACRISPR plasmid (Table S1) using the similar method but with the addition of 0.2% arabinose in the growth medium and plated with 50 μg/ml tetracycline and 150 μg/ml carbenicillin. For the second crossover the resulting colonies were grown in liquid LB at 37 ˚C for 2 hours, afterwards arabinose was added to 0.2% to induce the expression of the editing system. Cells were further incubated for 2 hours and streaked on LB agar plate containing 5% sucrose. On the next day colony PCR was used to confirm the presence of desired mutations. PCR fragment of the genome around the mutation was extracted with Zymoclean Gel DNA Recovery Kit (Zymo Research, USA) and sequenced with Sanger method (Eurofins Scientific, Luxembourg).

Phenotypic screening of aceEF mutants

Validation of pyruvate secretion

To further validate the *aceEF* mutants, pyruvate secretion was measured on HPLC-U1 as described above. 9 mL SCFM cultures were inoculated in 12 mL inoculation tubes and incubated at 37 C and 250 rpm in an orbital shaker. Samples were taken at 0, 4, 8 and 24 hours by measuring OD of 1 mL in cuvettes, transferring 850 μL to e. tubes, centrifuging at 21xG for 7 minutes at 4 C and transferring 750 μL supernatant to new e. tubes, which were stored at -80 C until HPLC.

MIC determination

MIC concentrations were determined by microdilution experiments. First, overnight cultures in SCFM and LB respectively were standardized to OD_{600} = 0.5 and serial diluted to a final dilution of 1:2500 to reach 5x 10^5 CFU/mL in 10 mL fresh media. From this inoculation, 190 μL were transferred to each well in columns of 96-well microtiter plates. Antibiotic stocks were set up with 20x the desired concentration in each well and 10 μL were added to the wells for a final volume of 200 μL. Growth curves were measured at 37 C and 250 rpm for 24 hours and MIC determined as the minimum concentration necessary to inhibit growth, shown as final OD.

Oxidative stress

3 mL of overlay LB agar (0.5 %) was inoculated with 100 μL of LB overnight culture standardized to OD_{600} = 1. The inoculated overlay agar was poured on a pre-cast LB agar plate and set to solidify for 10 minutes. Diffusion disks made of filter-paper was saturated with 5 μL of fresh 30 % H_2O_2 and placed in triplicate on the solidified overlay agar. Resistance to oxidative stress was measured as the diameter of the clearance zone around disks after incubation at 37 C for 24 hours.

Pyoverdine production

Overnight cultures were prepared in King's B medium. OD was measured and supernatant sampled by centrifugation at 17 G for 5 min. Relative pyoverdine concentration was measured as the fluorescence at 400/460 nm excitation/emission on a Synergy H1 Hybrid Multi-Mode Reader (BioTek Instruments, Winooski, VT, USA) and relative pyoverdine production calculated by normalizing against OD_{600}.

Biofilm formation

Potential for biofilm formation was assayed by measuring attachment ratio to NUNC peg lids [242]. Strains were grown at 37 °C at 150 rpm in Nunc 96-well plates with 150 μl of LB medium and sealed with parafilm to avoid evaporation. Peg lids (NUNC cat no. 445497) were used instead of the standard plate lids. After 24 hours, OD_{600} was measured and used as reference of planktonic growth. The peg lids were washed with 180 μl PBS and transferred for 15 min to a microtiter plate containing 160 μl of 0.01% crystal violet. The peg lids were then washed three times with 180 μl PBS to remove unbound crystal violet. The peg lids were transferred to a microtiter plate containing 180 μl of 99% ethanol, to detach the adhering cells from the peg lid and to read the OD_{590}. Surface attachment ratio was calculated as OD_{590}/OD_{600}.

Motility assay

LB agar motility plates were prepared with agar concentrations of 0.3 % (swimming), 0.6 % (swarming) and 1.5 % (twitching). Single colonies of the strains from LB plates were transferred with a sterile 10 μL pipette tip. For swimming plate, strain is deposited in the middle of the plate. For swarming, the colony is placed on the surface of the agar plate. For twitching, the colony is stabbed through the agar to the bottom of the plate. Motility was

measured as the diameter of the motility zone around the deposited colony after incubation at 37 C for 24 hours for swimming and swarming and 48 hours in the case of twitching.

Infection of ALI cultures

GFP-Tagging of *aceEF* mutants

aceEF mutants were tagged with GFP, following a previously described method for 4 parental mating using a mini Tn7 delivery-method [243]. Briefly, a conjugation mixture was prepared from overnight cultures in LB for the helper strains *E. coli* BF13 (100 μg/mL Ampicillin) and *E. coli* prK600 (6 μg/mL Chloramphenicol), as well as the *P. aeruginosa* target strain (No antibiotics) and *E. coli* Tn7(GFP)-vector strain (100 μg/mL Ampicillin) in a ratio of 1:1:1:3 and supplemented with prewarmed LB to final volume of 1 mL. The mixture was spun down at 7,000 G for 2 min. to avoid damage to surface pili required for conjugation and washed twice in 1 mL prewarmed LB. The conjugation mix was resuspended in 30 μL prewarmed LB and plated on a 13-mm cellulose acetate filter membrane placed on nonselective LB agar and incubated at 37 C overnight. After incubation, the bacterial lawn was resuspended in 200 μL LB and vortexed for 30-60 seconds. 100 μL of undiluted and 1:10 diluted suspension respectively was plated on selective *Pseudomonas* isolation agar plates with Gentamycin (30 μg/mL) and supplemented with 5 mM acetate to ensure growth of PDHc dysregulated target strains and incubated at 37 C overnight. Transformant colonies were identified by green fluorescence and grown in LB with gentamycin (30 μg/mL) for glycerol stocks. Identity of transformants was validated by comparing growth rate to the untagged target strain.

Cell culture

The human multipotent airway Basal Cell Immortalized Non-Smoker 1.1 (BCi-NS1.1) line was isolated from a bronchial brushing of a healthy non-smoker subject and immortalized using the retrovirus-mediated expression of human telomerase reverse transcriptase (hTERT) [244]. BCi-NS1.1 cells were cultured in Pneumacult-Ex Plus medium (STEMCELL Technologies, 05040) supplemented with Pneumacult-Ex 50x supplement (STEMCELL Technologies, 05008), 96 ng/mL hydrocortisone (STEMCELL Technologies, 07925) and 10 µM Y-27632 ROCK inhibitor (Bio-Techne #1254/10) in a 37°C, 5% CO_2 humidified incubator. Following expansion, 1.5 x 10^5

cells were seeded onto 6.5-diameter-size transwells with 0.4 μm pore polyester membrane inserts (Corning Incorporated, 3470) previously coated with human type I collagen (Gibco, A1048301). Air-Liquid Interface (ALI) was established once cells reached full confluency by removing media from the apical chamber and replacing media in the basolateral chamber with Pneumacult-ALI maintenance medium (STEMCELL Technologies, 05001). Pneumacult-ALI maintenance medium was supplemented with Pneumacult-ALI 10x supplement (STEMCELL Technologies, 05003), Pneumacult-ALI maintenance supplement (STEMCELL Technologies, 05006), 480 ng/mL hydrocortisone and 4 μg/mL heparin (STEMCELL Technologies, 07980). ALI cultures were grown in a 37 ºC, 5% CO_2 humidified incubator for 30 days, with media replacement every 2-3 days. Epithelial polarization was monitored by measurements of the transepithelial electrical resistance (TEER) using a chopstick electrode (STX2; World Precision Instruments). Following 15 days under ALI conditions, the apical surface was washed with 1x Phosphate Buffered Saline (PBS) every media change to remove accumulated mucus.

Bacteria and infection of ALI cultures

All strains were streaked from glycerol stocks onto lysogeny broth (LB) agar plates and grown at 37°C overnight. Following growth, a single colony was picked from the plate and grown overnight in LB medium at 37°C with agitation (220 rpm). Before infection, bacteria in the stationary phase were diluted to an OD_{600} of 0.05 grown in LB medium to the exponential phase (OD_{600} = 0.4 – 0.6), washed and resuspended in PBS at a density of 10^5 CFU/mL. Fully-differentiated BCi-NS1.1 cells were inoculated with 10^3 CFU from the apical side diluted in 10 μL PBS. Control wells were incubated with PBS-free bacteria. The initial inoculum was confirmed by plating serial dilutions on an LB-agar plate and counting the colonies. Cells were incubated for 14h at 37 ºC. Following infection, 200 μL of PBS was added to the apical side and the TEER was measured. This apical solution and the basolateral media were collected to quantify CFU on both chambers of the transwells. The apical and basolateral CFU were determined by platting 10 μL of 6-fold serial dilutions on LB-agar plates in technical replicates. Additionally, the basolateral media was collected for measuring LDH release (see Measurements of Lactate dehydrogenase (LDH) release section) and BCi-NS1.1 cells were stained (see Confocal Microscopy section).

Confocal Microscopy

BCi-NS1.1 cells on transwell inserts were rinsed once with PBS and fixed by adding 4% (wt/vol) paraformaldehyde (PFA) to both apical and basolateral chambers for 20 min at 4 °C. After washing, cells were permeabilized and blocked for 1 h with a buffer containing 3% Bovine Serum Albumin (BSA), 1% Saponin and 1% Triton X-100 in PBS. Cells were stained on the apical side with Phalloidin-AF488 (Invitrogen, 65-0863-14) and TO-PRO3 (Biolegend, 304008) diluted in a staining buffer (3% BSA and 1% Saponin in PBS) at a 1:500 dilution for 2h at room temperature. Transwells were removed from their supports with a scalpel and mounted on glass slides with VECTASHIELD® Antifade Mounting Medium (VWR, VECTH-1000). Images were acquired with a Carl Zeiss LSM 510 Confocal Laser Scanning Microscope (40× magnification, 1.3 oil) and analysed using the ImageJ software.

Measurements of Lactate dehydrogenase (LDH) release

Following infection, the LDH release was quantified to determine induced epithelial cytotoxicity, using the kit Invitrogen™ CyQUANT™ LDH Cytotoxicity Assay Kit (Invitrogen, C20301) according to the manufacturer´s instructions. LDH release was measured using 50 μL of basolateral media per sample in triplicates. The absorbance was measured at 680 nm and 490 nm.

Statistical Analysis

All statistical analyses were performed in GraphPad Prism 9 (GraphPad Software, CA, USA). Data are represented as mean ± standard error of the mean (SEM). Replicates represent independent experiments performed with cells from different passages. Statistical comparisons were calculated using Two-Way ANOVA for TEER and CFU measurements and One-Way ANOVA for LDH and IL-8 measurements. Statistical significance was considered for p-value < 0.05.

Figure legends

Figure 1: Selection of clinical isolates based on growth and WGS data

A) The growth rate (hour^{-1}) of each clinical isolate is shown as circles (early), triangles (late) and square (PAO1 control), coloured by clone type. The fold change from early to late clinical isolate of each clone type is shown as bar chart and as number value at the base of each bar. B) The maximal optical density (maxOD) of all isolates, grouped by early vs. late. Overall, maxOD is higher for early than for late isolates. Statistical significance was calculated by Unpaired Welch t-test and significance is indicated as *** ($p < 0.001$). C) Growth rate (hour^{-1}) of each strain in M9 minimal media containing 20 mM of a single carbon source glucose (Glu), lactate (Lac) or succinate (Suc). Growth rates are shown in coloured cell plot with a gradient from 0 (white) to 1.2 (dark blue) hour^{-1}. PAO1 is included under 'Early' and crossed out under 'Late'. D) Phylogenetic bootstrap consensus tree constructed by maximum parsimony analysis using the subtree-pruning-regrafting algorithm with search level 1, 10 replicates and a bootstrap consensus value of 50 % using the software MEGAX [245–247]. The tree was inferred from concatenated strings of 8600 positions in the genome containing non-intergenic SNPs in one or more strains, relative to PAO1 from WGS. Strain is indicated by the same symbols as panel a-b and by written clone type in blue (early) and red (late). E) Stacked bar chart showing the frequency of mutation types in each infection lineage by four categories: Indels (orange), Nonsense SNPs (blue), Missense SNPs (green) and Intergenic mutations (red). The total number of mutations (accumulated or reverted) in the specific infection lineage is written above each bar. F) Enrichment analysis of COG-categories from lists of mutated Locus Tags in each infection lineage, using the DAVID Functional Annotation Bioinformatics Microarray Analysis tool with the reference genome set as *Pseudomonas aeruginosa*. The fold-enrichment in each lineage is shown in purple boxes for all COG-categories enriched in one or more lineages.

Figure 2: Exometabolomic analysis shows adapted metabotypes characterized by secretion of acetate and pyruvate

A) Principal Component Analysis (PCA) showing the separation of strains based on their exo-metabolomes at 8 time-points in biological duplicates. Clinical isolates are shown as circles (early) and triangles (late) and coloured by clone type, while PAO1 is shown as a black square. Dashed arrows in the colour of the specific clone type shows some of the most noticeable

trajectories from early to late isolate in a given infection lineage. The analysis was done on covariance for concentrations of all 20 metabolites quantified. B) Hierarchical cluster analysis (HCA) of the same data, using Ward's method, showing a general separation into three clusters: 1) DK12-Late; 2) All other late isolates; and 3) All early isolates and PAO1. Early isolates are indicated as blue, late isolates as red and PAO1 as black. C) Assimilation hierarchies of each strain. Symbols/colours indicate strain, following the same system as panel A, and each dot represents the half-life (OD_{50}) of a specific metabolite mapped to a single x-axis showing OD in log-scale. The change in assimilation hierarchy during adaptation is indicated by semi-transparent lines in the colour of the clone type, connecting the half-life of a specific metabolite in the early isolate with its half-life in the corresponding late isolate. D) Secretion plots showing the concentrations of acetate, pyruvate and formate (mM) plotted against relative growth (OD_{600}), separated into early and late isolates. Clone types are indicated by colour, with shaded areas representing the 95 % confidence intervals. E) Table showing the total amount (mM) of carbon sources assimilated for each strain. Clone Types are separated by grey boxes with "E" indicating early and "L" indicating late isolate.

Figure 3: Proteomic analysis of metabolism for clinical isolates

A) Wide Principal Component Analysis (PCA) showing the separation of clinical strains based on correlation for proteomes at mid-exponential phase when grown in SCFM. Clinical isolates are shown as circles (early) and triangles (late) and coloured by clone type, while PAO1 is shown as a black square. Dashed arrows in the colour of the specific clone type shows some of the most noticeable trajectories from early to late isolate in a given infection lineage. Proteomes were defined as mean Log2(abundance) of five replicates for each of the 2061 proteins quantified by whole-cell proteomics. B) Dendrogram for Hierarchical Cluster Analysis (HCA) of the same data, using Ward's method, showing the same clustering as seen by PCA (cluster 1 containing DK03 early and late strains, cluster 3 containing the DK12, DK17, DK36 and DK55 late strains clearly separated by PCA and cluster 2 containing all remaining clinical strains along with the PAO1 reference strain). Clinical isolates are displayed the same as in panel A and labelled by clone type in blue (early), red (late) or black (PAO1). C) Dendrogram of the 8 infection lineages, based on the same method for Log2(fold-change) of the 235

proteins from COG categories related to metabolism that were found to be differentially expressed in at least one lineage (cluster A containing DK03, DK13, DK15 and DK41; cluster B containing DK12, DK17, DK36 and DK55). Clone types are displayed as circles following same colouring as panels A-B. D) Overlayed parallel plots showing the sum of instances of differentially expressed proteins in cluster A (Blue, shaded) compared with cluster B (red, transparent), broken down by COG categories related to metabolism. E) Metabolic maps showing the differences between early clinical strain vs PAO1 (left) and late vs early clinical strains (right) in pathways related to the catabolism of nutrients present in SCFM through central carbon metabolism. Arrows represent individual metabolite-conversions and are coloured by the pathway they belong to if at least one enzyme involved in that conversion is differentially expressed in more than one clone type – either with dashed (downregulated) or full (upregulated) lines, or both. Enzymes responsible for each reaction are indicated by numbered circles. For details on individual enzymes, see Figure S2. Transporters shown below the map as arrows crossing bacterial cell membrane with specific proteins labelled in parenthesis. Asp, Glu and Acetate are labelled with stars to indicate that they are represented in two places on the map, due to being involved in different parts of central carbon metabolism.

Figure 4: Proteomic analysis of virulence for clinical isolates

A) Enrichment analysis separated into KEGG and GO terms. Icons represent individual lineages, separated by specific the specific comparisons (Early vs. PAO1; Late vs. PAO1; Late vs. Early) and coloured by fold-enrichment. Red indicates the fold-enrichment of upregulated proteins, while blue indicates the fold-enrichment of downregulated proteins. B) Differential expression of virulence factors in early clinical strains vs. PAO1. Icons represent specific differentially expressed proteins, coloured by lineage and separated by category. The y-axis indicates Log2(Fold change). C) Differential expression of virulence factors in late vs. early clinical strains, shown by hierarchical cluster analysis of differentially expressed proteins separated into alginate biosynthesis, phenazine biosynthesis, PQS and T6SS respectively. Colour indicates Log2(Fold change), red for upregulated and blue for downregulated proteins.

Figure 5: Phenotypic screening of *aceEF* mutants and effects of acetate supplementation

A) Schematic of the location and type of mutation for the *aceE* (left) and *aceF* (right) clinical mutations found in DK36 and DK12 late strains and inserted into PAO1 wild type respectively. B) Growth rate ($hour^{-1}$) in SCFM2 (blue) and SCFM2 supplemented with 5 mM acetate (red) for PAO1 wt and *aceEF* mutant strains, as well as the DK12 & DK36 late clinical isolates carrying each mutation respectively. Icons represent biological replicates. Significance of differences in growth rate for each strain grown in SCFM2 +/- acetate was assessed by two-tailed unpaired parametric Welch t-test and indicated as * ($p < 0.05$), ** ($p < 0.01$) or **** ($p < 0.0001$). C) Pyruvate secretion (mM) of PAO1 wt (yellow), as well as *aceE* (cyan) and *aceF* (magenta) mutant strains after 4, 8 and 24 hours of growth in SCFM2. Icons represent biological replicates. D) PCA and HCA of whole-cell proteomics. Icons indicate the proteomes of strains grown in SCFM2 in presence (unfilled) and absence (filled) of acetate. HCA dendrogram is shown in top right corner of PCA plot. E) Number of differentially expressed proteins for each strain, when comparing the same strain grown in presence vs. absence of acetate (purple) or when comparing each mutant strain to the PAO1 reference, either in absence (orange) or presence (green) of acetate. F) Subset of metabolic map seen on Fig. 3 with arrows indicating differential expression of metabolic enzymes related to pyruvate and acetyl-CoA metabolism for mutant strains vs. PAO1 in absence (left) or presence (right) of acetate. G) Differential expression of virulence factors in the *aceE* (left) and *aceF* (right) mutant strains vs. PAO1 in SCFM2 without acetate. Icons indicate specific proteins that are upregulated (red plus) or downregulated (blue circle).

Figure 6**:** PAO1 *aceF* shows a decreased ability of infecting airway epithelial cells

A) Mean ± SEM for Transepithelial Electrical Resistance (TEER) ($\Omega \cdot cm^2$) indicating tight-junction disruption, LDH release into the basolateral media indicating cytotoxicity and Colony Forming Units (CFU) in the apical and basolateral ALI compartments, as well as B) IL-8 release into the basolateral media indicating immunogenicity caused by the invading bacteria following 14 hours of infection with the different strains in fully-differentiated BCi-NS1.1 cells and of the TEER before infection. Icons indicate biological replicates of PAO1 (yellow), *aceE* (cyan), *aceF* (magenta), Δ*pscC* (green) and empty control 'Mock' (black). Statistical

significance was determined by Two-Way ANOVA for TEER and CFU measurements and One-Way ANOVA for LDH and IL-8 measurements and indicated as * ($p < 0.05$), ** ($p < 0.01$), *** ($p < 0.001$) and **** ($p < 0.0001$). C) Confocal images of ALI transwells following infection with *P. aeruginosa* in green (GFP), epithelium in red (Phalloidin) and nuclei in blue (To-pro). Scale bar = 40 μm.

Acknowledgements

The work was supported by the Novo Nordisk Foundation (NNF Grant number: NNF20CC0035580) and the CF Trust.

Proteomics was carried out by the DTU Biosustain Analytics Core for clinical isolates and by the DTU Bioengineering Proteomics Core for mutant strains.

The Basal Cell Immortalized Non-Smoker 1.1 (BCi-NS1.1) cell line was a kind gift from Professor Ronald G. Cristal (Weil Cornell Medical College, New York, USA).

Chapter 4: Discussion

4.1 Clinical strains show EPS-LPS switching consistent with itaconate utilizing phenotype

The reduced flux of pyruvate through the PDHc caused by increased inhibition by PDK is known to disrupt TCA activity and divert the citrate-derived *cis*-aconitate toward the production of itaconate [227,231], which is a central metabolite in regulating the immune response [223,224]. Itaconate also has direct antibacterial properties, interfering with their metabolism through inhibition of both the enzyme Isocitrate Lyase and the ability to assimilate acetate [223]. It has been suggested that *P. aeruginosa* has a relatively unique genetic ability to adapt metabolically to utilize itaconate for biofilm production, while replacing LPS with EPS to induce further itaconate production, turning immune cells into feeder cells that help sustain *P. aerugionsa* biofilms [233], while presumably making the environment more hostile for competing microbes. This LPS to EPS switching phenotype was reported based on increased gene-expression of the EPS-associated *algADRUQ* and *pelA* genes and a reduced expression of the LPS-associated *wbpAGY* genes. This is consistent with what we see for protein expression in all clinical strains compared to PAO1 – but especially in the case of DK03, which may be related to its atypical proteome allocation. Figure 10 shows a schematic of the proposed interaction, as well as the differential expression of EPS and LPS related genes and proteins in Riquelme *et al.*, (2020) and the current study, respectively.

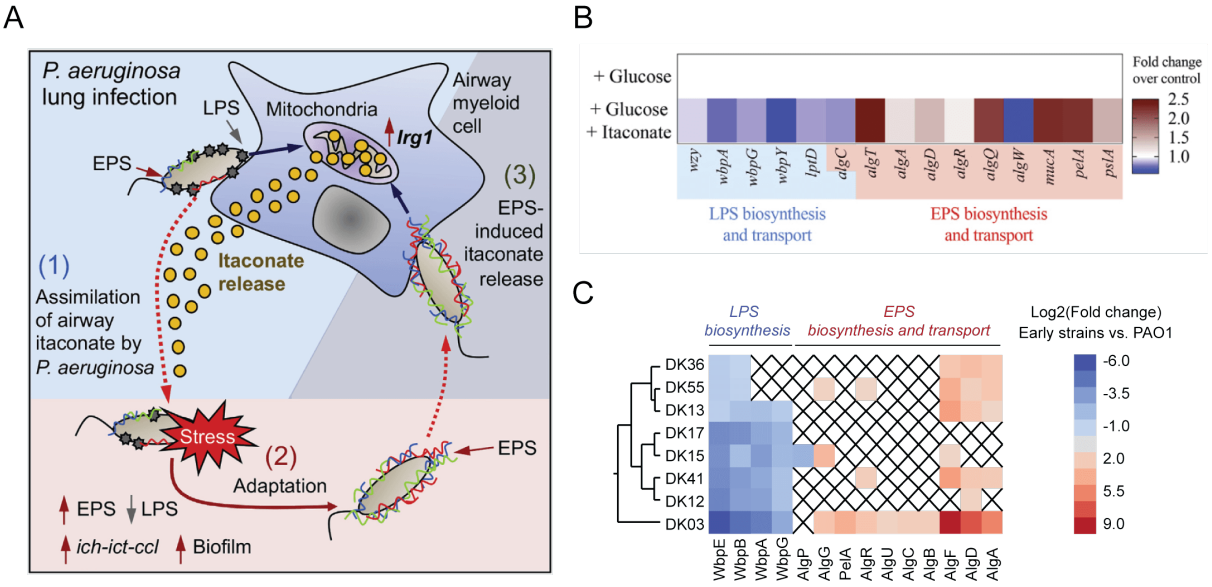

Figure 10: Panel A-B from Riquelme et al. (2020), Cell Metabolism. A) Schematic of the proposed mechanism for hijacking of host immune cells. B) LPS and EPS related genes found to be expressed at decreased and increased levels respectively are also differentially expressed in same direction for PAO1 in Glucose, when supplemented with Itaconate. C) Differential expressions of LPS and EPS related proteins follow same pattern in early clinical isolates vs PAO1 (Same holds for late strains vs PAO1).

It is beyond the scope of this thesis to delve into this type of host-pathogen interactions in more detail. However, future work is necessary to determine how the modulated secretion of pyruvate by *P. aeruginosa* may affect the immune system during chronic infections.

4.2 Pseudomonas Quinolone System (PQS) upregulated in clinical strains

The biggest difference in protein expression between clinical strains (early and late) and PAO1, both in terms of abundance and convergence, is the downregulation of the four LPS O-antigen related proteins WbpABEG discussed in the previous section and the upregulation of the four PQS related proteins PqsABCD (See Appendix C). PQS is one of three quorum sensing systems important for chronic infections [248], iron acquisition, cytotoxicity, outer-membrane vesicle biogenesis, and modulation of the host immune system [117], as well as stimulating the destruction of damaged cells and reducing metabolic activity in response to oxidative stress [118]. Because of its crucial role in regulating virulence, the PQS system has been heavily studied as a potential target for development of novel antimicrobials, although most of the focus has been on PqsR [248–255]. Another potential target that has been heavily studied is PqsE, which regulates most traits controlled by the transcription factor RhlR [248,256–258] and is required for the expression of H3-T6SS [108,259]. However, neither of these potential targets show any differential expression in clinical strains, with PqsE being the only protein of the *pqsABCDE* operon where this is the case.

PqsD, which we do find to be convergently and substantially upregulated in all 16 clinical strains, has also been suggested as a potential target for the phage-protein Qst which, in addition to facilitating infection, leads to reprogramming of acetyl-CoA related metabolism and inhibits cell division in *P. aeruginosa* [260]. The highly convergent and substantial upregulation of PqsD in clinical strains, in contrast with the lack of any differential expression observed for PqsR and PqsE, may suggest it holds more promise as a potential target for antibacterial therapies aimed at *P. aeruginosa* CF airway infections.

4.3 Dnr is downregulated in adapted metabotypes

The Dnr transcriptional regulator is mainly known for being required for denitrification [261–264] in *P. aeruginosa* but has also been implicated in the regulation of H2-T6SS [265] and AckA [71]

under anaerobic conditions similar to those of the CF lungs. AckA is one of the enzymes required for converting acetate to acetyl-CoA, which presumably is what re-establishes normal growth rates in PDHc dysregulated strains by replacing pyruvate with acetate as a source of acetyl-CoA, allowing continued TCA activity. Figure 11 shows the differential expression of Dnr in late clinical strains and the *aceE* mutant strain, as well as a schematic of the conversion of pyruvate and acetate into acetyl-CoA.

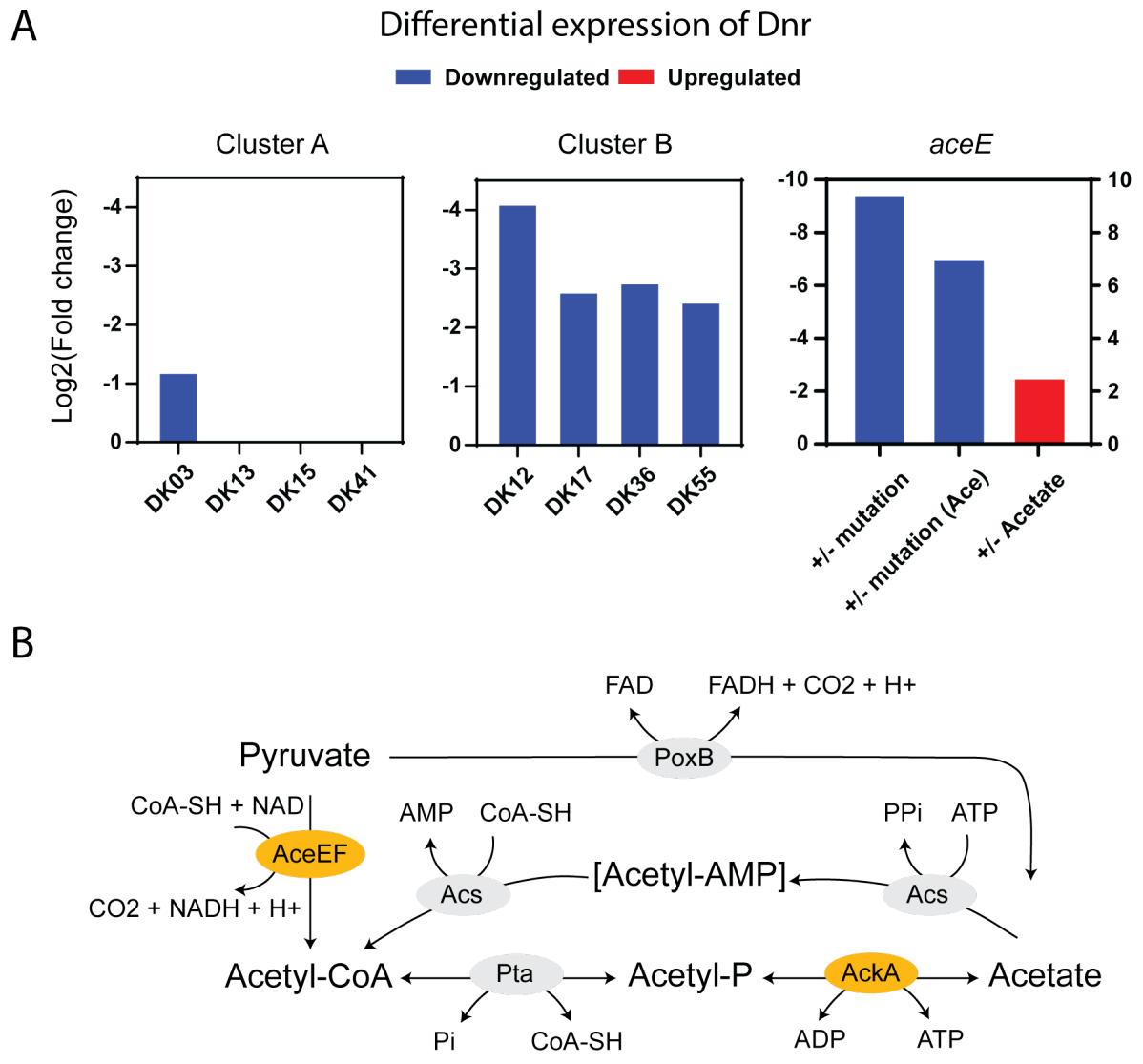

Figure 11: A) The -Log2(Fold change) of the Dnr transcriptional regulator in late vs early clinical isolates (Same holds for late strains vs PAO1) for lineages in Cluster A (left) and B (middle), as well as in the aceE mutant strain (right) when compared to PAO1 wt in SCFM2 in absence (+/- mutation) and presense (Ace) of acetate or when compared to itself in presence of acetate (+/- Acetate). B) Schematic showing the metabolism of pyruvate and acetate as it relates to the TCA cycle with the roles of aceEF and AckA coloured orange.

Interestingly, Dnr is extremely downregulated by insertion of the *aceE* clinical mutation and slightly upregulated by acetate supplementation. However, it is completely unaffected by

insertion of the *aceF* clinical mutation. Moreover, Dnr was specifically downregulated in the late clinical strains of all lineages with proteome allocations that cluster separately from the typical PAO1-like cluster but not in any of the early strains, suggesting some adaptive role for reduced expression of Dnr in the CF airways, potentially making it a relevant target for novel therapies aimed at reducing fitness of the chronic infections.

4.4 BfmRS may coordinate metabolism and virulence mediated by Acetyl-P

One potential mechanism for the regulation of virulence through PDHc mutations is the Two-Component system BfmRS, which is an orthologue of the RhpRS system in *Pseudomonas syringae*, where it coordinates metabolism and virulence in response to environmental conditions [266–268], as seen on Figure 12.

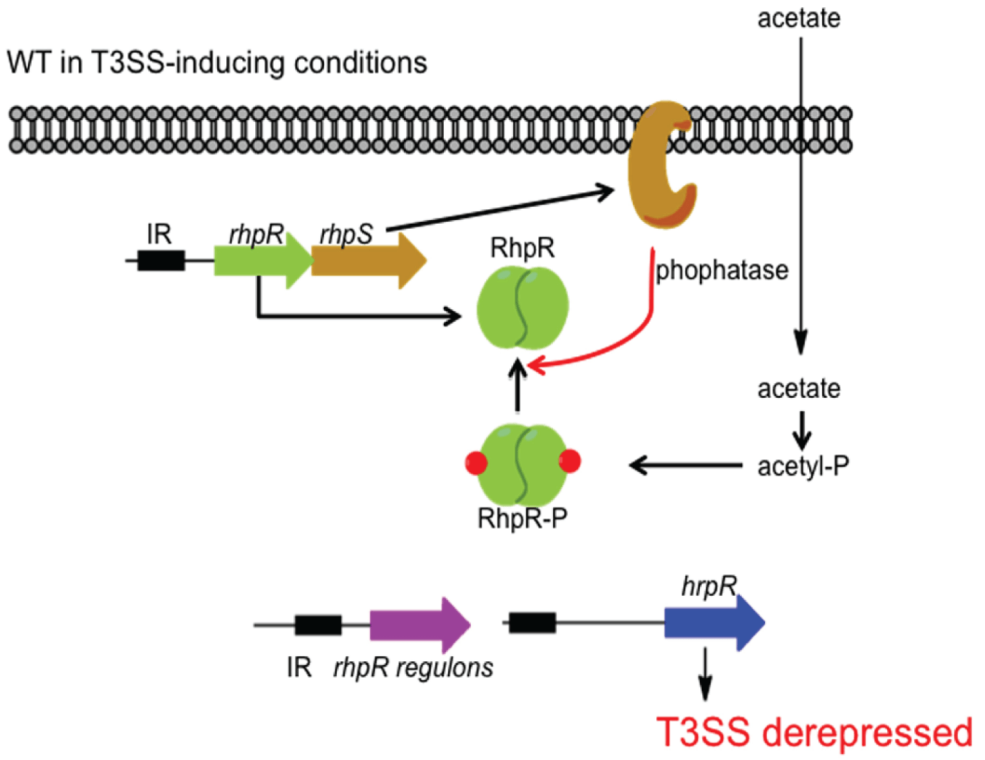

Figure 12: Deng et al. (2014), Nucleic acids research. Schematic of proposed model for acetyl-P mediated RhpRS regulation of T3SS in P. syringae.

This system is regulated in part by endogenous acetyl-P levels, which can be modulated by supplementation with acetate [266], since acetyl-P is an intermediary product of the conversion of acetate to acetyl-CoA. Thus, when acetyl-CoA is depleted in PDHc dysregulated strains, due to their inability to derive it from pyruvate, this would lead to reduced levels of acetyl-P and

potentially inhibit the BfmRS virulence response. Conversely, acetate supplementation should restore normal physiological levels of acetyl-P in the cell, reactivating its capacity for this virulence response. Notably, the *bfmRS* genes are wholly deleted early in certain infection lineages of *P. aeruginosa* CF airway infections [18] but are fully intact in both early and late clinical strains of the Clone Types DK12, DK36 & DK55 where we see dysregulation of PDHc in the current study, supporting the idea that suppressing this system is pathoadaptive. It may be that the metabolic mutations in PDHc provides an alternative mechanism for inhibition of this system in a less all-or-nothing way than complete deletion of the genes, allowing modulation and coordination with metabolism and growth phenotype for the virulence response in a way that is more responsive to changes in the environment.

4.5 Pyruvate plays an important role in many different types of pathologies

Pyruvate is a metabolite of critical importance in almost all living cells due to its role as master fuel for the highly conserved central carbon metabolism of the TCA cycle and as such plays an important role in many different areas of human health and disease [269]. Several studies have suggested treatments targeted toward the activity of PDHc and regulation of pyruvate in different contexts. For example, PDK-mediated inhibition of PDHc has been suggested both as a potential anti-inflammation therapy for chronic metabolic diseases [220] and as a cancer treatment by targeting the metabolic Warburg effect in tumour cells, which functions very similar to the overflow metabolism observed here for *P. aeruginosa* [221]. Conversely, treatment with active PDHc for the depletion of pyruvate has been suggested as anti-biofilm therapy against *P. aeruginosa* infections [219]. Indeed, pyruvate has also been associated with biofilm formation in several pathogens other than *P. aeruginosa*, including *E. coli, S. aureus*, *Clostridioides difficile*, *Candida albicans*, *Candida tropicalis* and *Streptococci* [270–277]. Recently, pyruvate has also been studied as a potential biomarker for Covid-19 due to high circulation in critically ill patients [278]. All this suggests a highly complex and near universal role of pyruvate in a diverse set of pathologies, which must be taken into consideration when designing treatments targeted at its role in one specific context.

Chapter 5: Conclusion and future directions

The aims of this project were to:

- Develop a method for high-throughput dynamic metabolomic screening of large collections of isolates for differences in metabolic profiles.
- Apply this method to search for adaptive metabotypes in clinical isolates of *P. aeruginosa* CF airway infections.
- Study the effects of the candidate pathoadaptive genes *aceEF* in a clean genetic background.

In summary, the dilution-based method for high-throughput sampling accurately captures the metabolic dynamics of low-throughput time-resolved methods and allows for more detailed and direct analysis of metabolic variation in large collections of strains than was previously feasible. This approach could be enhanced with few modifications by integrating it with automated liquid handling robots, making it feasible to scale up experiments to test numerous different variables including how variations in media composition affects the metabolism of different lineages. By applying this method to clinical strains of different infection scenarios before and after the substantial decrease in growth rates typical of chronic phenotypes, I was able to identify a general adapted metabotype common for all scenarios, characterized by the secretion of acetate and increased assimilation of amino acids, and a more specific one, characterized in part by the secretion of pyruvate, for lineages with impactful mutations in the *aceEF* genes encoding the key metabolic regulator pyruvate dehydrogenase. Inserting these clinical mutations in the PAO1 clean genetic background demonstrated their pathoadaptive nature by recapitulating the chronic phenotype to varying degrees. Beyond the reduction in growth rate and secretion of pyruvate, *aceEF* mutations also led to an upregulation of T6SS and biosynthesis of phenazines and alginate, as well as a reduction in T3SS and bacterial recognition by host cells.

Further studies are required to elucidate how these changes are modulated by the specific effects of the many different missense SNPs in *aceEF* genes seen for different infection lineages. For example, it may be interesting to couple enzymatic assays of the specific activity of different PDHs with competition assays of mutant strains in infection models to see if the specific activity of the enzyme is balanced around some fitness peak. It would also be very

interesting to see how much of the naïve phenotype can be restored by inserting fully functional *aceEF* genes in the clinical strains to determine the extent to which the chronic phenotype is under direct control of PDHc activity in strains that have many more adaptive mutations accumulated in concert with *aceEF*. Additionally, although *aceEF* mutant strains did not show increased antibiotic resistance, the question still remains if the altered metabolism and growth dynamics could confer some degree of antibiotic tolerance to the strains by promoting the survival of a small number of cells that may then regrow once antibiotic treatment has been suspended. Moreover, the effects that different pyruvate secretion profiles by *P. aeruginosa* may have on host immune cells require further study in infection models that more accurately capture the host-pathogen interactions *in vivo* e.g. by introducing immune cells to the ALI culture model. More work is also required to decipher the exact mechanism by which *aceEF* mutations affect e.g. virulence factors in the transition to the chronic phenotype. For example, double mutants of *aceEF* and the regulators *bfmRS* or *dnr* respectively may help determine if either of these regulatory systems mediate the effects PDHc dysregulation on virulence and help explain the broader physiological consequences in more detail. Additionally, it would be interesting to measure the effects of *aceEF* mutations on endogenous acetyl-P levels. Acetyl-P is an important signalling molecule involved in many different regulatory systems related to virulence [211,279–281] and the fact that it is also an intermediate of the conversion between acetate and acetyl-CoA makes it likely to be affected by the reduced acetyl-CoA production caused by mutations in PDHc.

Another emerging application of the large data sets that are becoming more and more feasible to generate with the increase in high-throughput methods is the construction of Genome-Scale Models that integrate genomic, transcriptomic, proteomic and metabolomic data to construct *in silico* models of organisms that predict behaviour under novel conditions [282,283]. Although mainly applied in *E. coli* due to the amount of knowledge and data available for this organism, the method has also been used e.g. to predict gene essentiality and links between growth and virulence in the PAO1 and PA14 laboratory strains [284]. In principle, the WGS data already available for clinical strains, along with the proteomic and metabolomic data generated in the current study could be integrated with further studies to generate strain-specific metabolic network models of *P. aeruginosa* that take into account different clinically relevant evolutionary histories.

Metabolism is the most foundational and conserved aspect of biology across all living organisms. In particular, the biochemistry of the TCA cycle and its role in the production of energy remains much the same for widely different organisms. This gives changes in metabolism a certain reach to affect physiological changes both endogenously and by interference for a wide array of organisms, including both host and pathogen cells. Since pathogens like *P. aeruginosa* are actually evolving during infections, whereas the host is not, this presents a highly asymmetrical set of opportunities for the pathogen to adapt its metabolism to the host environment, including changes that directly interfere with the host metabolism. Such changes can be further coordinated with endogenous changes, e.g. the formation of biofilm as may be the case for the altered flux of pyruvate in *P. aeruginosa* persistent infections supported by overflow metabolism from assimilation of large amounts of amino acids from the environment. One promising albeit preliminary finding that is worth noting is that the CFTR modulator treatment Trikafta seems to reduce the concentration of amino acids in the CF airway sputum, which may help undermine the fitness of these adapted metabotypes, reshaping the niche space to require different metabotypes for achieving chronicity in the future [285].

Although the challenge of eradicating persistent airways infections of *P. aeruginosa* in patients with CF is itself of great importance, this reach and foundational nature of metabolic adaptations makes them likely to be of general importance beyond the specific bacterial species or underlying disease. Thus, to help address the antimicrobial resistance crisis, future research into the development of persistent infections must include a more detailed understanding of what metabolic strategies are available to the infecting pathogens and how those strategies can be effectively undermined.

References

1. United Nations Global Compact & KPMG. Healthcare & Life Sciences New. *SDG Industry Matrix* (2015).
2. O'Neill, J. Tackling Drug-resistant Infections Globally: Final Report and Recommendations. *Review on Antimicrobial Resistance* (2016).
3. de Kraker, M. E. A., Stewardson, A. J. & Harbarth, S. Will 10 Million People Die a Year due to Antimicrobial Resistance by 2050? *PLoS Med* **13**, (2016).
4. Murray, C. J. *et al.* Global burden of bacterial antimicrobial resistance in 2019: a systematic analysis. *Lancet* **399**, 629–655 (2022).
5. Towse, A. & Bonnifield, R. S. An Ambitious USG Advanced Commitment for Subscription-Based Purchasing of Novel Antimicrobials and Its Expected Return on Investment. *Center for Global Development* (2022).
6. Theuretzbacher, U., Outterson, K., Engel, A. & Karlén, A. The Global Preclinical Antibacterial Pipeline. *Nat Rev Microbiol* **18**, 275–285 (2020).
7. Dheman, N. *et al.* An Analysis of Antibacterial Drug Development Trends in the United States, 1980-2019. *Clin Infect Dis* **73**, E4444–E4450 (2021).
8. Theuretzbacher, U. *et al.* Analysis of the clinical antibacterial and antituberculosis pipeline. *Lancet Infect Dis* **19**, e40–e50 (2019).
9. Butler, M. S. *et al.* Analysis of the Clinical Pipeline of Treatments for Drug-Resistant Bacterial Infections: Despite Progress, More Action Is Needed. (2022).
10. Jonas, O. B., Irwin, A., Berthe, F. C. J., Le Gall, F. G. & Marquez, P. V. *Drug-resistant infections: a threat to our economic future (Vol. 2)*. (2017).
11. Bonnifield, R. S. & Towse, A. Estimating the European Union's Return on Investment from an Ambitious Program to Incentivize New Antibiotics. *Center for Global Development* (2022).
12. Bonnifield, R. S. & Towse, A. Estimating the UK's Return on Investment from an Ambitious Program to Incentivize New Antibiotics. *Center for Global Development* (2022).
13. Bonnifield, R. S. & Towse, A. Estimating Canada's Return on Investment from an Ambitious Program to Incentivize New Antibiotics. *Center for Global Development* (2022).
14. Bonnifield, R. S. & Towse, A. Estimating Japan's Return on Investment from an Ambitious Program to Incentivize New Antibiotics. *Center for Global Development* (2022).
15. Centers for Disease Control and Prevention. Covid-19 U.S. Impact on Antimicrobial Resistance. *Atlanta, GA: U.S. Department of Health and Human Services, CDC; 2022.* 1–44 (2022).
16. Shrivastava, S. R., Shrivastava, P. S. & Ramasamy, J. Global priority list of antibiotic-resistant bacteria to guide research, discovery, and development of new antibiotics. *JMS - Journal of Medical Society* **32**, 76–77 (2018).
17. Rice, L. B. Federal funding for the study of antimicrobial resistance in nosocomial pathogens: No ESKAPE. *Journal of Infectious Diseases* vol. 197 1079–1081 Preprint at https://doi.org/10.1086/533452 (2008).
18. Marvig, R. L., Sommer, L. M., Molin, S. & Johansen, H. K. Convergent evolution and adaptation of Pseudomonas aeruginosa within patients with cystic fibrosis. *Nat Genet* **47**, 57–64 (2015).
19. la Rosa, Johansen & Molin. Adapting to the Airways: Metabolic Requirements of Pseudomonas aeruginosa during the Infection of Cystic Fibrosis Patients. *Metabolites* **9**, 234 (2019).
20. Folkesson, A. *et al.* Adaptation of Pseudomonas aeruginosa to the cystic fibrosis airway: An evolutionary perspective. *Nat Rev Microbiol* **10**, 841–851 (2012).
21. Ahlgren, H. G. *et al.* Clinical outcomes associated with Staphylococcus aureus and Pseudomonas aeruginosa airway infections in adult cystic fibrosis patients. *BMC Pulm Med* **15**, (2015).
22. Cystic Fibrosis Foundation. 2018 Patient Registry Annual Data Report. *Cystic Fibrosis Foundation Patient Registry 2018 Annual Data Report* 92 (2018).
23. Rossi, E. *et al.* Pseudomonas aeruginosa adaptation and evolution in patients with cystic fibrosis. *Nat Rev Microbiol* (2020) doi:10.1038/s41579-020-00477-5.

24. Johansen, H. K. *et al.* Antibody response to Pseudomonas aeruginosa in cystic fibrosis patients: a marker of therapeutic success?--A 30-year cohort study of survival in Danish CF patients after onset of chronic P. aeruginosa lung infection. *Pediatr Pulmonol* **37**, 427–432 (2004).

25. Habib, A. R. R. *et al.* A Systematic Review of the Clinical Efficacy and Safety of CFTR Modulators in Cystic Fibrosis. *Sci Rep* **9**, 1–9 (2019).

26. Molinski, S. v *et al.* Orkambi(R) and amplifier co-therapy improves function from a rare CFTR mutation in gene-edited cells and patient tissue. *EMBO Mol Med* **9**, 1224–43 (2017).

27. van Goor, F. *et al.* Rescue of CF airway epithelial cell function in vitro by a CFTR potentiator, VX-770. *Proc Natl Acad Sci USA* **106**, 18825–30 (2009).

28. van Goor, F. *et al.* Correction of the F508del-CFTR protein processing defect in vitro by the investigational drug VX-809. *Proc Natl Acad Sci USA* **108**, 18843–8 (2011).

29. Armstrong, D. K., Cunningham, S., Davies, J. C. & Alton, E. W. F. W. Gene therapy in cystic fibrosis. *Arch Dis Child* **99**, 465–8 (2014).

30. Elborn, J. S. Personalised medicine for cystic fibrosis: treating the basic defect. *Eur Respir Rev* **22**, 3–5 (2013).

31. Quon, B. S. & Rowe, S. M. New and emerging targeted therapies for cystic fibrosis. *BMJ* **352**, i859 (2016).

32. Chaudary, N. Triplet CFTR modulators: future prospects for treatment of cystic fibrosis. *Ther Clin Risk Manag* **14**, 2375–2383 (2018).

33. Frost, F. J., Nazareth, D. S., Charman, S. C., Winstanley, C. & Walshaw, M. J. Ivacaftor Is Associated with Reduced Lung Infection by Key Cystic Fibrosis Pathogens. A Cohort Study Using National Registry Data. *Ann Am Thorac Soc* **16**, 1375–1382 (2019).

34. Gifford, A. H. & Heltshe, S. L. Does ivacaftor taken twice a day keep the pseudomonas away? *Ann Am Thorac Soc* **16**, 1366–1367 (2019).

35. Allison, K. R., Brynildsen, M. P. & Collins, J. J. Metabolite-enabled eradication of bacterial persisters by aminoglycosides. *Nature* **473**, 216–220 (2011).

36. Brynildsen, M. P., Winkler, J. A., Spina, C. S., MacDonald, I. C. & Collins, J. J. Potentiating antibacterial activity by predictably enhancing endogenous microbial ROS production. *Nat Biotechnol* **31**, 160–165 (2013).

37. Stokes, J. M., Lopatkin, A. J., Lobritz, M. A. & Collins, J. J. Bacterial Metabolism and Antibiotic Efficacy. *Cell Metab* **30**, 251–259 (2019).

38. Zheng, E. J., Stokes, J. M. & Collins, J. J. Eradicating Bacterial Persisters with Combinations of Strongly and Weakly Metabolism-Dependent Antibiotics. *Cell Chem Biol* **27**, 1–9 (2020).

39. Lopatkin, A. J. *et al.* Bacterial metabolic state more accurately predicts antibiotic lethality than growth rate. *Nat Microbiol* **4**, 2109–2117 (2019).

40. Crabbé, A., Jensen, P. Ø., Bjarnsholt, T. & Coenye, T. Antimicrobial Tolerance and Metabolic Adaptations in Microbial Biofilms. *Trends Microbiol* **27**, 850–863 (2019).

41. Lopatkin, A. J. *et al.* Clinically relevant mutations in core metabolic genes confer antibiotic resistance. *Science (1979)* **0862**, 1–8 (2021).

42. Schrader, S. M. *et al.* Multiform antimicrobial resistance from a metabolic mutation. *Sci Adv* **7**, (2021).

43. la Rosa, R., Johansen, H. K. & Molin, S. Convergent metabolic specialization through distinct evolutionary paths in Pseudomonas aeruginosa. *mBio* **9**, (2018).

44. Crone, S. *et al.* The environmental occurrence of Pseudomonas aeruginosa. *Apmis* 1–12 (2019) doi:10.1111/apm.13010.

45. Walker, T. S. *et al.* Pseudomonas aeruginosa-plant root interactions. Pathogenicity, biofilm formation, and root exudation. *Plant Physiol* **134**, 320–331 (2004).

46. Mushin, R. & Ziv, G. An epidemiological study of Pseudomonas aeruginosa in cattle and other animals by pyocine typing. *J Hyg (Lond)* **71**, 113–122 (1973).

47. Haenni, M. *et al.* Population structure and antimicrobial susceptibility of Pseudomonas aeruginosa from animal infections in France. *BMC Vet Res* **11**, (2015).

48. Eklöf, J. *et al.* Pseudomonas aeruginosa and risk of death and exacerbations in patients with chronic obstructive pulmonary disease: an observational cohort study of 22 053 patients. *Clin Microbiol Infect* **26**, 227–234 (2020).

49. Barbier, F., Andremont, A., Wolff, M. & Bouadma, L. Hospital-acquired pneumonia and ventilator-associated pneumonia: recent advances in epidemiology and management. *Curr Opin Pulm Med* **19**, 216–228 (2013).

50. Kerr, K. G. & Snelling, A. M. Pseudomonas aeruginosa: a formidable and ever-present adversary. *J Hosp Infect* **73**, 338–344 (2009).

51. Silby, M. W., Winstanley, C., Godfrey, S. A. C., Levy, S. B. & Jackson, R. W. Pseudomonas genomes: diverse and adaptable. *FEMS Microbiol Rev* **35**, 652–680 (2011).

52. Ball, C. A. *et al.* Integrating functional genomic information into the Saccharomyces Genome Database. *Nucleic Acids Res* **28**, 77 (2000).

53. Freschi, L. *et al.* The Pseudomonas aeruginosa Pan-Genome Provides New Insights on Its Population Structure, Horizontal Gene Transfer, and Pathogenicity. *Genome Biol Evol* **11**, 109 (2019).

54. Turner, K. H., Wessel, A. K., Palmer, G. C., Murray, J. L. & Whiteley, M. Essential genome of Pseudomonas aeruginosa in cystic fibrosis sputum. *Proceedings of the National Academy of Sciences* **112**, 4110–4115 (2015).

55. Klockgether, J., Cramer, N., Wiehlmann, L., Davenport, C. F. & Tümmler, B. Pseudomonas aeruginosa Genomic Structure and Diversity. *Front Microbiol* **2**, (2011).

56. Stewart, L. *et al.* Draft genomes of 12 host-adapted and environmental isolates of Pseudomonas aeruginosa and their positions in the core genome phylogeny. *Pathog Dis* **71**, 20–25 (2014).

57. Frimmersdorf, E., Horatzek, S., Pelnikevich, A., Wiehlmann, L. & Schomburg, D. How Pseudomonas aeruginosa adapts to various environments: a metabolomic approach. *Environ Microbiol* **12**, 1734–1747 (2010).

58. Nikel, P. I., Martínez-García, E. & de Lorenzo, V. Biotechnological domestication of pseudomonads using synthetic biology. *Nat Rev Microbiol* **12**, 368–379 (2014).

59. Alonso, A., Rojo, F. & Martínez, J. L. Environmental and clinical isolates of Pseudomonas aeruginosa show pathogenic and biodegradative properties irrespective of their origin. *Environ Microbiol* **1**, 421–430 (1999).

60. Dolan, S. K. *et al.* Contextual flexibility in pseudomonas aeruginosa central carbon metabolism during growth in single carbon sources. *Molecular Biology and Physiology* **11**, 1–20 (2020).

61. Perinbam, K., Chacko, J. v., Kannan, A., Digman, M. A. & Siryaporn, A. A Shift in Central Metabolism Accompanies Virulence Activation in Pseudomonas aeruginosa. *mBio* **11**, (2020).

62. May, T. B. & Chakrabarty, A. M. Pseudomonas aeruginosa: genes and enzymes of alginate synthesis. *Trends Microbiol* **2**, 151–157 (1994).

63. Chubukov, V., Gerosa, L., Kochanowski, K. & Sauer, U. Coordination of microbial metabolism. *Nat Rev Microbiol* **12**, 327–340 (2014).

64. Yang, L. *et al.* In situ growth rates and biofilm development of Pseudomonas aeruginosa populations in chronic lung infections. *J Bacteriol* **190**, 2767–2776 (2008).

65. Palmer, K. L., Aye, L. M. & Whiteley, M. Nutritional cues control Pseudomonas aeruginosa multicellular behavior in cystic fibrosis sputum. *J Bacteriol* **189**, 8079–8087 (2007).

66. Singh, R., Mailloux, R. J., Puiseux-Dao, S. & Appanna, V. D. Oxidative stress evokes a metabolic adaptation that favors increased NADPH synthesis and decreased NADH production in Pseudomonas fluorescens. *J Bacteriol* **189**, 6665–6675 (2007).

67. Rossi, E., Falcone, M., Molin, S. & Johansen, H. K. High-resolution in situ transcriptomics of Pseudomonas aeruginosa unveils genotype independent patho-phenotypes in cystic fibrosis lungs. *Nat Commun* **9**, (2018).

68. Alvarez-Ortega, C. & Harwood, C. S. Responses of Pseudomonas aeruginosa to low oxygen indicate that growth in the cystic fibrosis lung is by aerobic respiration. *Mol Microbiol* **65**, 153–165 (2007).

69. Rossi, E. *et al.* Pseudomonas aeruginosa adaptation and evolution in patients with cystic fibrosis. *Nat Rev Microbiol* **19**, 331–342 (2021).

70. Wauven, C. v., Pierard, A., Kley-Raymann, M. & Haas, D. Pseudomonas aeruginosa mutants affected in anaerobic growth on arginine: evidence for a four-gene cluster encoding the arginine deiminase pathway. *J Bacteriol* **160**, 928 (1984).

71. Eschbach, M. *et al.* Long-term anaerobic survival of the opportunistic pathogen Pseudomonas aeruginosa via pyruvate fermentation. *J Bacteriol* **186**, 4596–4604 (2004).

72. Schreiber, K. *et al.* Anaerobic survival of Pseudomonas aeruginosa by pyruvate fermentation requires an Usp-type stress protein. *J Bacteriol* **188**, 659–668 (2006).

73. Cornforth, D. M. *et al.* Pseudomonas aeruginosa transcriptome during human infection. *Proc Natl Acad Sci U S A* **115**, (2018).

74. Kordes, A. *et al.* Genetically diverse Pseudomonas aeruginosa populations display similar transcriptomic profiles in a cystic fibrosis explanted lung. *Nat Commun* **10**, (2019).

75. Schiessl, K. T. *et al.* Phenazine production promotes antibiotic tolerance and metabolic heterogeneity in Pseudomonas aeruginosa biofilms. *Nature Communications 2019 10:1* **10**, 1–10 (2019).

76. de Sousa, T. *et al.* Genomic and Metabolic Characteristics of the Pathogenicity in Pseudomonas aeruginosa. *Int J Mol Sci* **22**, (2021).

77. Delepelaire, P. Type I secretion in gram-negative bacteria. *Biochim Biophys Acta Mol Cell Res* **1694**, 149–161 (2004).

78. Ma, Q., Zhai, Y., Schneider, J. C., Ramseier, T. M. & Saier, M. H. Protein secretion systems of Pseudomonas aeruginosa and P. fluorescens. *Biochim Biophys Acta Biomembr* **1611**, 223–233 (2003).

79. Matsumoto, K. Role of bacterial proteases in pseudomonal and serratial keratitis. *Biol Chem* **385**, 1007–1016 (2004).

80. Guzzo, J., Pages, J. M., Duong, F., Lazdunski, A. & Murgier, M. Pseudomonas aeruginosa alkaline protease: evidence for secretion genes and study of secretion mechanism. *J Bacteriol* **173**, 5290–5297 (1991).

81. Costa, T. R. D. *et al.* Secretion systems in Gram-negative bacteria: structural and mechanistic insights. *Nat Rev Microbiol* **13**, 343–359 (2015).

82. Cianciotto, N. P. Type II secretion: a protein secretion system for all seasons. *Trends Microbiol* **13**, 581–588 (2005).

83. Ball, G., Durand, É., Lazdunski, A. & Filloux, A. A novel type II secretion system in Pseudomonas aeruginosa. *Mol Microbiol* **43**, 475–485 (2002).

84. Allured, V. S., Collier, R. J., Carroll, S. F. & McKay, D. B. Structure of exotoxin A of Pseudomonas aeruginosa at 3.0-Angstrom resolution. *Proc Natl Acad Sci U S A* **83**, 1320–1324 (1986).

85. Casilag, F. *et al.* The LasB Elastase of Pseudomonas aeruginosa Acts in Concert with Alkaline Protease AprA To Prevent Flagellin-Mediated Immune Recognition. *Infect Immun* **84**, 162–171 (2015).

86. Korotkov, K. v., Sandkvist, M. & Hol, W. G. J. The type II secretion system: biogenesis, molecular architecture and mechanism. *Nat Rev Microbiol* **10**, 336–351 (2012).

87. Ostroff, R. M., Vasil, A. I. & Vasil, M. L. Molecular comparison of a nonhemolytic and a hemolytic phospholipase C from Pseudomonas aeruginosa. *J Bacteriol* **172**, 5915–5923 (1990).

88. Sawa, T., Shimizu, M., Moriyama, K. & Wiener-Kronish, J. P. Association between Pseudomonas aeruginosa type III secretion, antibiotic resistance, and clinical outcome: a review. *Crit Care* **18**, (2014).

89. Jia, J. *et al.* c-Jun NH2-terminal kinase-mediated signaling is essential for Pseudomonas aeruginosa ExoS-induced apoptosis. *Infect Immun* **71**, 3361–3370 (2003).

90. Rangel, S. M., Logan, L. K. & Hausera, A. R. The ADP-ribosyltransferase domain of the effector protein ExoS inhibits phagocytosis of Pseudomonas aeruginosa during pneumonia. *mBio* **5**, (2014).

91. Rangel, S. M., Diaz, M. H., Knoten, C. A., Zhang, A. & Hauser, A. R. The Role of ExoS in Dissemination of Pseudomonas aeruginosa during Pneumonia. *PLoS Pathog* **11**, (2015).

92. Engel, J. & Balachandran, P. Role of Pseudomonas aeruginosa type III effectors in disease. *Curr Opin Microbiol* **12**, 61–66 (2009).

93. Bleves, S. *et al.* Protein secretion systems in Pseudomonas aeruginosa: A wealth of pathogenic weapons. *Int J Med Microbiol* **300**, 534–543 (2010).

94. Urbanowski, M. L., Lykken, G. L. & Yahr, T. L. A secreted regulatory protein couples transcription to the secretory activity of the Pseudomonas aeruginosa type III secretion system. *Proc Natl Acad Sci U S A* **102**, 9930–9935 (2005).

95. McCaw, M. L., Lykken, G. L., Singh, P. K. & Yahr, T. L. ExsD is a negative regulator of the Pseudomonas aeruginosa type III secretion regulon. *Mol Microbiol* **46**, 1123–1133 (2002).

96. Wolfgang, M. C. *et al.* Conservation of genome content and virulence determinants among clinical and environmental isolates of Pseudomonas aeruginosa. *Proc Natl Acad Sci U S A* **100**, 8484–8489 (2003).

97. Zhou, L., Wang, J. & Zhang, L. H. Modulation of bacterial Type III secretion system by a spermidine transporter dependent signaling pathway. *PLoS One* **2**, (2007).

98. Filloux, A. Protein Secretion Systems in Pseudomonas aeruginosa: An Essay on Diversity, Evolution, and Function. *Front Microbiol* **2**, (2011).

99. Wilhelm, S., Tommassen, J. & Jaeger, K. E. A novel lipolytic enzyme located in the outer membrane of Pseudomonas aeruginosa. *J Bacteriol* **181**, 6977–6986 (1999).

100. Wilhelm, S., Gdynia, A., Tielen, P., Rosenau, F. & Jaeger, K. E. The autotransporter esterase EstA of Pseudomonas aeruginosa is required for rhamnolipid production, cell motility, and biofilm formation. *J Bacteriol* **189**, 6695–6703 (2007).

101. Salacha, R. *et al.* The Pseudomonas aeruginosa patatin-like protein PlpD is the archetype of a novel Type V secretion system. *Environ Microbiol* **12**, 1498–1512 (2010).

102. Borlee, B. R. *et al.* Pseudomonas aeruginosa uses a cyclic-di-GMP-regulated adhesin to reinforce the biofilm extracellular matrix. *Mol Microbiol* **75**, 827–842 (2010).

103. Allsopp, L. P. *et al.* RsmA and AmrZ orchestrate the assembly of all three type VI secretion systems in Pseudomonas aeruginosa. *Proc Natl Acad Sci U S A* **114**, 7707–7712 (2017).

104. Basler, M., Ho, B. T. & Mekalanos, J. J. Tit-for-tat: Type VI secretion system counterattack during bacterial cell-cell interactions. *Cell* **152**, 884–894 (2013).

105. Whitney, J. C. *et al.* Genetically distinct pathways guide effector export through the type VI secretion system. *Mol Microbiol* **92**, 529–542 (2014).

106. Russell, A. B. *et al.* Type VI secretion delivers bacteriolytic effectors to target cells. *Nature* **475**, 343–349 (2011).

107. Basler, M., Pilhofer, M., Henderson, G. P., Jensen, G. J. & Mekalanos, J. J. Type VI secretion requires a dynamic contractile phage tail-like structure. *Nature 2012 483:7388* **483**, 182–186 (2012).

108. Lesic, B., Starkey, M., He, J., Hazan, R. & Rahme, L. G. Quorum sensing differentially regulates Pseudomonas aeruginosa type VI secretion locus I and homologous loci II and III, which are required for pathogenesis. *Microbiology (N Y)* **155**, 2845 (2009).

109. de Kievit, T. R., Gillis, R., Marx, S., Brown, C. & Iglewski, B. H. Quorum-sensing genes in Pseudomonas aeruginosa biofilms: their role and expression patterns. *Appl Environ Microbiol* **67**, 1865–1873 (2001).

110. Miller, M. B. & Bassler, B. L. Quorum sensing in bacteria. *Annu Rev Microbiol* **55**, 165–199 (2001).

111. Venturi, V. Regulation of quorum sensing in Pseudomonas. *FEMS Microbiol Rev* **30**, 274–291 (2006).

112. Liu, L. *et al.* Structural and functional studies on Pseudomonas aeruginosa DspI: implications for its role in DSF biosynthesis. *Sci Rep* **8**, (2018).

113. Gallagher, L. A., McKnight, S. L., Kuznetsova, M. S., Pesci, E. C. & Manoil, C. Functions required for extracellular quinolone signaling by Pseudomonas aeruginosa. *J Bacteriol* **184**, 6472–6480 (2002).

114. Kviatkovski, I. *et al.* Pseudomonas aeruginosa activates the quorum sensing LuxR response regulator through secretion of 2-aminoacetophenone. *Chem Commun (Camb)* **51**, 3258–3261 (2015).

115. Pearson, J. P., Pesci, E. C. & Iglewski, B. H. Roles of Pseudomonas aeruginosa las and rhl quorum-sensing systems in control of elastase and rhamnolipid biosynthesis genes. *J Bacteriol* **179**, 5756–5767 (1997).

116. Bjarnsholt, T. *et al.* Quorum sensing and virulence of Pseudomonas aeruginosa during lung infection of cystic fibrosis patients. *PLoS One* **5**, (2010).

117. Lin, J., Cheng, J., Wang, Y. & Shen, X. The Pseudomonas quinolone signal (PQS): Not just for quorum sensing anymore. *Frontiers in Cellular and Infection Microbiology* vol. 8 Preprint at https://doi.org/10.3389/fcimb.2018.00230 (2018).

118. Häussler, S. & Becker, T. The Pseudomonas Quinolone Signal (PQS) Balances Life and Death in Pseudomonas aeruginosa Populations. *PLoS Pathog* **4**, e1000166 (2008).

119. Yang, L. *et al.* Distinct roles of extracellular polymeric substances in Pseudomonas aeruginosa biofilm development. *Environ Microbiol* **13**, 1705–1717 (2011).

120. Rasamiravaka, T., Labtani, Q., Duez, P. & el Jaziri, M. The formation of biofilms by Pseudomonas aeruginosa: a review of the natural and synthetic compounds interfering with control mechanisms. *Biomed Res Int* **2015**, (2015).

121. Ma, L., Jackson, K. D., Landry, R. M., Parsek, M. R. & Wozniak, D. J. Analysis of Pseudomonas aeruginosa conditional psl variants reveals roles for the psl polysaccharide in adhesion and maintaining biofilm structure postattachment. *J Bacteriol* **188**, 8213–8221 (2006).

122. Gilbert, K. B., Kim, T. H., Gupta, R., Greenberg, E. P. & Schuster, M. Global position analysis of the Pseudomonas aeruginosa quorum-sensing transcription factor LasR. *Mol Microbiol* **73**, 1072–1085 (2009).

123. Sakuragi, Y. & Kolter, R. Quorum-sensing regulation of the biofilm matrix genes (pel) of Pseudomonas aeruginosa. *J Bacteriol* **189**, 5383–5386 (2007).

124. Badal, D., Jayarani, A. V., Kollaran, M. A., Kumar, A. & Singh, V. Pseudomonas aeruginosa biofilm formation on endotracheal tubes requires multiple two-component systems. *J Med Microbiol* **69**, 906–919 (2020).

125. Franklin, M. J., Nivens, D. E., Weadge, J. T. & Lynne Howell, P. Biosynthesis of the Pseudomonas aeruginosa Extracellular Polysaccharides, Alginate, Pel, and Psl. *Front Microbiol* **2**, (2011).

126. Friedman, L. & Kolter, R. Genes involved in matrix formation in Pseudomonas aeruginosa PA14 biofilms. *Mol Microbiol* **51**, 675–690 (2004).

127. Valentini, M. & Filloux, A. Biofilms and Cyclic di-GMP (c-di-GMP) Signaling: Lessons from Pseudomonas aeruginosa and Other Bacteria. *J Biol Chem* **291**, 12547–12555 (2016).

128. Goodman, A. L. *et al.* A signaling network reciprocally regulates genes associated with acute infection and chronic persistence in Pseudomonas aeruginosa. *Dev Cell* **7**, 745–754 (2004).

129. Mulcahy, H. *et al.* Pseudomonas aeruginosa RsmA plays an important role during murine infection by influencing colonization, virulence, persistence, and pulmonary inflammation. *Infect Immun* **76**, 632–638 (2008).

130. Sauer, K. *et al.* The biofilm life cycle: expanding the conceptual model of biofilm formation. *Nature Reviews Microbiology 2022 20:10* **20**, 608–620 (2022).

131. Taylor, P. K., Yeung, A. T. Y. & Hancock, R. E. W. Antibiotic resistance in Pseudomonas aeruginosa biofilms: towards the development of novel anti-biofilm therapies. *J Biotechnol* **191**, 121–130 (2014).

132. Sauer, K., Camper, A. K., Ehrlich, G. D., Costerton, J. W. & Davies, D. G. Pseudomonas aeruginosa displays multiple phenotypes during development as a biofilm. *J Bacteriol* **184**, 1140–1154 (2002).

133. Xu, K. D., Stewart, P. S., Xia, F., Huang, C. T. & McFeters, G. A. Spatial physiological heterogeneity in Pseudomonas aeruginosa biofilm is determined by oxygen availability. *Appl Environ Microbiol* **64**, 4035–4039 (1998).

134. Yoon, S. S. *et al.* Pseudomonas aeruginosa anaerobic respiration in biofilms: relationships to cystic fibrosis pathogenesis. *Dev Cell* **3**, 593–603 (2002).

135. Worlitzsch, D. *et al.* Effects of reduced mucus oxygen concentration in airway Pseudomonas infections of cystic fibrosis patients. *J Clin Invest* **109**, 317–325 (2002).

136. Ciofu, O. & Tolker-Nielsen, T. Tolerance and Resistance of Pseudomonas aeruginosa Biofilms to Antimicrobial Agents-How P. aeruginosa Can Escape Antibiotics. *Front Microbiol* **10**, (2019).

137. Høiby, N. *et al.* The clinical impact of bacterial biofilms. *Int J Oral Sci* **3**, 55–65 (2011).

138. Jensen, P. Ø., Givskov, M., Bjarnsholt, T. & Moser, C. The immune system vs. Pseudomonas aeruginosa biofilms. *FEMS Immunol Med Microbiol* **59**, 292–305 (2010).

139. Costerton, J. W., Irvin, R. T. & Cheng, K. J. The bacterial glycocalyx in nature and disease. *Annu Rev Microbiol* **35**, 299–324 (1981).

140. Meshulam, T., Obedeanu, N., Merzbach, D. & Sobel, J. D. Phagocytosis of mucoid and nonmucoid strains of Pseudomonas aeruginosa. *Clin Immunol Immunopathol* **32**, 151–165 (1984).

141. Simpson, J. A., Smith, S. E. & Dean, R. T. Scavenging by alginate of free radicals released by macrophages. *Free Radic Biol Med* **6**, 347–353 (1989).

142. Cabral, D. A., Loh, B. A. & Speert, D. P. Mucoid Pseudomonas aeruginosa resists nonopsonic phagocytosis by human neutrophils and macrophages. *Pediatr Res* **22**, 429–431 (1987).

143. Meshulam, T., Verbrugh, H. A. & Verhoef, J. Opsonization and phagocytosis of mucoid and non-mucoid Pseudomonas aeruginosa strains. *Eur J Clin Microbiol* **1**, 112–117 (1982).

144. Pedersen, S. S., Kharazmi, A., Espersen, F. & Hoiby, N. Pseudomonas aeruginosa alginate in cystic fibrosis sputum and the inflammatory response. *Infect Immun* **58**, 3363 (1990).

145. Govan, J. R. & Deretic, V. Microbial pathogenesis in cystic fibrosis: mucoid Pseudomonas aeruginosa and Burkholderia cepacia. *Microbiol Rev* **60**, 539–574 (1996).

146. Martin, D. W. *et al.* Mechanism of conversion to mucoidy in Pseudomonas aeruginosa infecting cystic fibrosis patients. *Proc Natl Acad Sci U S A* **90**, 8377 (1993).

147. Boucher, J. C., Yu, H., Mudd, M. H. & Deretic, V. Mucoid Pseudomonas aeruginosa in cystic fibrosis: characterization of muc mutations in clinical isolates and analysis of clearance in a mouse model of respiratory infection. *Infect Immun* **65**, 3838–3846 (1997).

148. Wood, L. F. & Ohman, D. E. Identification of Genes in the σ22 Regulon of Pseudomonas aeruginosa Required for Cell Envelope Homeostasis in Either the Planktonic or the Sessile Mode of Growth. *mBio* **3**, (2012).

149. Ramsey, D. M. & Wozniak, D. J. Understanding the control of Pseudomonas aeruginosa alginate synthesis and the prospects for management of chronic infections in cystic fibrosis. *Mol Microbiol* **56**, 309–322 (2005).

150. Chitnis, C. E. & Ohman, D. E. Genetic analysis of the alginate biosynthetic gene cluster of Pseudomonas aeruginosa shows evidence of an operonic structure. *Mol Microbiol* **8**, 583–590 (1993).

151. DeVries, C. A. & Ohman, D. E. Mucoid-to-nonmucoid conversion in alginate-producing Pseudomonas aeruginosa often results from spontaneous mutations in algT, encoding a putative alternate sigma factor, and shows evidence for autoregulation. *J Bacteriol* **176**, 6677 (1994).

152. Deretic, V., Schurr, M. J., Boucher, J. C. & Martin, D. W. Conversion of Pseudomonas aeruginosa to mucoidy in cystic fibrosis: environmental stress and regulation of bacterial virulence by alternative sigma factors. *J Bacteriol* **176**, 2773 (1994).

153. Wood, L. F. & Ohman, D. E. Use of cell wall stress to characterize sigma 22 (AlgT/U) activation by regulated proteolysis and its regulon in Pseudomonas aeruginosa. *Mol Microbiol* **72**, 183–201 (2009).

154. Wood, L. F. & Ohman, D. E. Identification of Genes in the σ22 Regulon of Pseudomonas aeruginosa Required for Cell Envelope Homeostasis in Either the Planktonic or the Sessile Mode of Growth. *mBio* **3**, (2012).

155. Hauser, A. R., Jain, M., Bar-Meir, M. & McColley, S. A. Clinical significance of microbial infection and adaptation in cystic fibrosis. *Clin Microbiol Rev* **24**, 29–70 (2011).

156. Imlay, J. A. & Linn, S. DNA damage and oxygen radical toxicity. *Science* **240**, 1302–1309 (1988).

157. Imlay, J. A. Iron-sulphur clusters and the problem with oxygen. *Mol Microbiol* **59**, 1073–1082 (2006).

158. Ernst, R. K. *et al.* The Pseudomonas aeruginosa lipid A deacylase: selection for expression and loss within the cystic fibrosis airway. *J Bacteriol* **188**, 191–201 (2006).

159. Ernst, R. K. *et al.* Unique lipid a modifications in Pseudomonas aeruginosa isolated from the airways of patients with cystic fibrosis. *J Infect Dis* **196**, 1088–1092 (2007).

160. Hancock, R. E. W. *et al.* Pseudomonas aeruginosa isolates from patients with cystic fibrosis: a class of serum-sensitive, nontypable strains deficient in lipopolysaccharide O side chains. *Infect Immun* **42**, 170–177 (1983).

161. Kim, S. K. *et al.* Bacterial ornithine lipid, a surrogate membrane lipid under phosphate-limiting conditions, plays important roles in bacterial persistence and interaction with host. *Environ Microbiol* **20**, 3992–4008 (2018).

162. Marvig, R. L. *et al.* Within-host evolution of Pseudomonas aeruginosa reveals adaptation toward iron acquisition from hemoglobin. *mBio* **5**, (2014).

163. Klockgether, J., Cramer, N., Fischer, S., Wiehlmann, L. & Tümmler, B. Long-Term Microevolution of Pseudomonas aeruginosa Differs between Mildly and Severely Affected Cystic Fibrosis Lungs. *Am J Respir Cell Mol Biol* **59**, 246–256 (2018).

164. Bartell, J. A. *et al.* Evolutionary highways to persistent bacterial infection. *Nat Commun* **10**, (2019).

165. Folkesson, A. *et al.* Adaptation of Pseudomonas aeruginosa to the cystic fibrosis airway: an evolutionary perspective. *Nat Rev Microbiol* **10**, 841–851 (2012).

166. Behrends, V., Williams, H. D. & Bundy, J. G. Pseudomonas methods and protocols Chapter 23 - Metabolic Footprinting: Extracellular Metabolomic Analysis. *Methods Mol Biol* **1149**, 281–292 (2014).

167. Paczia, N. *et al.* Extensive exometabolome analysis reveals extended overflow metabolism in various microorganisms. *Microb Cell Fact* **11**, 1–14 (2012).

168. Allen, J. *et al.* High-throughput classification of yeast mutants for functional genomics using metabolic footprinting. *Nat Biotechnol* **21**, 692–696 (2003).

169. Mas, S., Villas-Bôas, S. G., Hansen, M. E., Åkesson, M. & Nielsen, J. A Comparison of Direct Infusion MS and GC-MS for Metabolic Footprinting of Yeast Mutants. *Biotechnology and Bionengineering* **96**, 1014–1022 (2006).

170. Kaderbhai, N. N., Broadhurst, D. I., Ellis, D. I., Goodacre, R. & Kell, D. B. Functional genomics via metabolic footprinting: Monitoring metabolite secretion by Escherichia coli tryptophan metabolism mutants using FT-IR and direct injection electrospray mass spectrometry. *Comp Funct Genomics* **4**, 376–391 (2003).

171. Sue, T., Obolonkin, V., Griffiths, H. & Villas-Bôas, S. G. An exometabolomics approach to monitoring microbial contamination in microalgal fermentation processes by using metabolic footprint analysis. *Appl Environ Microbiol* **77**, 7605–7610 (2011).

172. Henriques, I. D. S., Aga, D. S., Mendes, P., O'Connor, S. K. & Love, N. G. Metabolic footprinting: A new approach to identify physiological changes in complex microbial communities upon exposure to toxic chemicals. *Environ Sci Technol* **41**, 3945–3951 (2007).

173. Monti, M. R., Smania, A. M., Fabro, G., Alvarez, M. E. & Argaraña, C. E. Engineering Pseudomonas fluorescens for biodegradation of 2,4-dinitrotoluene. *Appl Environ Microbiol* **71**, 8864–8872 (2005).

174. Howell, K. S., Cozzolino, D., Bartowsky, E. J., Fleet, G. H. & Henschke, P. A. Metabolic profiling as a tool for revealing Saccharomyces interactions during wine fermentation. *FEMS Yeast Res* **6**, 91–101 (2006).

175. Cheraiti, N., Guezenec, S. & Salmon, J. M. Redox interactions between Saccharomyces cerevisiae and Saccharomyces uvarum in mixed culture under enological conditions. *Appl Environ Microbiol* **71**, 255–260 (2005).

176. Panagiotou, G., Kouskoumvekaki, I., Jónsdóttir, S. O. & Olsson, L. Monitoring novel metabolic pathways using metabolomics and machine learning: Induction of the phosphoketolase pathway in Aspergillus nidulans cultivations. *Metabolomics* **3**, 503–516 (2007).

177. La Rosa, R., Behrends, V., Williams, H. D., Bundy, J. G. & Rojo, F. Influence of the Crc regulator on the hierarchical use of carbon sources from a complete medium in Pseudomonas. *Environ Microbiol* **18**, 807–818 (2016).

178. Molina, L., La Rosa, R., Nogales, J. & Rojo, F. Influence of the Crc global regulator on substrate uptake rates and the distribution of metabolic fluxes in Pseudomonas putida KT2440 growing in a complete medium. *Environ Microbiol* **21**, 4446–4459 (2019).

179. Mapelli, V., Olsson, L. & Nielsen, J. Metabolic footprinting in microbiology: methods and applications in functional genomics and biotechnology. *Trends Biotechnol* **26**, 490–497 (2008).

180. Van Ditmarsch, D. & Xavier, J. B. High-resolution time series of Pseudomonas aeruginosa gene expression and rhamnolipid secretion through growth curve synchronization. *BMC Microbiol* **11**, (2011).

181. López-Sánchez, A., Jiménez-Fernández, A., Calero, P., Gallego, L. D. & Govantes, F. New methods for the isolation and characterization of biofilm-persistent mutants in Pseudomonas putida. *Environ Microbiol Rep* **5**, 679–685 (2013).

182. Behrends, V., Ebbels, T. M. D., Williams, H. D. & Bundy, J. G. Time-resolved metabolic footprinting for nonlinear modeling of Bacterial substrate utilization. *Appl Environ Microbiol* **75**, 2453–2463 (2009).

183. Depke, T., Häussler, S. & Brönstrup, M. The peptide chain release factor methyltransferase prmc influences the pseudomonas aeruginosa pa14 endo-and exometabolome. *Metabolites* **10**, 1–8 (2020).

184. Yung, Y. P. *et al.* Reverse diauxie phenotype in Pseudomonas aeruginosa biofilm revealed by exometabolomics and label-free proteomics. *NPJ Biofilms Microbiomes* **5**, (2019).

185. Behrends, V. *et al.* Metabolic adaptations of Pseudomonas aeruginosa during cystic fibrosis chronic lung infections. *Environ Microbiol* **15**, 398–408 (2013).

186. Brown, S. A., Palmer, K. L. & Whiteley, M. Revisiting the host as a growth medium. *Nat Rev Microbiol* **6**, 657–666 (2008).

187. Malik-Kale, P. *et al.* Salmonella- at home in the host cell. *Front Microbiol* **2**, 1–9 (2011).

188. Flannagan, R. S., Cosío, G. & Grinstein, S. Antimicrobial mechanisms of phagocytes and bacterial evasion strategies. *Nat Rev Microbiol* **7**, 355–366 (2009).

189. Diaz, M. R., King, J. M. & Yahr, T. L. Intrinsic and extrinsic regulation of type III secretion gene expression in Pseudomonas aeruginosa. *Front Microbiol* **2**, 1–10 (2011).

190. Li, L., Meng, H., Gu, D., Li, Y. & Jia, M. Molecular mechanisms of Vibrio parahaemolyticus pathogenesis. *Microbiol Res* **222**, 43–51 (2019).

191. La Rosa, R., Johansen, H. K. & Molin, S. Convergent Metabolic Specialization through Distinct Evolutionary Paths in Pseudomonas aeruginosa. *mBio* **9**, e00269-18 (2018).

192. Behrends, V. *et al.* Metabolite Profiling to Characterize Disease-related Bacteria. *Journal of Biological Chemistry* **288**, 15098–15109 (2013).

193. Rossi, E. *et al.* Pseudomonas aeruginosa adaptation and evolution in patients with cystic fibrosis. *Nat Rev Microbiol* **19**, 331–342 (2021).

194. La Rosa, R., Johansen, H. K. & Molin, S. Adapting to the Airways: Metabolic Requirements of Pseudomonas aeruginosa during the Infection of Cystic Fibrosis Patients. *Metabolites* **9**, 234 (2019).

195. Palmer, K. L., Aye, L. M. & Whiteley, M. Nutritional Cues Control Pseudomonas aeruginosa Multicellular Behavior in Cystic Fibrosis Sputum. *J Bacteriol* **189**, 8079–8087 (2007).

196. La Rosa, R., Johansen, H. K. & Molin, S. Persistent Bacterial Infections, Antibiotic Treatment Failure, and Microbial Adaptive Evolution. *Antibiotics* **11**, 419 (2022).

197. Haney, E. F. & Hancock, R. E. W. Addressing Antibiotic Failure—Beyond Genetically Encoded Antimicrobial Resistance. *Frontiers in Drug Discovery* **2**, 1–7 (2022).

198. Marvig, R. L., Sommer, L. M., Molin, S. & Johansen, H. K. Convergent evolution and adaptation of Pseudomonas aeruginosa within patients with cystic fibrosis. *Nat Genet* **47**, 57–64 (2015).

199. Yang, L. *et al.* Evolutionary dynamics of bacteria in a human host environment. *Proceedings of the National Academy of Sciences* **108**, 7481–7486 (2011).

200. La Rosa, R., Rossi, E., Feist, A. M., Johansen, H. K. & Molin, S. Compensatory evolution of Pseudomonas aeruginosa's slow growth phenotype suggests mechanisms of adaptation in cystic fibrosis. *Nat Commun* **12**, 3186 (2021).

201. Lopatkin, A. J. *et al.* Clinically relevant mutations in core metabolic genes confer antibiotic resistance. *Science (1979)* **371**, eaba0862 (2021).

202. Martínez, J. L. & Rojo, F. Metabolic regulation of antibiotic resistance. *FEMS Microbiol Rev* **35**, 768–789 (2011).

203. Chung, J. C. S., Rzhepishevska, O., Ramstedt, M. & Welch, M. Type III secretion system expression in oxygen-limited Pseudomonas aeruginosa cultures is stimulated by isocitrate lyase activity. *Open Biol* **3**, (2013).

204. Linares, J. F. *et al.* Overexpression of the multidrug efflux pumps MexCD-OprJ and MexEF-OprN is associated with a reduction of type III secretion in Pseudomonas aeruginosa. *J Bacteriol* **187**, 1384–1391 (2005).

205. Dacheux, D. *et al.* Activation of the Pseudomonas aeruginosa type III secretion system requires an intact pyruvate dehydrogenase aceAB operon. *Infect Immun* **70**, 3973–3977 (2002).

206. Price-Whelan, A., Dietrich, L. E. P. & Newman, D. K. Pyocyanin Alters Redox Homeostasis and Carbon Flux through Central Metabolic Pathways in Pseudomonas aeruginosa PA14. *J Bacteriol* **189**, 6372–6381 (2007).

207. Schiessl, K. T. *et al.* Phenazine production promotes antibiotic tolerance and metabolic heterogeneity in Pseudomonas aeruginosa biofilms. *Nat Commun* **10**, 1–10 (2019).

208. Hauser, A. R. The type III secretion system of Pseudomonas aeruginosa: Infection by injection. *Nature Reviews Microbiology* vol. 7 654–665 Preprint at https://doi.org/10.1038/nrmicro2199 (2009).

209. Williams McMackin, E. A., Djapgne, L., Corley, J. M. & Yahr, T. L. Fitting Pieces into the Puzzle of Pseudomonas aeruginosa Type III Secretion System Gene Expression. *J Bacteriol* **201**, (2019).

210. Behrends, V., Geier, B., Williams, H. D. & Bundy, J. G. Direct assessment of metabolite utilization by Pseudomonas aeruginosa during growth on artificial sputum medium. *Appl Environ Microbiol* **79**, 2467–2470 (2013).

211. Bernal, V., Castaño-Cerezo, S. & Cánovas, M. Acetate metabolism regulation in Escherichia coli: carbon overflow, pathogenicity, and beyond. *Applied Microbiology and Biotechnology* vol. 100 8985–9001 Preprint at https://doi.org/10.1007/s00253-016-7832-x (2016).

212. Millard, P., Enjalbert, B., Uttenweiler-Joseph, S., Portais, J. C. & Létisse, F. Control and regulation of acetate overflow in escherichia coli. *Elife* **10**, (2021).

213. Fiske, M. J., Whitaker, R. J. & Jensen, R. A. Hidden overflow pathway to L-phenylalanine in Pseudomonas aeruginosa. *J Bacteriol* **154**, 623–631 (1983).

214. Paczia, N. *et al.* Extensive exometabolome analysis reveals extended overflow metabolism in various microorganisms. *Microb Cell Fact* **11**, 1–14 (2012).

215. Peebo, K. *et al.* Coordinated activation of PTA-ACS and TCA cycles strongly reduces overflow metabolism of acetate in Escherichia coli. *Appl Microbiol Biotechnol* **98**, 5131–5143 (2014).

216. Li, H. *et al.* Dihydrolipoamide Acetyltransferase AceF Influences the Type III Secretion System and Resistance to Oxidative Stresses through RsmY/Z in Pseudomonas aeruginosa. *Microorganisms* **10**, (2022).

217. Dacheux, D. *et al.* Activation of the Pseudomonas aeruginosa type III secretion system requires an intact pyruvate dehydrogenase aceAB operon. *Infect Immun* **70**, 3973–3977 (2002).

218. Petrova, O. E., Schurr, J. R., Schurr, M. J. & Sauer, K. Microcolony formation by the opportunistic pathogen Pseudomonas aeruginosa requires pyruvate and pyruvate fermentation. *Mol Microbiol* **86**, 819–835 (2012).

219. Goodwine, J. *et al.* Pyruvate-depleting conditions induce biofilm dispersion and enhance the efficacy of antibiotics in killing biofilms in vitro and in vivo. *Sci Rep* **9**, (2019).

220. Min, B. K. *et al.* Pyruvate dehydrogenase kinase is a metabolic checkpoint for polarization of macrophages to the M1 phenotype. *Front Immunol* **10**, (2019).

221. Zhang, W., Zhang, S. L., Hu, X. & Tam, K. Y. Targeting Tumor Metabolism for Cancer Treatment: Is Pyruvate Dehydrogenase Kinases (PDKs) a Viable Anticancer Target? *Int J Biol Sci* **11**, 1390 (2015).

222. Li, J. *et al.* VSIG4 inhibits proinflammatory macrophage activation by reprogramming mitochondrial pyruvate metabolism. *Nat Commun* **8**, (2017).

223. O'Neill, L. A. J. & Artyomov, M. N. Itaconate: the poster child of metabolic reprogramming in macrophage function. *Nat Rev Immunol* **19**, 273–281 (2019).

224. Domínguez-Andrés, J. *et al.* The Itaconate Pathway Is a Central Regulatory Node Linking Innate Immune Tolerance and Trained Immunity. *Cell Metab* **29**, 211-220.e5 (2019).

225. Røst, L. M., Louet, C., Bruheim, P., Flo, T. H. & Gidon, A. Pyruvate Supports RET-Dependent Mitochondrial ROS Production to Control Mycobacterium avium Infection in Human Primary Macrophages. *Front Immunol* **13**, (2022).

226. McCall, C. E. *et al.* Pyruvate dehydrogenase complex stimulation promotes immunometabolic homeostasis and sepsis survival. *JCI Insight* **3**, (2018).

227. Zhu, X. *et al.* Stimulating pyruvate dehydrogenase complex reduces itaconate levels and enhances TCA cycle anabolic bioenergetics in acutely inflamed monocytes. *J Leukoc Biol* **107**, 467–484 (2020).

228. McCall, C. E. *et al.* Sepsis, pyruvate, and mitochondria energy supply chain shortage. *J Leukoc Biol* **112**, (2022).

229. Abusalamah, H., Reel, J. M. & Lupfer, C. R. Pyruvate affects inflammatory responses of macrophages during influenza A virus infection. *Virus Res* **286**, (2020).

230. Bailey, J. D. *et al.* Nitric Oxide Modulates Metabolic Remodeling in Inflammatory Macrophages through TCA Cycle Regulation and Itaconate Accumulation. *Cell Rep* **28**, 218-230.e7 (2019).

231. Meiser, J. *et al.* Pro-inflammatory macrophages sustain pyruvate oxidation through pyruvate dehydrogenase for the synthesis of itaconate and to enable cytokine expression. *Journal of Biological Chemistry* **291**, 3932–3946 (2016).

232. Palmieri, E. M. *et al.* Nitric oxide orchestrates metabolic rewiring in M1 macrophages by targeting aconitase 2 and pyruvate dehydrogenase. *Nat Commun* **11**, (2020).

233. Riquelme, S. A. *et al.* Pseudomonas aeruginosa Utilizes Host-Derived Itaconate to Redirect Its Metabolism to Promote Biofilm Formation. *Cell Metab* **0**, 1–16 (2020).

234. Chakhtoura, M. *et al.* Ethyl pyruvate modulates murine dendritic cell activation and survival through their immunometabolism. *Front Immunol* **10**, 30 (2019).

235. Deschamps, E. *et al.* Membrane phospholipid composition of Pseudomonas aeruginosa grown in a cystic fibrosis mucus-mimicking medium. *Biochimica et Biophysica Acta (BBA) - Biomembranes* **1863**, 183482 (2021).

236. Pedersen, B. H. *et al.* High-throughput dilution-based growth method enables time-resolved exo-metabolomics of Pseudomonas putida and Pseudomonas aeruginosa. *Microb Biotechnol* **0**, 1–13 (2021).

237. Callister, S. J. *et al.* Normalization approaches for removing systematic biases associated with mass spectrometry and label-free proteomics. *J Proteome Res* **5**, 277–286 (2006).

238. Cavaleiro, A. M., Kim, S. H., Seppälä, S., Nielsen, M. T. & Nørholm, M. H. H. Accurate DNA assembly and genome engineering with optimized uracil excision cloning. *ACS Synth Biol* **4**, 1042–1046 (2015).

239. Chen, W. *et al.* CRISPR/Cas9-based genome editing in Pseudomonas aeruginosa and cytidine deaminase-mediated base editing in Pseudomonas species. *iScience* **6**, 222–231 (2018).

240. Chen, W. *et al.* CRISPR/Cas9-based genome editing in Pseudomonas aeruginosa and cytidine deaminase-mediated base editing in Pseudomonas species. *iScience* **6**, 222–231 (2018).

241. Choi, K. H., Kumar, A. & Schweizer, H. P. A 10-min method for preparation of highly electrocompetent Pseudomonas aeruginosa cells: Application for DNA fragment transfer between chromosomes and plasmid transformation. *J Microbiol Methods* **64**, 391–397 (2006).

242. Bartell, J. A. *et al.* Evolutionary highways to persistent bacterial infection. *Nat Commun* **10**, 629 (2019).

243. Choi, K. H. & Schweizer, H. P. mini-Tn7 insertion in bacteria with single attTn7 sites: example Pseudomonas aeruginosa. *Nat Protoc* **1**, 153–161 (2006).

244. Walters, M. S. *et al.* Generation of a human airway epithelium derived basal cell line with multipotent differentiation capacity. *Respir Res* **14**, 135 (2013).

245. Felsenstein, J. Confidence limits on phylogenies: An approach using the bootstrap. *Evolution (N Y)* 783–791 (1985).

246. Nei, M. & Kumar, S. Molecular Evolution and Phylogenetics. *Oxford University Press, New York* (2000).

247. Kumar, S., Stecher, G., Li, M., Knyaz, C. & Tamura, K. MEGA X: Molecular Evolutionary Genetics Analysis across computing platforms. *Mol Biol Evol* 1547–1549 (2018).

248. Borgert, S. R. *et al.* Moonlighting chaperone activity of the enzyme PqsE contributes to RhlR-controlled virulence of Pseudomonas aeruginosa. (2022) doi:10.1038/s41467-022-35030-w.

249. Schütz, C. *et al.* A New PqsR Inverse Agonist Potentiates Tobramycin Efficacy to Eradicate Pseudomonas aeruginosa Biofilms. *Advanced Science* **8**, 2004369 (2021).

250. Kitao, T. *et al.* Molecular Insights into Function and Competitive Inhibition of Pseudomonas aeruginosa Multiple Virulence Factor Regulator. *mBio* **9**, e02158-17 (2018).

251. Soukarieh, F. *et al.* Hit Identification of New Potent PqsR Antagonists as Inhibitors of Quorum Sensing in Planktonic and Biofilm Grown Pseudomonas aeruginosa. *Front. Chem.* **8**, 204 (2020).

252. Sabir, S. *et al.* Thioether-linked dihydropyrrol-2-one analogues as PqsR antagonists against antibiotic resistant Pseudomonas aeruginosa. *Bioorg. Med. Chem.* **31**, 115967 (2021).

253. Grossman, S. *et al.* Novel quinazolinone inhibitors of the Pseudomonas aeruginosa quorum sensing transcriptional regulator PqsR. *Eur. J. Med. Chem.* **208**, 112778 (2020).

254. Zender, M. *et al.* Flexible Fragment Growing Boosts Potency of Quorum-Sensing Inhibitors against Pseudomonas aeruginosa Virulence. *ChemMedChem* **15**, 188–194 (2020).

255. Maura, D. & Rahme, L. G. Pharmacological Inhibition of the Pseudomonas aeruginosa MvfR Quorum-Sensing System Interferes with Biofilm Formation and Potentiates Antibiotic-Mediated Biofilm Disruption. *Antimicrob. Agents Chemother.* **61**, e01362-17 (2017).

256. Mukherjee, S. *et al.* The PqsE and RhlR proteins are an autoinducer synthase-receptor pair that control virulence and biofilm development in Pseudomonas aeruginosa. *Proc Natl Acad Sci U S A* **115**, E9411–E9418 (2018).

257. Letizia, M. *et al.* PqsE Expands and Differentially Modulates the RhlR Quorum Sensing Regulon in Pseudomonas aeruginosa. *Microbiol Spectr* **10**, (2022).

258. Groleau, M., Pereira, T. D. O., Dekimpe, V. & Déziela, E. PqsE Is Essential for RhlR-Dependent Quorum Sensing Regulation in Pseudomonas aeruginosa Marie-Christine. *mSystems* **5**, 1–13 (2020).

259. Lin, J. *et al.* A Pseudomonas T6SS effector recruits PQS-containing outer membrane vesicles for iron acquisition. *Nature Communications 2017 8:1* **8**, 1–12 (2017).

260. Hendrix, H. *et al.* Metabolic reprogramming of Pseudomonas aeruginosa by phage-based quorum sensing modulation. *Cell Rep* **38**, 110372 (2022).

261. Arai, H., Igarashi, Y. & Kodama, T. Expression of the nir and nor genes for denitrification of Pseudomonas aeruginosa requires a novel CRP/FNR-related transcriptional regulator, DNR, in addition to ANR. *FEBS Lett* **371**, 73–76 (1995).

262. Krieger, R., Rompf, A., Schobert, M. & Jahn, D. The Pseudomonas aeruginosa hemA promoter is regulated by Anr, Dnr, NarL and Integration Host Factor. *Mol Genet Genomics* **267**, 409–417 (2002).

263. Ye, R. W. *et al.* Anaerobic activation of the entire denitrification pathway in Pseudomonas aeruginosa requires Anr, an analog of Fnr. *J Bacteriol* **177**, 3606–3609 (1995).

264. Aral, H., Kodama, T. & Igarashi, Y. Cascade regulation of the two CRP/FNR-related transcriptional regulators (ANR and DNR) and the denitrification enzymes in Pseudomonas aeruginosa. *Mol Microbiol* **25**, 1141–1148 (1997).

265. Dang, J., Wang, T., Wen, J. & Liang, H. An Important Role of the Type VI Secretion System of Pseudomonas aeruginosa Regulated by Dnr in Response to Anaerobic Environments. *Microbiol Spectr* (2022) doi:10.1128/spectrum.01533-22.

266. Deng, X. *et al.* Molecular mechanisms of two-component system RhpRS regulating type III secretion system in Pseudomonas syringae. *Nucleic Acids Res* **42**, 11472–11486 (2014).

267. Xie, Y. *et al.* Pseudomonas savastanoi two-component system RhpRS switches between virulence and metabolism by tuning phosphorylation state and sensing nutritional conditions. *mBio* **10**, (2019).

268. Xie, Y., Shao, X. & Deng, X. Regulation of type III secretion system in Pseudomonas syringae. *Environ Microbiol* **21**, 4465–4477 (2019).

269. Gray, L. R., Tompkins, S. C. & Taylor, E. B. Regulation of pyruvate metabolism and human disease. *Cellular and Molecular Life Sciences* **71**, 2577 (2014).

270. Cheng, X. *et al.* Plasticity of the pyruvate node modulates hydrogen peroxide production and acid tolerance in multiple oral streptococci. *Appl Environ Microbiol* **84**, (2018).

271. Redanz, S. *et al.* Pyruvate secretion by oral streptococci modulates hydrogen peroxide dependent antagonism. *ISME Journal* **14**, 1074–1088 (2020).

272. Zeng, L., Walker, A. R., Burne, R. A. & Taylor, Z. A. Glucose Phosphotransferase System Modulates Pyruvate Metabolism, Bacterial Fitness, and Microbial Ecology in Oral Streptococci. *J Bacteriol* (2022) doi:10.1128/JB.00352-22.

273. Krzysciak, W. *et al.* Relationship between Pyruvate Kinase Activity and Cariogenic Biofilm Formation in Streptococcus mutans Biotypes in Caries Patients. *Front Microbiol* **8**, (2017).

274. Miyagi, M. *et al.* Indole-3-acetic acid synthesized through the indole-3-pyruvate pathway promotes Candida tropicalis biofilm formation. *PLoS One* **15**, (2020).

275. Rai, L. S., Chauvel, M., Permal, E., d'Enfert, C. & Bachellier-Bassi, S. Transcript profiling reveals the role of PDB1, a subunit of the pyruvate dehydrogenase complex in Candida albicans biofilm formation. *Res Microbiol* 104014 (2022) doi:10.1016/j.resmic.2022.104014.

276. Ogasawara, H. *et al.* Regulatory role of pyruvate-sensing BtsSR in biofilm formation by Escherichia coli K-12. *FEMS Microbiol Lett* **366**, (2019).

277. Tremblay, Y. D. N. *et al.* Metabolic adaption to extracellular pyruvate triggers biofilm formation in Clostridioides difficile. *ISME J* **15**, 3623–3635 (2021).

278. Ceperuelo-Mallafré, V. *et al.* Circulating pyruvate is a potent prognostic marker for critical COVID-19 outcomes. *Front Immunol* **13**, (2022).

279. Wolfe, A. J. The Acetate Switch. *Microbiology and Molecular Biology Reviews* **69**, 12–50 (2005).

280. Lynnes, T., Prüß, B. M. & Samanta, P. Acetate metabolism and Escherichia coli biofilm: New approaches to an old problem. *FEMS Microbiology Letters* vol. 344 95–103 Preprint at https://doi.org/10.1111/1574-6968.12174 (2013).

281. Valgepea, K. *et al.* Systems biology approach reveals that overflow metabolism of acetate in Escherichia coli is triggered by carbon catabolite repression of acetyl-CoA synthetase. *BMC Syst Biol* **4**, (2010).

282. Fang, X., Lloyd, C. J. & Palsson, B. O. Reconstructing organisms in silico: genome-scale models and their emerging applications. *Nat Rev Microbiol* **18**, 731–743 (2020).

283. Palsson, B. O. Genome-Scale Models. *Metab Eng* 23–71 (2021) doi:10.1002/9783527823468.CH2.

284. Bartell, J. A. *et al.* Reconstruction of the metabolic network of Pseudomonas aeruginosa to interrogate virulence factor synthesis. *Nat Commun* **8**, (2017).

285. Sosinski, L. M. *et al.* A restructuring of microbiome niche space is associated with Elexacaftor-Tezacaftor-Ivacaftor therapy in the cystic fibrosis lung. *Journal of Cystic Fibrosis* (2021) doi:10.1016/j.jcf.2021.11.003.

Appendix A: Supplementary Materials for "High-throughput dilution-based growth method enables time-resolved exo-metabolomics of *Pseudomonas putida* and *Pseudomonas aeruginosa*", Microbial Biotechnology (2021)

Supplementary Figure 1

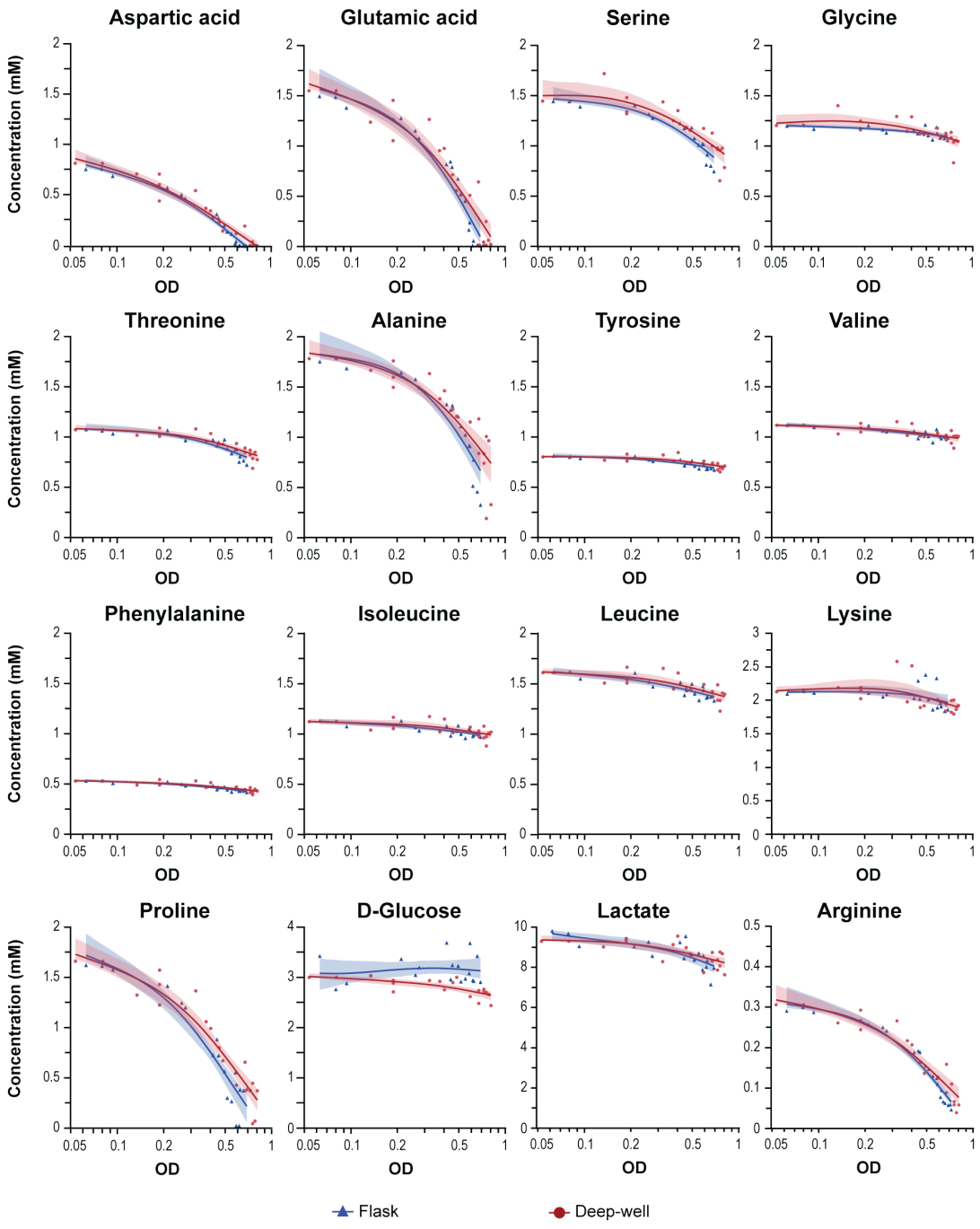

Figure 13: Assimilation plots of all quantified metabolites for Pseudomonas aeruginosa *PAO1 cultivated in SCFM. The concentration of each metabolite in Erlenmeyer flasks (blue symbols and lines), and deep-well plates (red symbols and lines) is shown relative to the OD at which supernatant samples were collected. Shaded areas indicate the 95% confidence intervals of the curves (cubic spline fitting).*

Supplementary Figure 2

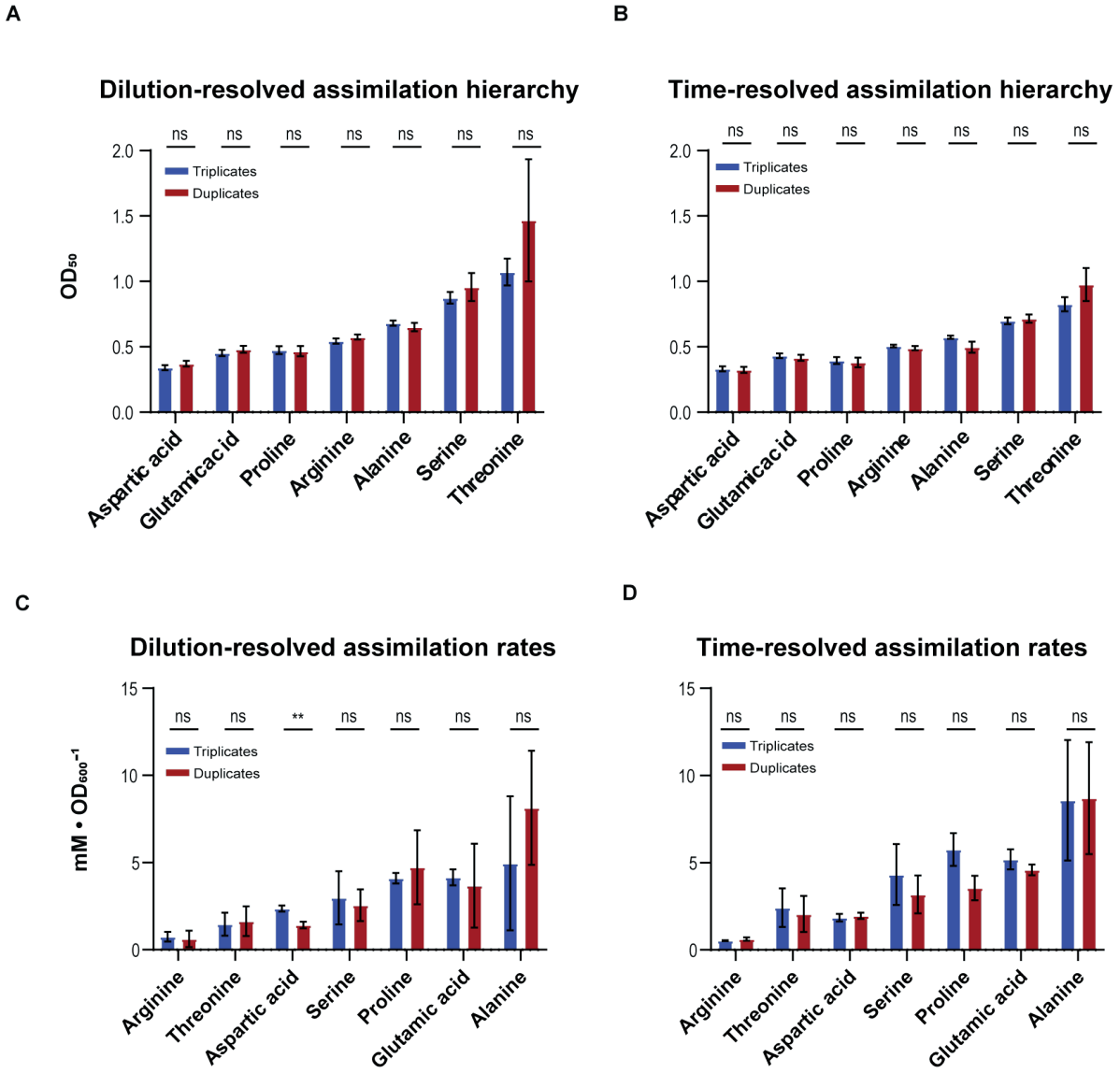

*Figure 14: Assimilation hierarchy (A and B) and assimilation rate (C and D) determined using the data from three (blue bars) or two (red bars) biological replicates for the dilution-resolved (A and C) and time-resolved (B and D) methods. The error bar indicates the SEM (Standard Error of the Mean). Differences between rates were evaluated by Unpaired Welch t-test with significance indicated as 'ns' where P > 0.05 and '**' where P < 0.01.*

Supplementary Table 1

All data is available in online version of paper (DOI: 10.1111/1751-7915.13905; ISSN: 1751-7915).

Appendix B: Supplementary Materials for "Metabolic specialization drives reduced pathogenicity in *Pseudomonas aeruginosa* infections in cystic fibrosis patients", In preparation (2023).

Supplementary Figure 1

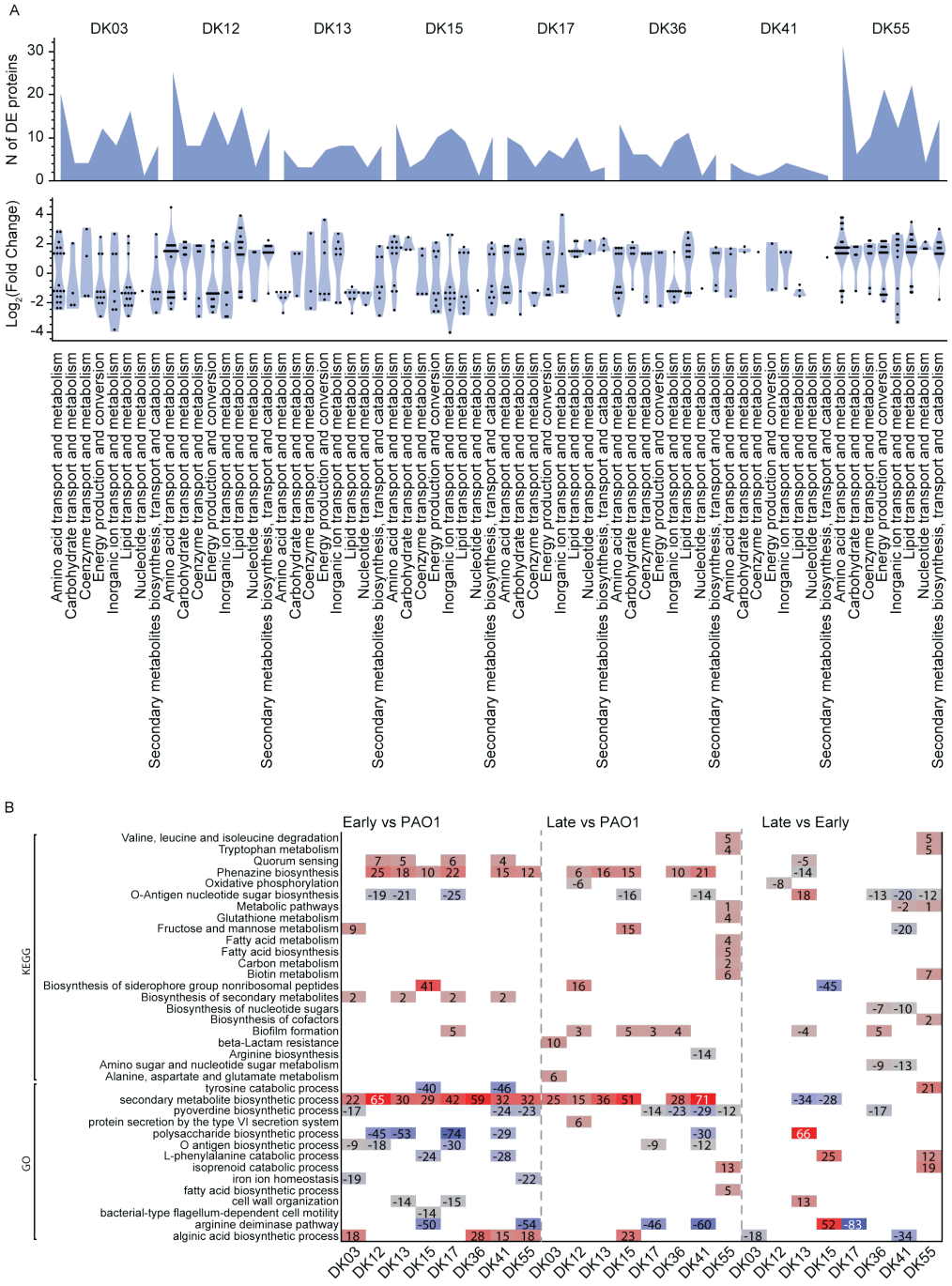

Figure 15: A) Number of differentially expressed proteins (top) and Log2(Fold change) of individual differentially expressed proteins in late vs. early clinical isolates, separated by lineage and on the x-axis by COG categories. B) Complete enrichment analysis showing fold-enrichments separated by comparison and lineage on x-axis and by KEGG and GO terms on y-axis.

Supplementary Figure 2

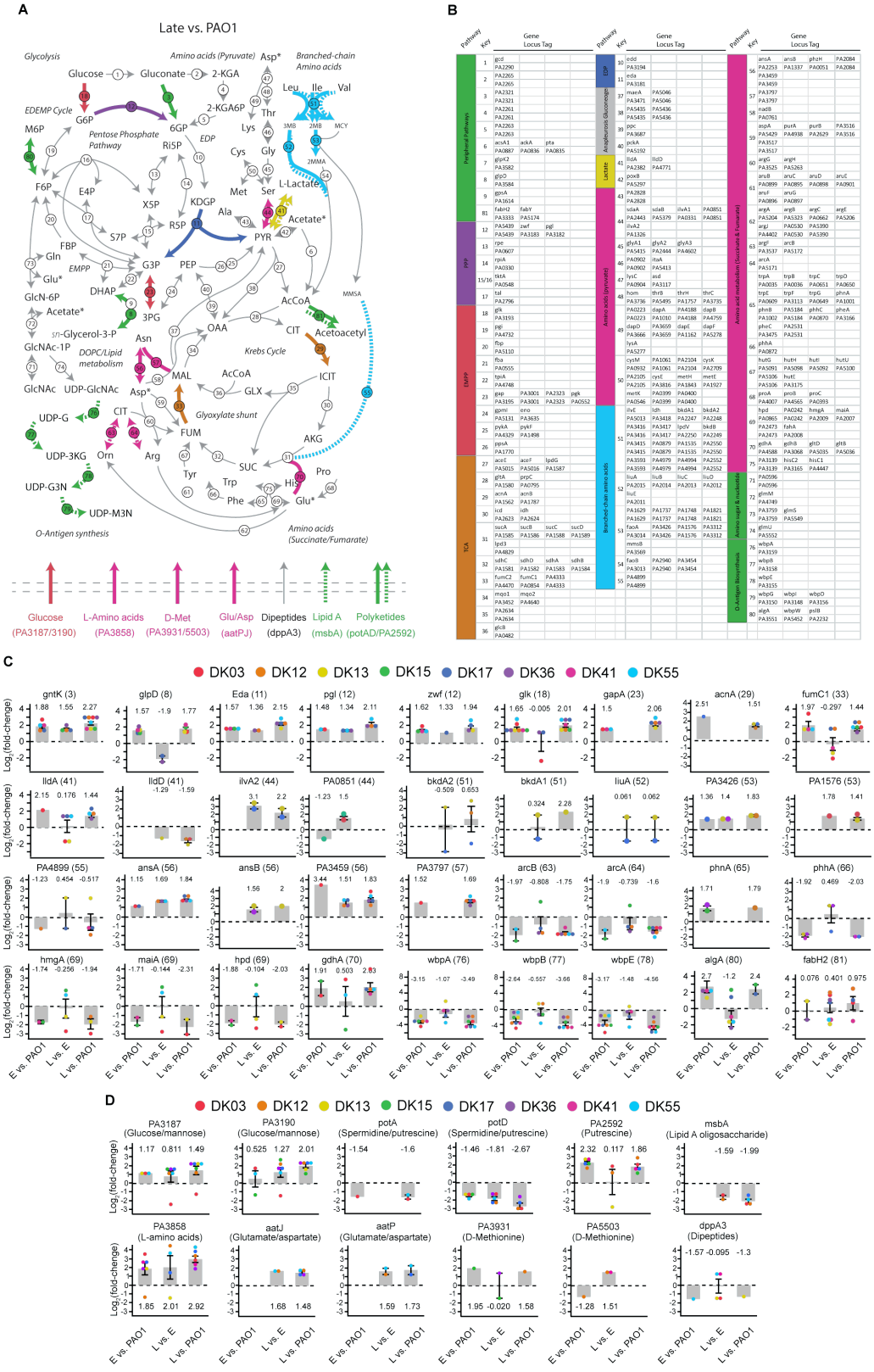

Figure 16: A) Metabolic map in the same style as Fig. 3E for late clinical strains vs PAO1. B) Table of genes/Locus Tags of all metabolic enzymes included in the map. C-D) Bar charts showing Log2(Fold change) of all differentially expressed proteins highlighted on the metabolic maps. Icons coloured by lineage and separated into three comparisons on x-axis (Early vs PAO1; Late vs Early; Late vs PAO1). Panel C contains metabolic enzymes and panel D contains transporters.

Supplementary Figure 3

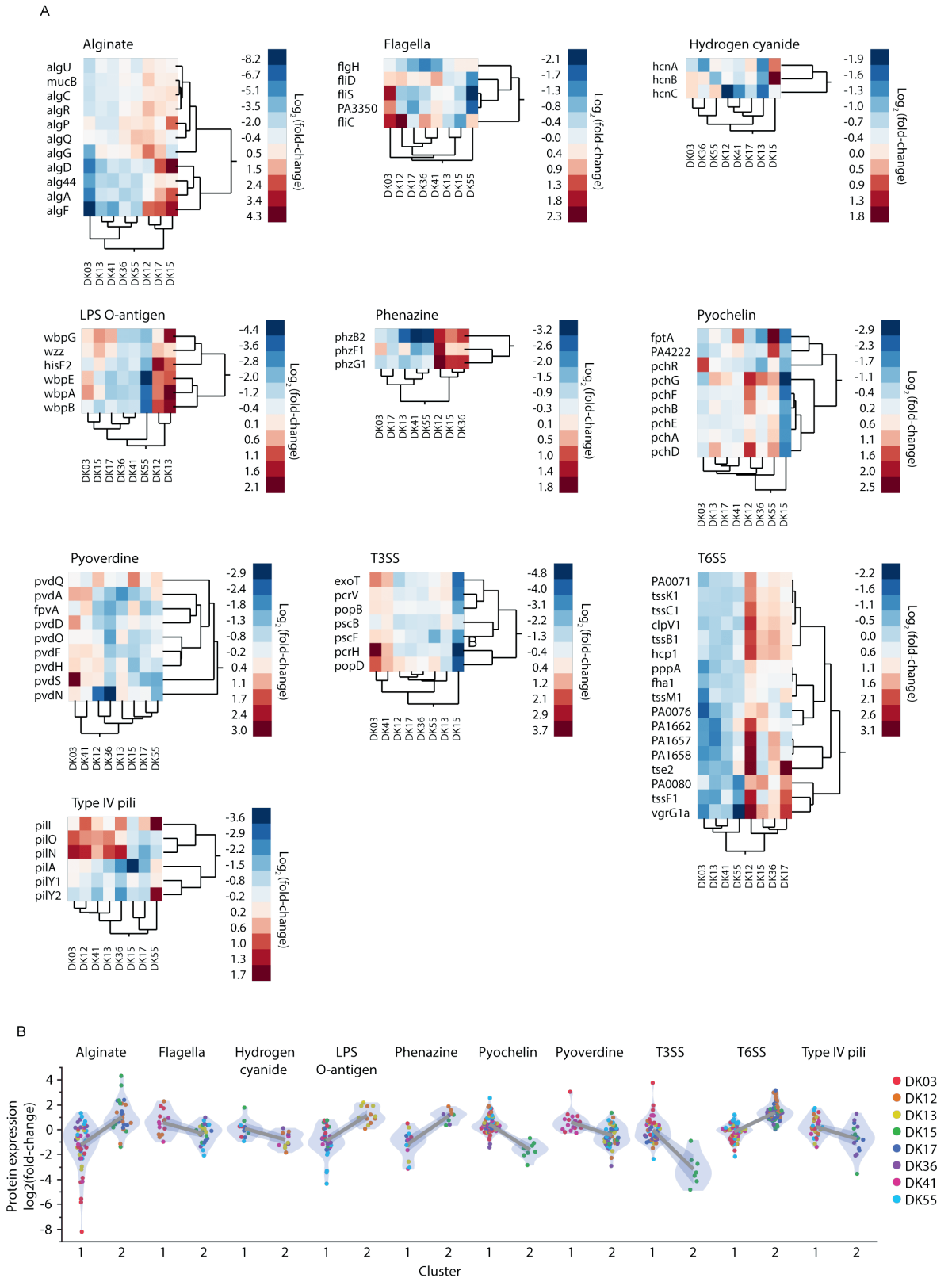

Figure 17: A) Hierarchical cluster analysis in the same style as Fig. 4C, showing differential expression in late vs early clinical strains for several more virulence categories. B) The Log2(Fold change) of differentially expressed proteins in late vs early clinical strains separated into the relevant virulence categories and further separated into the two main clusters from panel A. Icons are coloured by lineage and lines depict the difference in mean Log2(Fold change) between the two clusters.

Supplementary Figure 4

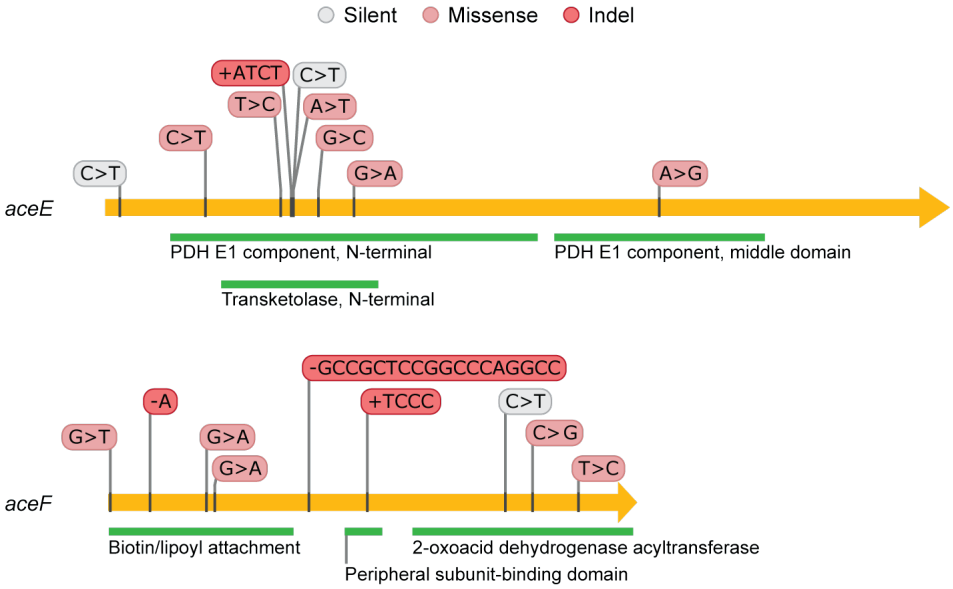

Figure 18: Schematic of all 18 unique mutations observed for aceE (top) and aceF (bottom) in our collection of clinical isolates of P. aeruginosa. Grey lines indicate mutation site and letters indicate nucleotide-sequence coloured by type of mutation.

Supplementary Figure 5

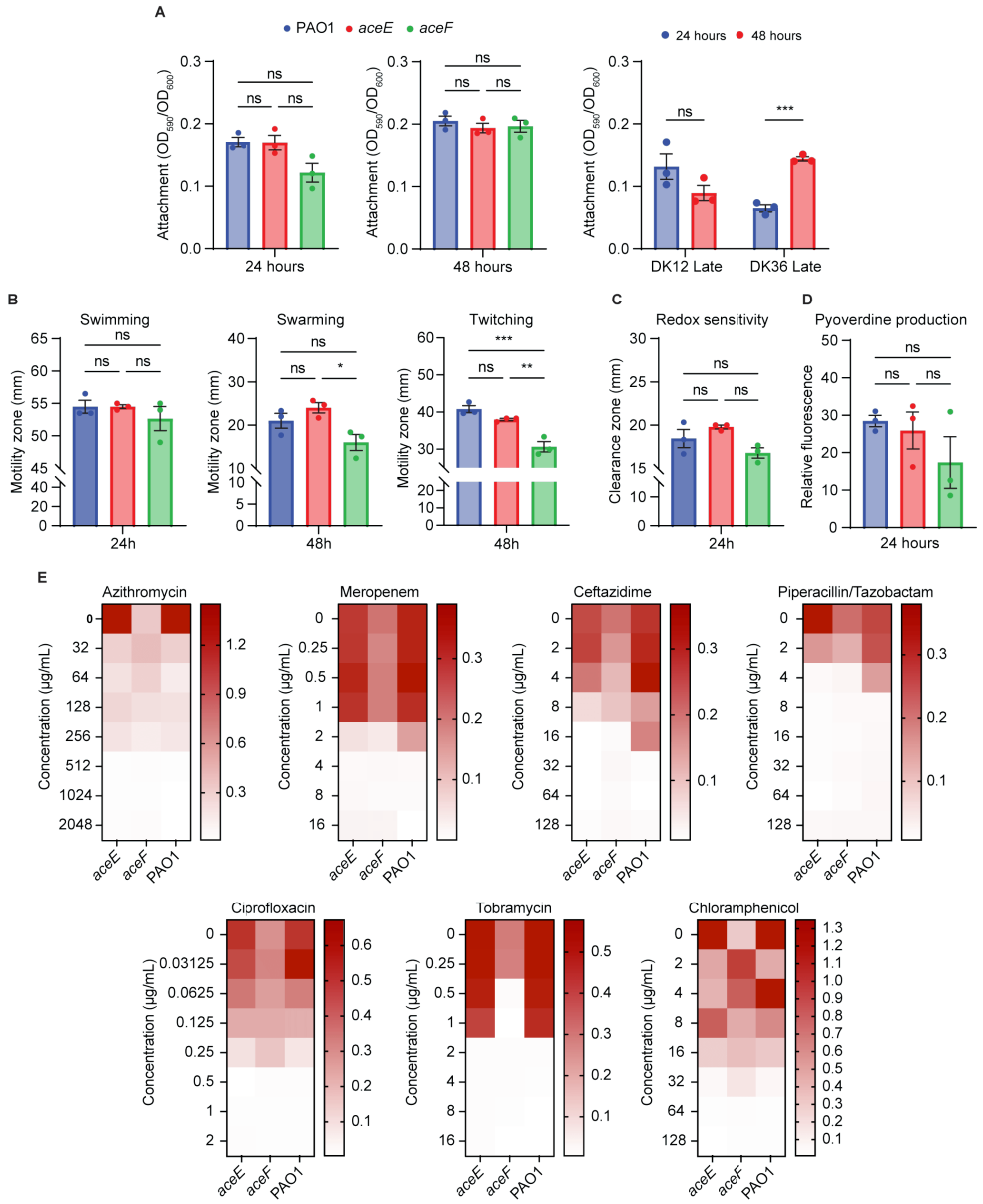

*Figure 19: A) Potential for biofilm formation (surface attachment) of PAO1 wt (blue), as well as aceE (red) and aceF (green) mutant strains and DK12 & DK36 late clinical strains after 24 and 48 hours respectively. For the clinical isolates, strain is indicated on the x-axes and incubation time is indicated as blue (24 hours) and red (48 hours). Attachment is measured as the ratio of surface-attached cells (OD_{590}) to total number of cells (OD_{600}) after incubation. For PAO1 wt and aceEF mutants, all strains were compared by One-Way ANOVA. For clinical isolates, each strain was compared to itself after 24 and 48 hours of incubation respectively, using two-tailed unpaired parametric Welch t-test. Significance is indicated as 'ns' ($p > 0.05$), * ($p < 0.05$), ** ($p < 0.01$), *** ($p < 0.001$). Same colouring and statistical analysis for PAO1 and mutant strains in panel B-D. B) Motility measured as the diameter (mm) of the zone of growth in motility plates (LB agar). Swimming motility was clearly visible after 24 hours of incubation. Swarming and twitching plates required 48 hours of incubation. C) Redox sensitivity measured as the diameter of the clearance zone (mm) on bacterial lawns (LB agar) of each strain from H_2O_2 diffusion disks after 24 hours. D) Pyoverdine production measured as relative fluorescence (F/OD_{600}) of each strain after 24 hours of growth in King's B medium. For panel A-D, icons indicate biological replicates and bars represent the mean ± SEM. E) MICs of PAO1 wt and aceEF mutant strains. Each cell represents the maxOD of growth curves under the given condition, following the colour gradient to the right of each heatmap. The MIC is the concentration where no growth is observed (white). Each heat map shows the MIC for all three strains for a given antibiotic (Ceftazidime, Meropenem, Piperacillin, Azithromycin, Chloramphenicol, Ciprofloxacin and Tobramycin). Concentrations (µg/mL) increase 2-fold downward on the vertical axis and the specific strain is given on the horizontal axis. Azithromycin MICs were determined in LB, while all other MICs were determined in SCFM2. Piperacillin was used in combination with the ß-lactamase inhibitor Tazobactam.*

Supplementary Figure 6

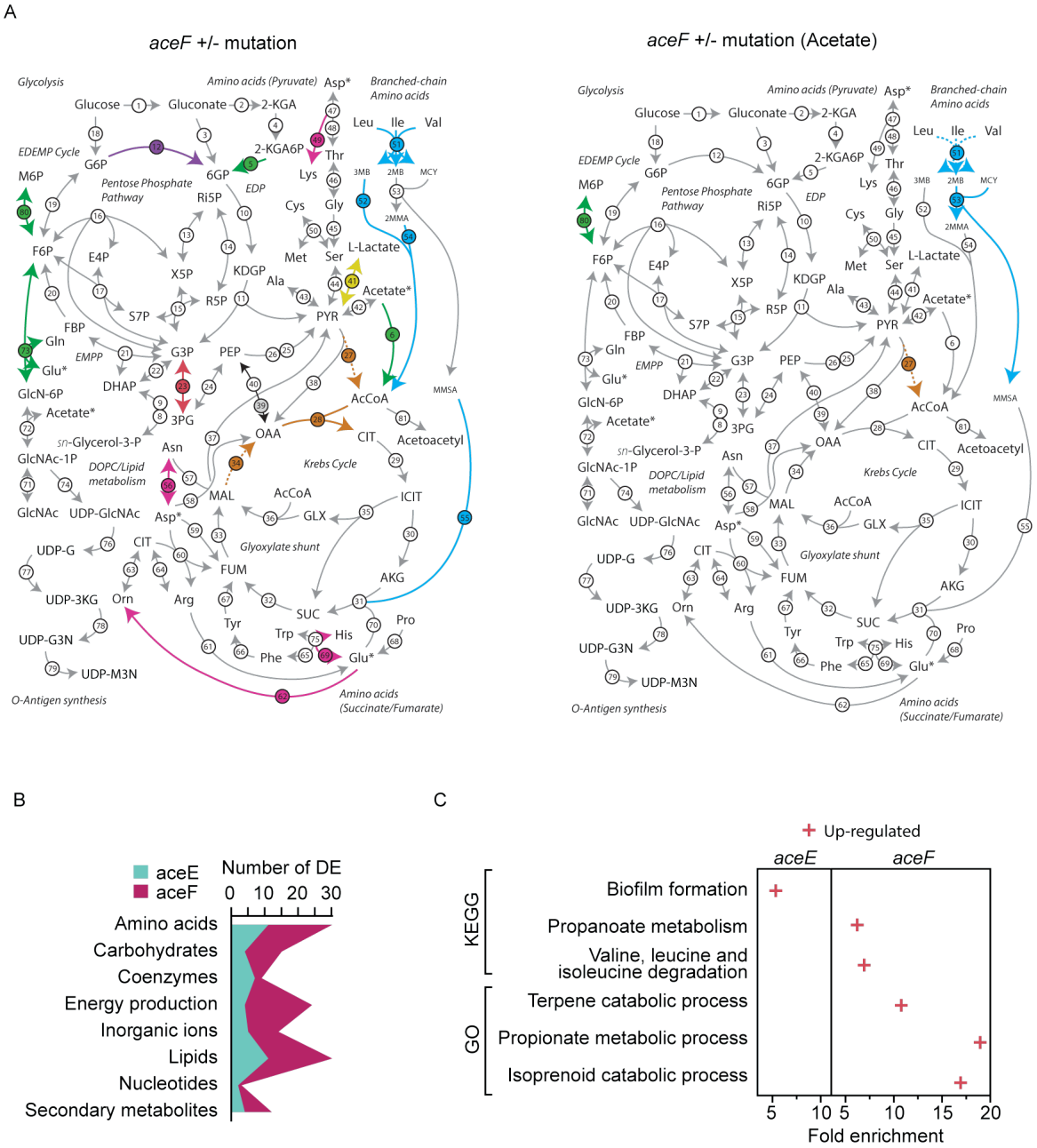

Figure 20: A) Metabolic map in the same style as Fig. 3E for aceF mutant strain vs PAO1 reference in SCFM2 in absence (left) and presence (right) of acetate. B) Parallel plot showing the number of differentially expressed proteins, separated by metabolic COG categories, in aceE (cyan) and aceF (magenta) mutant strains vs PAO1. C) Enrichment analysis showing fold enrichment on x-axis separated by KEGG and GO terms on y-axis for aceE (left) and aceF (right) mutant strains vs PAO1.

Supplementary Figure 7

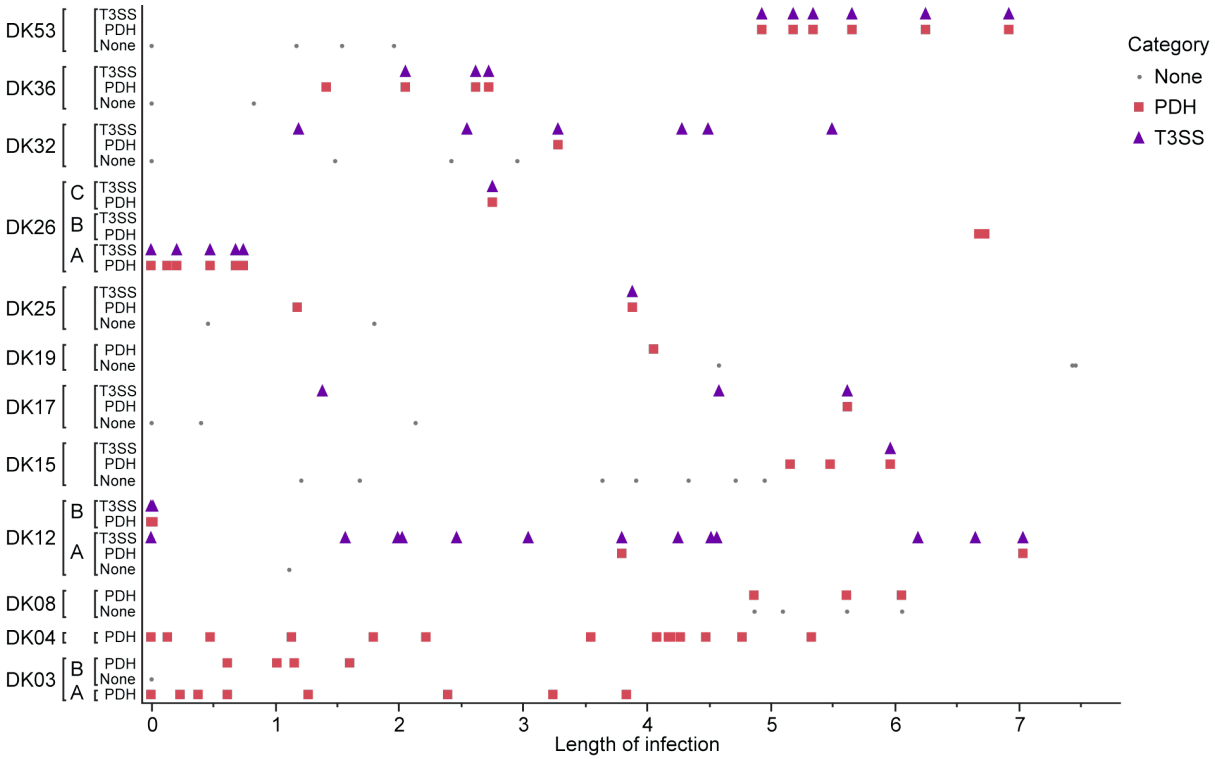

Figure 21: Longitudinal collection of P. aeruginosa clinical isolates from CF airways. Icons indicate isolates carrying mutations in genes encoding PDHc (red squares) and/or T3SS (purple triangles) proteins, as well as isolates with no mutations in either (grey dots). Isolates are separated by Clone Type and further separated by patient-specific lineages within Clone Types (A, B, C). The x-axis shows the length of infection (years) since the first isolate of the given lineage.

Supplementary Table 1: Strains and plasmids used in this study

Strain	**Genotype**	**Source**
PAO1	*P. aeruginosa* PAO1 wild type	Lab stock
PA018	*P. aeruginosa* PAO1; *aceE* t551c	This work
PA019	*P. aeruginosa* PAO1; *aceF* +tccc 816-819	This work
PA020	*P. aeruginosa* PAO1; *aceF* Δgccgctccggcccaggcc 618-636	This work
Plasmid	**Description**	**Source**
pCasPA	Vector carrying P_{ara}-*cas9* and λ Red recombination system; Tet^R	239
pACRISPR	Template vector for homology flanks and sgRNA integration; Cab^R	239
pIP243	Editing plasmid to introduce *aceF* +tccc 816-819; Cab^R	This work
pIP244	Editing plasmid to introduce *aceF* Δgccgctccggcccaggcc 618-636; Cab^R	This work
pIP251	Editing plasmid to introduce *aceE* t551c; Cab^R	This work

Supplementary Table 2: Primers used in this study

Primer name	Sequence	Description
PNJ1377	ACACAUTATACGAGCCGGATGATTAATTGTC	Reverse to amplify the backbone of pACRISPR
PNJ1378	ACTTTTCAUACTCCCGCCATTCAGAAG	Forward to amplify the backbone of pACRISPR
PNJ1379	AGACCAUGGGTATGGACAGATCTCA	Reverse to amplify sgRNA
PNJ1533	ATGTGUGGGATGCGACCCTTGGGACCGCGTT TTAGAGCTAGAAATAGCAAGTTAAAATAA	Forward to amplify sgRNA, *aceF* +tccc
PNJ1534	ATGGTCUAGAGCCAGCGTCCAGGACATCAAGG	Forward, *aceF* +tccc left flank
PNJ1535	ACCGCUGGCTTTCACTTCGCTC	Reverse , *aceF* +tccc left flank
PNJ1536	AGCGGUCCCTCCCAAGGGTCGCATCCTCAAGG	Forward, *aceF* +tccc right flank
PNJ1537	ATGAAAAGUCTCGAGACCGGGACCAGCAGGCCGTC	Reverse , *aceF* +tccc right flank
PNJ1541	ATGTGUGGACCGGCAGCCGCTCCGGCCCGTTTTAGAGCTAGAAATAGCAAGT TAAAATAA	Forward to amplify sgRNA, *aceF* –N18
PNJ1542 b	ATGGTCUAGAAATCCCCAGTCCCAAGGCCGGG	Forward, *aceF* –N18 left flank
PNJ1543	AGCGGCGCCUTCCACCTTCAG	Reverse , *aceF* –N18 left flank
PNJ1544	AGGCGCCGCUCCGGCAGCCGAAGAGCAACCGGCAGCGGCGCCCGCCGCCGA GCAG	Forward, *aceF* –N18 right flank
PNJ1545	ATGAAAAGUCTCGAGATCGGCAGTACGGTCAGCTTGAC	Reverse , *aceF* –N18 right flank
PNJ1568	ATGCCGAUATACTATGCCGATGATTAATTGTCAACAATTAATTAAAGG	Forward to amplify sgRNA *aceE* t551c
PNJ1569	ATCGGCAUAGGTGGGGAACTGCCAGAAGTCGTTTTAGAGCTAGAAATAGCAA GTTAAAAT	Reverse to amplify sgRNA *aceE* t551c

Data availability

All data are available upon request.

Appendix C: Additional comments on proteomic convergence

In addition to the enzymes shown on the map, we also found convergence (defined as > 1 CTs) in the differential expression of enzymes related to fructose and glyoxylate (alg44, algD, algG, PA1500), as well as many proteins related to Arginine (arcC, ureAC, spdH, aguB) and other amino acids (dhcB, mmsA, PA1337, hisF2). Additionally, proteins related to oxygen (ccoP1, PA0141) and nitrogen (nirS, nosZ) were convergently downregulated during infection. Proteins related to methane (PA3628) and GTP (PA3043) were upregulated, while PA4645 related to GMP was downregulated. The transporters msbA (lipids) and potD (polyketides) were convergently downregulated, while aatJ (Glu/Asp) was upregulated in late isolates. A number of proteins related to secondary metabolites were also differentially expressed in a convergent fashion, namely Glycan (algF, wbpG, ponA), phenazines (phzB2, phzG1), folate (folC), butanoate (dhcB), porphyrin (hemN), cyanide (hcnC), Acetaldehyde-P (phnX), pyochelin (pchDG), glutathione (PA2813, PA4511) and NADPH-quinone (PA1225).

We also found convergent upregulation in the Two Component systems phoP, pfeR, copR, dctP and hxuR, modulation of mexXY and downregulation of algR, oprD and pilA. The quorum sensing proteins pqsABCD were all the most strongly upregulated proteins in early isolates and subsequently downregulated in late isolates, albeit still expressed at much higher levels than PAO1. Additionally, many proteins of the T6SS injectosome are upregulated during infection (clpV1/V2, hcp1/C1/C2, vgrG1/G2a, tssB1/C1/J1), while the secreted factor secF is downregulated. For motility, proteins associated with flagellar (fliCD, PA1095) were severely downregulated already in the early isolates and remained so, while proteins related to chemotaxis (dppA3, pctB) were more affected in late isolates.

Metabolism

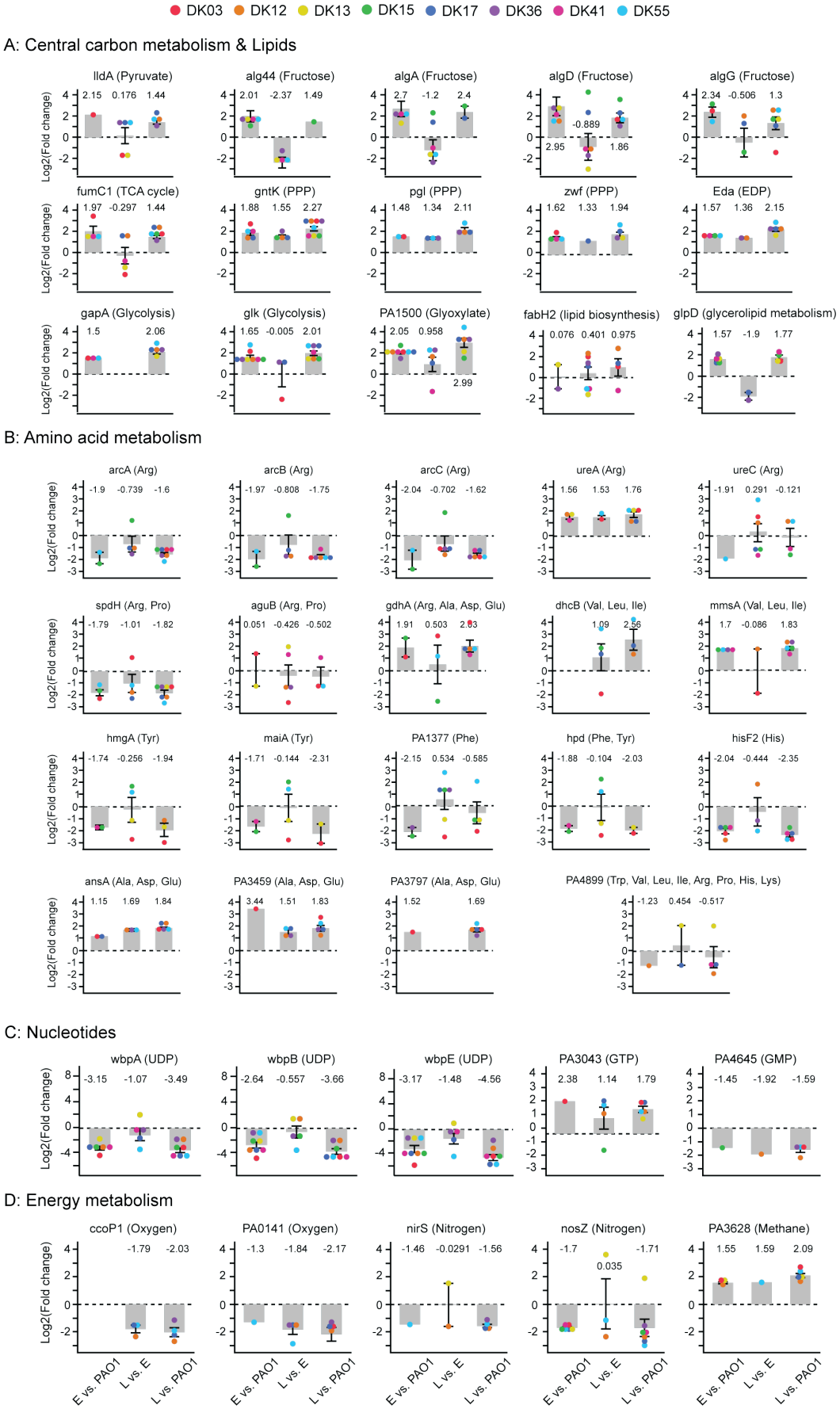
DK03 DK12 DK13 DK15 DK17 DK36 DK41 DK55
A: Central carbon metabolism & Lipids
lldA (Pyruvate)
alg44 (Fructose)
algA (Fructose)
algD (Fructose)
algG (Fructose)
fumC1 (TCA cycle)
gntK (PPP)
pgl (PPP)
zwf (PPP)
Eda (EDP)
gapA (Glycolysis)
glk (Glycolysis)
PA1500 (Glyoxylate)
fabH2 (lipid biosynthesis)
glpD (glycerolipid metabolism)
B: Amino acid metabolism
arcA (Arg)
arcB (Arg)
arcC (Arg)
ureA (Arg)
ureC (Arg)
spdH (Arg, Pro)
aguB (Arg, Pro)
gdhA (Arg, Ala, Asp, Glu)
dhcB (Val, Leu, Ile)
mmsA (Val, Leu, Ile)
hmgA (Tyr)
maiA (Tyr)
PA1377 (Phe)
hpd (Phe, Tyr)
hisF2 (His)
ansA (Ala, Asp, Glu)
PA3459 (Ala, Asp, Glu)
PA3797 (Ala, Asp, Glu)
PA4899 (Trp, Val, Leu, Ile, Arg, Pro, His, Lys)
C: Nucleotides
wbpA (UDP)
wbpB (UDP)
wbpE (UDP)
PA3043 (GTP)
PA4645 (GMP)
D: Energy metabolism
ccoP1 (Oxygen)
PA0141 (Oxygen)
nirS (Nitrogen)
nosZ (Nitrogen)
PA3628 (Methane)
Log2(Fold change)
E vs. PAO1
L vs. E
L vs. PAO1

Non-metabolic proteins

Two-Component Systems

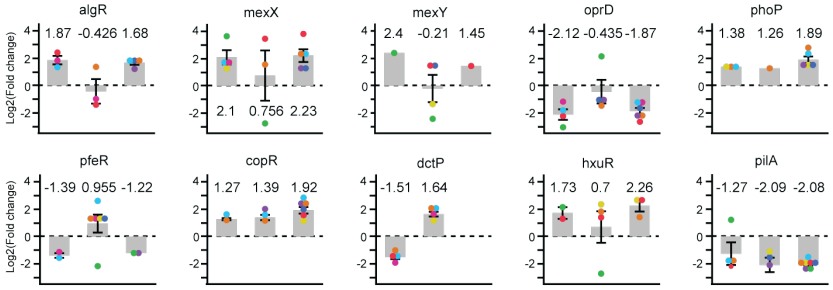

Bacterial secretion system

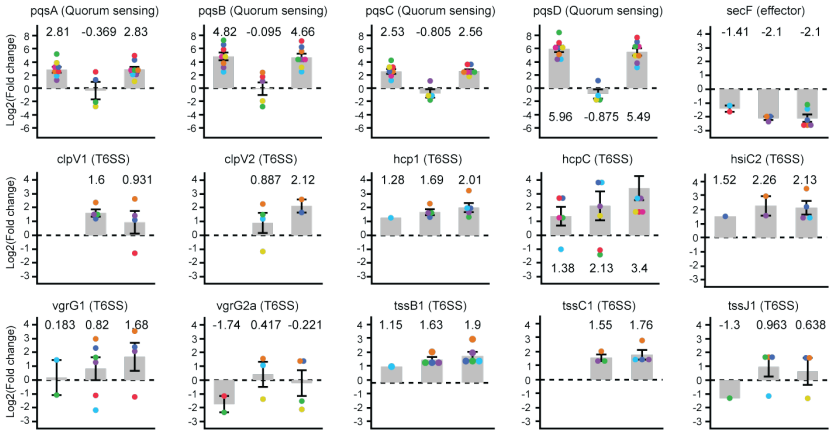

Secondary metabolites

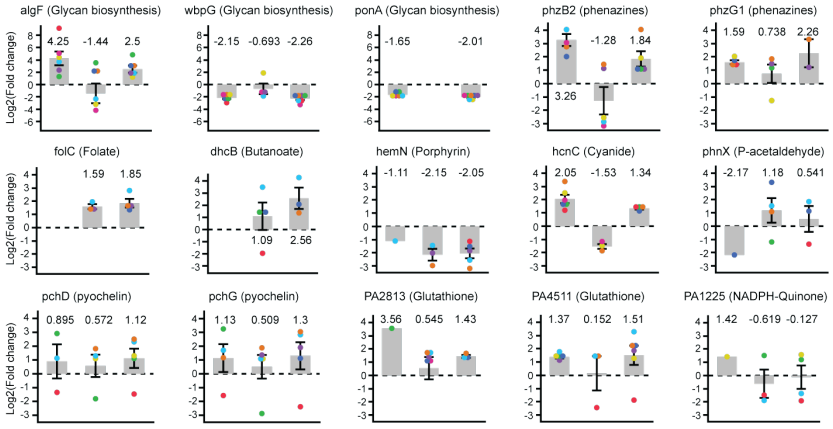

Motility

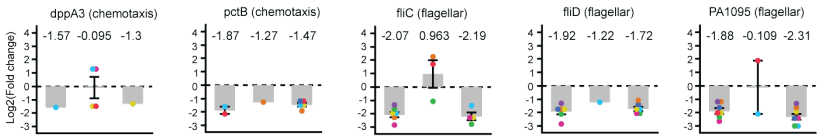

ABC Transporters